INSTITUT SUPERIEUR DE L'AERONAUTIQUE ET DE L'ESPACE
DEPARTMENT OF AERODYNAMICS, ENERGETICS AND PROPULSION
MSC AEROSPACE MECHANICS AND AVIONICS
MAJOR ON AERODYNAMICS

Large Eddy Simulation of the Film Cooling Flow System of Turbine Blades: Public Shaped Holes

Master Thesis

SIMIRIOTIS Nikolaos

Carried out at:

CERFACS
CENTRE EUROPÉEN DE RECHERCHE ET DE FORMATION AVANCÉE EN CALCUL SCIENTIFIQUE

Supervisors:
Dr. Laurent Gicquel , Senior Researcher at CERFACS
Dr. Florent Duchaine , Senior Researcher at CERFACS

Academic Supervisor:
Prof. Nicolas Gourdain

Toulouse

September, 2016

(PAGE INTENTIONALLY LEFT BLANK)

DECLARATION BY STUDENT

This assignment is entirely my own work. Quotations from literature are properly indicated with appropriated references in the text. All literature used in this piece of work is indicated in the bibliography placed at the end. I confirm that no sources have been used other than those stated.
I understand that plagiarism (copy without mentioning the reference) is a serious examinations offense that may result in disciplinary action being taken.

(PAGE INTENTIONALLY LEFT BLANK)

ABSTRACT

Gas turbines nowadays are used in many industrial applications. The thermal efficiency and the power output of gas turbines is associated with the increase of the turbine inlet rotor temperature. The needs in increasing the turbine inlet temperature is not accompanied by a significant breakthrough in terms of material technology. The turbine inlet temperature at this point is far above the melting point of the metal material used. Therefore, the turbine blades have to be cooled. The main application of external cooling is the film cooling technique. The goal of this thesis is to study numerically the flow phenomena present in a typical film cooling flow application utilizing shaped holes. It aims to assess a Large Eddy Simulation (LES) code on this type of configuration.

This thesis includes two parts. The first part is devoted to an extensive literature review so that the reader could get an idea on the basics of this field of research. It will become obvious that the add of shaping in the holes used for film cooling can lead to a by far improved cooling efficiency. Essentially, this type of flow could be viewed as a jet flow ejected to a cross-flow, a domain that has been researched a lot over the years with many questions still remaining unanswered. Many typical flow structures develop with the Counter Rotating Vortex Pair (CRVP) being the most important to the film cooling. A description and an interpretation of the flow mechanisms is attempted in this thesis as well.

In the second part simulations are carried out using AVBP, an LES code. The Public Shaped Hole, a design proposed by R. P. Schroeder, is studied. A simplified geometry including one hole bringing cold fluid over a flat surface is meshed and given appropriate boundary conditions representing as close as possible an experimental configuration. The effect of numerical schemes, wall modeling and turbulent injection were studied. Thermal and flow quantities were compared to experimental ones. The code was successfully validated. The TTGC (a Taylor-Galerkin based) convective scheme provided the best results among the others and a quite good prediction in general. The wall modeling approach did not seem to lead to an improvement of the estimation and the turbulence injected at the inlet of the computational domain had no apparent effect on the computed solution. Through flow field plots all the typical feature of the film cooling flow already identified in past literature were observed constituting AVBP a solver capable to predict the phenomena taking place.

(PAGE INTENTIONALLY LEFT BLANK)

CONTENTS

(PAGE INTENTIONALLY LEFT BLANK)

1. INTRODUCTION

The goal of this thesis is to study numerically the flow phenomena present in a typical film cooling flow application utilizing shaped holes. It aims to assess a Large Eddy Simulation code on this type of configuration which is of great importance for the industrial world.

Gas turbines nowadays are used in many industrial applications. The propulsion of aircrafts and the generation of mechanical power or electricity in land-based facilities are the main examples. The thermal efficiency and the power output of gas turbines is associated with the increase of the turbine inlet rotor temperature [1]. This can be clearly observed in figure 1.1 that exhibits the engine's power output as a function of the turbine inlet temperature. The ideal performance line corresponds to an engine working perfectly without any losses. Even the modest increase in efficiency is significant in the industrial world nowadays.

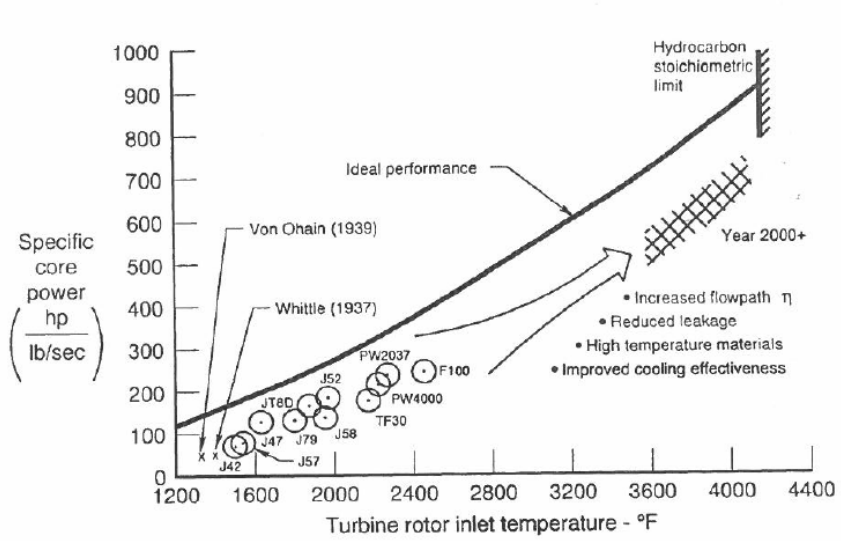

Figure 1.1: *Engine cycle power output as a function of the turbine inlet temperature [1].*

The dependence observed in this figure can be explained by taking a look at the ideal Brayton cycle that describes the work of a constant pressure engine. In figure 1.2 the temperature-entropy diagram of a Brayton cycle is depicted. The power output per unit mass flow is proportional to the enclosed area in this diagram. Increasing the temperature at the turbine inlet (i.e. T_4) by working in a higher compressor pressure ration, leads to an increase in thermal efficiency while keeping the power output per unit mass flow constant. This is of great importance (especially when referring to aircraft propulsion) as designers take into consideration the engine size (consequently the mass flow rate) when designing a new engine. Finally, regulations concerning the gas exhausts necessitate to keep the combustion temperature within a specific range due to constraints

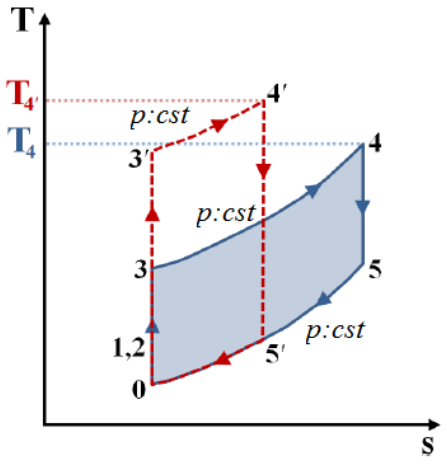

Figure 1.2: *Ideal Brayton cycles [2].*

of the NO_x emission problem. Concluding, to achieve a higher thermal efficiency for the same combustion temperatures the turbine inlet temperature should be higher. In that way more power is to be produced.

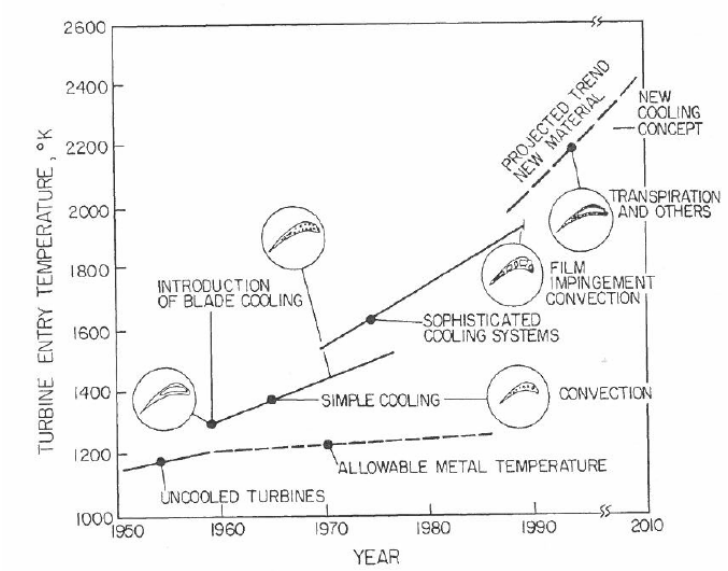

Figure 1.3: *Turbine entry temperature over the years compared to allowable metal temperature [1].*

However, the needs in increasing the turbine inlet temperature is not accompanied by a significant breakthrough in terms of material technology. The turbine inlet temperature at this point is far above the melting point of the metal material used in advanced gas turbines (figure 1.3). Therefore, the turbine blades have to be cooled. To ensure high performance and protection against the thermal material failure the industry is obliged to invest on development such as thermal barrier coating and sophisticated cooling schemes [1].

1.1. Turbine Blade Cooling

The engine cooling systems are responsible to ensure that the maximum temperature level at the surface of the blade along with the temperature gradients are compatible with the limitations of thermal stress imposed by the design. By reducing the heat transfer to the turbine blades they maintain the desired component life and the safe operating conditions.

The basic concept of turbine cooling systems is pretty simple: air is extracted from the compressor of the engine which later on is provided to the blades for cooling. This extraction results in a penalty in thermal efficiency as the bled air could otherwise be burned. Therefore, it is essential for the cooling technique to be optimized so that the extraction does not result in reduced engine performance but at the same time is sufficient to protect effectively the blade components. The blades are cooled internally and externally. Internal cooling is achieved by letting the coolant pass through serpentine like passages (rib-turbulated cooling) in the interior of the blade extracting the heat from the blades' surface [1]. Jet impinge-

ment and pin-fin cooling are also complementary internal cooling techniques.

The main application of external cooling is the film cooling technique. In film cooling, the coolant is injected from the interior of the blade to the mainstream of the hot gases through discrete holes on the blade's surface. The jet is then entrained by the main flow forming a thin protective layer of cool air covering the blade's surface reducing in that way the incident convective heat flux, protecting the blade from the hot combustion gases. The reader can see schematics of the techniques described in figure 1.4.

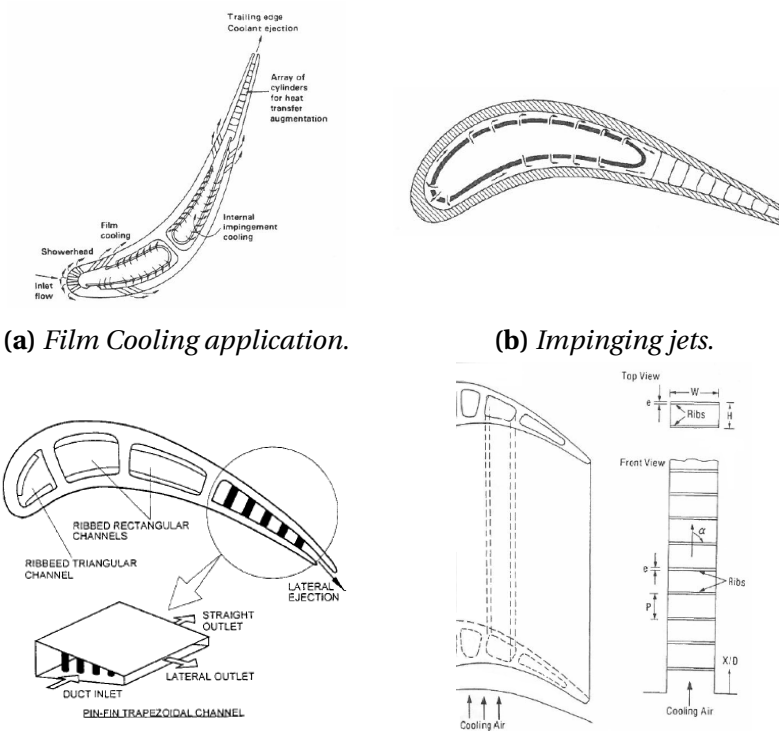

(a) *Film Cooling application.* **(b)** *Impinging jets.*

(c) *Pin-Fin technique.* **(d)** *Rib-turbulated cooling.*

Figure 1.4: *Schematic illustration of the different cooling techniques on a turbine blade [1], [3].*

1.1.1. Blade Film Cooling Basics

Film cooling techniques aim to provide protection versus the impacting heat flux on the surface of the blade by ejecting coolant through discrete holes on the blade's surface, shrouds, tips and endwalls (see figure 1.5). With the exception of the region of the trailing edge, the usage of slots for the cooling is not applicable due to constraints for structural integrity deriving from the high thermal and mechanical stress the components are subjected to [4]. As a result, most of the holes used in film cooling are drilled at an angle to the blade's surface.

There are however plenty of additional challenges when designing the application of a blade film cooling system. It is important for this type of technology to provide the maximum cooling efficiency. For that, sufficient mass flow rate should be provided. However, that flow rate should not exceed a certain limit after which the losses in thermal efficiency would be

greater than the increase achieved due to the higher inlet turbine temperature.

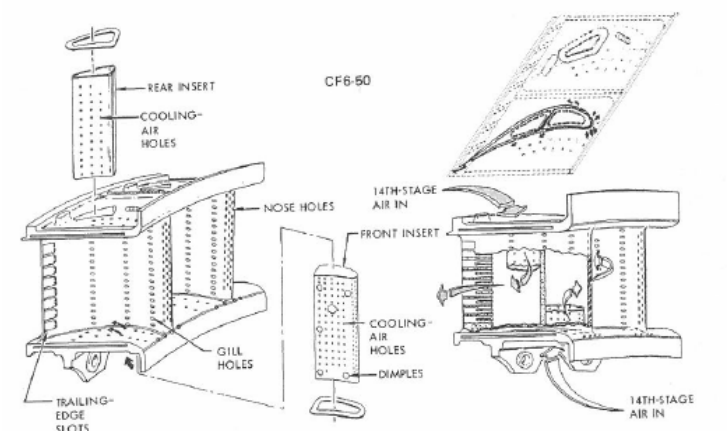

Figure 1.5: *Typical cooled nozzle vane of high pressure turbine [1].*

For that to happen there is a continuous effort for hole designs that eject a jet of coolant which stays attached to the (blade's) surface in order to cover it effectively and reduce the heat flux not only where the ejection takes place but also further downstream. These designs should also aim to reduce the turbulent mixing of the jet with the mainstream as much as possible in order to avoid the dilution of the coolant and deteriorate the aerodynamic losses due to the mixing of two means with different momentum (the coolant jet flow and the hot gases flow). In order to take into account all the aforementioned goals, one common direction in designing is the adding of proper shaping which, as it will be exhibited later on, leads to holes with superior cooling performance in most of the cases.

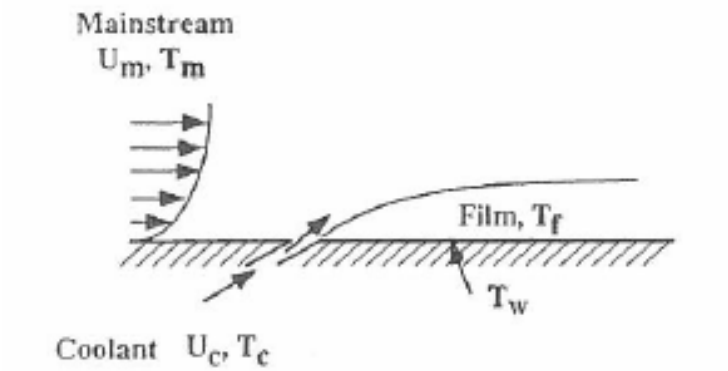

Figure 1.6: *Schematic of the film cooling concept [1] where T_f is the adiabatic wall temperature, T_c the coolant temperature and T_m the hot gas temperature.*

In literature, the performance of the film cooling technique is primarily evaluated in the scope of the heat transfer and the aerodynamic losses due to mixing only come second in consideration [2]. In terms of heat transfer, two are the performance variables of interest: the adiabatic effectiveness (η) and the convective heat transfers coefficient (h_f) [5]. A common definition in literature for the adiabatic effectiveness writes:

$$\eta = \frac{T_{m,rec} - T_{aw}}{T_{m,rec} - T_c} \tag{1.1}$$

where: $T_{m,rec}$ the hot gas recovery temperature (namely the temperature on the adiabatic wall without the film cooling influence), T_c the coolant temperature typically at the exit of the hole and T_{aw} the adiabatic wall temperature (defined as the temperature of the fluid covering the adiabatic wall when film cooling is applied). Generally, the $T_{m,rec}$ is defined locally [4] but from hereon will be associated with the constant temperature of the main (hot gas) flow. The adiabatic effectiveness is a metric providing information on the coverage (the footprint on the wall) of the cooling strategy.

The heat transfer coefficient with film cooling is given:

$$h_f = \frac{q_f}{T_{aw} - T_w} \tag{1.2}$$

and without film cooling:

$$h_0 = \frac{q_0}{T_{m,rec} - T_w} \tag{1.3}$$

where q_0 and q_f the heat loading for the two cases respectively and T_w the wall temperature that should be kept below the material melting point. The flow losses are often quantified with the discharge coefficient defined as the ratio of the real flow mass through the hole versus the ideal one and writes (assuming isentropic one-dimensional expansion) [13]:

$$c_D = \frac{m_{real}}{m_{ideal}} = \frac{m_{real}}{A \cdot p_{t,c} (\frac{p_m}{pt,c})^{\frac{\gamma+1}{2\gamma}} \sqrt{\frac{2\gamma}{(\gamma-1)RT_{t,c}} \left[(p_{t,c}/p_m)^{(\gamma-1)/\gamma} - 1 \right]}} \tag{1.4}$$

where: A the metering cross section area (for a shaped hole typically the constant cross-section of the cylindrical part), p_m and $p_{t,c}$ the static and total pressure at the exit and inlet of the hole respectively and $T_{t,c}$ the total temperature of the coolant (at the hole's inlet).

The film cooling effectiveness mainly depends on the typical flow structures resulting from the interaction of the main (hot gas) flow with the coolant jet. These flow structures in turn are directly associated with the geometrical parameters defining the design of the cooling holes and the operating conditions of each configuration. As a result, a large number of parameters seem to affect the flow in subject and the efficiency of the cooling technique. Typical flow parameters for this type of configurations, against which researchers try to scale their results are:

$$DR = \frac{\rho_c}{\rho_m} \quad , \quad M = \frac{\rho_c u_c}{\rho_m u_m} \quad , \quad I = \frac{\rho_c u_c^2}{\rho_m u_m^2}$$

where the index c refers to the coolant, the index m to the quantities of the mainstream, DR is the density ratio, M the mass flux ratio (also referred to in the literature as blowing ratio) and I the momentum flux (momentum ratio). Usual configuration parameters that are also taken into consideration are the ones that describe the free-stream conditions, such as the turbulence intensity T_u, the integral length scale Λ_x and the boundary layer characteristics

(displacement thickness δ_1, momentum thickness θ) of the approaching flow [2].

The geometric parameters of interest are those describing the configuration itself. The flow phenomena are mainly driven by the characteristics of the geometry and the performance is significantly affected by changes in the hole's design. Typical geometric parameters will be seen in following chapter (the reader could look for figure 2.6) and their effect will be briefly addressed through the literature review that follows.

1.2. Goals of the Project

In this project a Large Eddy Simulation (LES) of the Public Shaped Hole (a specific hole design described in the next chapter) is performed. The configuration consists of a "7-7-7" hole bringing coolant on a flat plate. The goal is to access AVBP, a parallel LES code, on its ability to estimate effectively the type of flow developed and validate it for this case versus experimental results. Numerical simulations offer great flexibility especially for cases where experiments is difficult to be performed in realistic conditions. Indeed, it is very rarely that test cases like this are experimentally tested in real engine-like conditions.

Having a validated (LES) tool in hand can also add up to the understanding of complex flows like the one in subject as there is almost no limit to the information that can be acquired and the variability of the cases that can be later on tested. Indeed, the typical flow structures that develop in a configuration like this have been the object of many experimental studies over the years. However, there is plenty of room for additional work since there are still many questions unanswered regarding the comprehension of the flow physics that take place. As there is a significant smaller number of numerical studies, this project can contribute to the understanding the research community has on the subject.

On a personal note, this project had offered the author a great chance to undergo a training in LES techniques through multiple sessions and everyday involvement with the computational procedure. By performing a systematic LES study a great deal of attributes were indeed acquired. Finally, the project provides with the opportunity to work in an important industrial application that is really interesting for the scientific community as well.

1.3. Outline

This thesis is organized in the following way:

Chapter 1. An introduction to the application/scientific field that is of interest has been made and the goals of the project have been set.

Chapter 2. Literature review of film cooling studies with a special emphasis on technical attributes and cooling performance. Review of R. P. Schroeder's work on Public Shapes holes.

Chapter 3 Review of "jet in a cross-flow" studies. These flows are often associated with the film-cooling ones. Overview of typical structures observed.

Chapter 4. A brief reference on Large Eddy Simulation (LES) and some specifics about the parallel LES code used in this project (AVBP).

Chapter 5 Results of the simulations versus the experimental ones. Validation of AVBP for this case and brief discussion.

Chapter 6. Summary of the thesis, some concluding remarks and a few suggestions for future work/continuation of this project.

1.4. About Cerfacs

The *Centre Européen de Recherche et de Formation Avancée en Calcul Scientifique* (CERFACS) is a fundamental and applied research center specializing on modeling and numerical simulation[1]. Strongly involved in the development and usage of numerical tools, CERFACS deals with problems of the public and industrial research taking advantage of the accumulated in-depth knowledge on High Performance Computing (HPC). Created in 1987, CERFACS has evolved to be implied in major projects, strongly interacting with its industrial partners (i.e. Airbus Group, Cnes, EDF, Météo France, Onera, Safran and Total) and is associated with important research centers.

CERFACS accommodates a number of interdisciplinary researchers (leading to the creation of corresponding multidisciplinary teams) developing innovative tools and methods that find application in the aeronautic, spatial, climate, energy and environmental fields of research. It also provides advanced training sessions dealing with dedicated disciplines of importance (e.g. applied mathematics, HPC topics, physics). Being involved in major scientific and industrial projects, CERFACS provides multiple offers of occupation and training for young engineers interested to delve into research. The present project was carried out during a six-month training period at CERFACS.

[1] http://www.cerfacs.fr/en/discover-cerfacs/

2. Literature Review

In this chapter literature examining the performance of film cooling is reviewed. Due to easiness in manufacturing, the standard in film cooling has been the design of simple cylindrical holes drilled at an angle to the surface of the turbine blade [4]. This (inclination) angle has to be as small as possible (according to manufacturing constraints) for the jet to be ejected close to the surface. Seminal studies (1974) performed by Goldstein et al. [6] exhibited that the cooling performance can be significantly improved with the application of proper shaping in the holes. They demonstrated that the coolant jet ejected from round (cylindrical) holes was detached from the surface for greater blowing ratios ($M > 0.5$) which dramatically affects the adiabatic effectiveness. On the other hand, shaped holes exhibited low sensitivity to the variation of the M and the values of adiabatic effectiveness remained superior to the ones acquired from cylindrical holes.

Nowadays, the use of shaping in holes has been a pretty common practice since they perform better in representative values for the M in real engines ($M \approx 2$). The film cooling holes consist of a round (cylindrical) part followed by an expanding (diffused) exit nozzle. The reader can see typical shape hole designs in figure 2.1. This expansion aids in the reduce of the jet's momentum and along with the Coanda effect [6] (as the holes are inclined) keeps the jet attached to the surface. This leads to lower aerodynamic mixing losses, greater lateral coverage of the surface and lower effective blowing ratios all resulting in an increment in cooling efficiency. The application of shaping of course does not come without its own limitations: available wall thickness is a requirement and the appropriate distance between neighboring holes should be kept and is always a concern. Moreover, there are still regions on an airfoil where shaping adds little to no value at all [4].

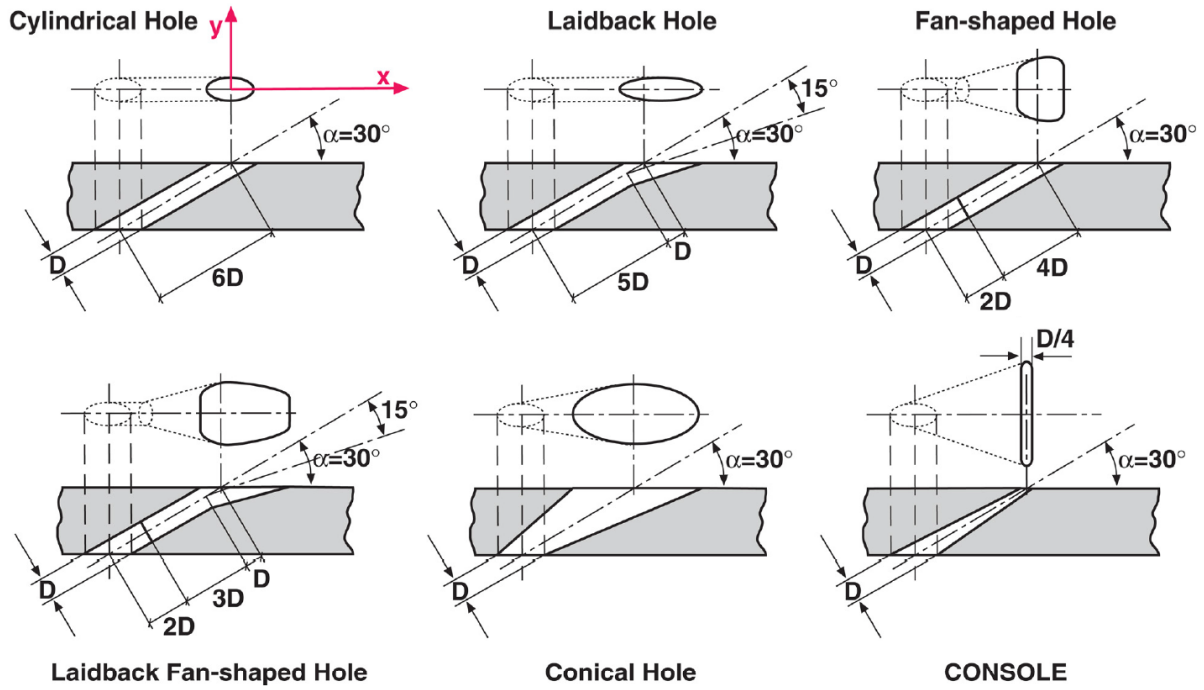

Figure 2.1: *Basic hole designs [7].*

2.1. Specifics of Shaped Holes

There are many key features in a film cooling flow and various phenomena that have been identified and reported through many years of research. Typically, a cooling hole can be fed with coolant by a plenum or a channel through which cooled-air cross-flow is provided. In either case, usually the fluid undergoes a huge turning leading to a separation bubble on the leeward side of the hole's wall, just after its inlet. The excess velocity of the fluid at the windward side of the hole is a result of this and is called "the jetting effect" ([14], [10]). In the case of the shaped hole, due to the non-uniform profile at the diffuser's inlet and the velocity deficit due to the jetting effect [8] a separation region is usually developed in the leeward side of the diffuser' wall. This separated fluid makes the rest of the flow concentrate on the sides of the hole forming a typical bimodal pattern on the footprint of the flow (see figure 2.2) outside of the hole and over the surface that is to be cooled.

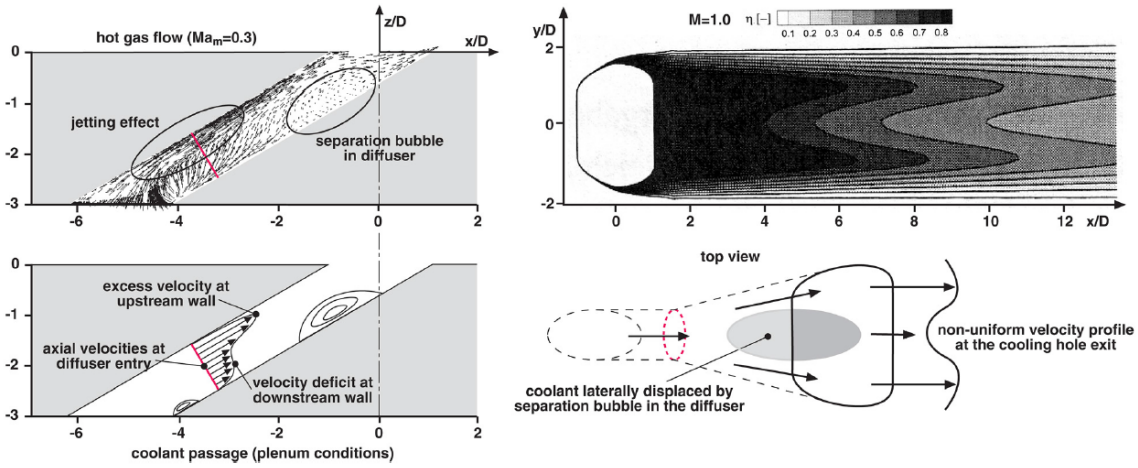

Figure 2.2: *Schematic representation of specific flow phenomena typically seen in film cooling flows with shaped holes [8].*

This separation region can be in many cases suppressed leading to the extinction of the bimodal pattern. However, as it can have both detrimental and desirable effects, no concluding remark has been made on whether it should be suppressed or not. Generally, even though it leads to non-uniform velocity profiles at the exit, associated with intense turbulence generation, and contains the momentum reduction of the jet [2], it also aids in the lateral spreading of the jet providing enhanced coverage.

The main feature of these flows however is the formation of a *Counter Rotating Vortex Pair* (CRVP) outside of the hole. This specific structure is typical (among others) to each configuration that includes a jet ejected in a cross-flow and has been associated with the film cooling flows over many years of research. It consists of a pair of longitudinal (in the direction of the mainstream) vortices formating after the interaction of the jet with the mainstream. This pair is rotating in a sense that brings the mainstream (hot gasses) under the jet and just above over the surface reducing the adiabatic effectiveness of the cooling jet (see figure 2.3). In addition to that, due to the nature of the vortex dynamics the induced velocity makes the jet further lift-off the surface.

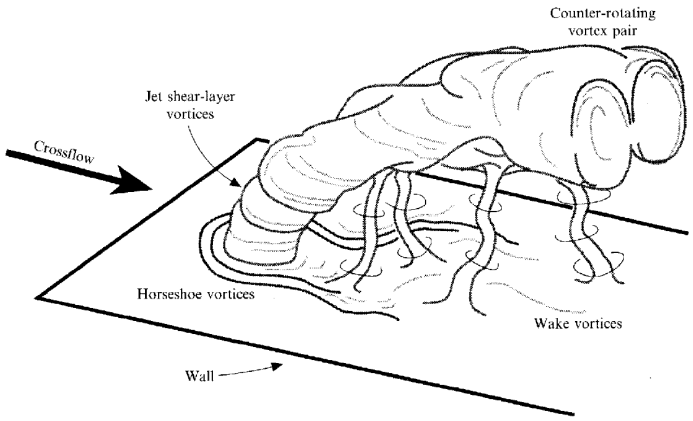

Figure 2.3: *Schematic representation of the different types of structures found in a jet-crossflow interaction - among them the CRVP [28].*

This structure that only has detrimental effects in the cooling process seems to be less pronounced in shaped holes and far more supreme when cylindrical holes are used. With the shaped holes the two vortices of the pair seem to move apart from each other and their induced results are suppressed. Additionally, their coherence breaks down due to various smaller vortical structures generated that tend to weaken the CRVP and format a far more complex flow field that is not anymore strongly governed just by this pair. That is yet another reason that shaping is a common direction when designing cooling holes nowadays. This part is going to be discussed separately in a following chapter in more extent.

At this point, what follows is a literature review over some experimental and numerical studies of film cooling on flat surfaces. The flat-surface models are generally used to study the singled-out effects that different parameters have with great ease and by lowering the cost (either computational or for the manufacturing of specimens to be tested experimentally). Moreover, studies have showed that results obtained from flat plate test cases can applied to turbine blades of real engines with some corrections [1]. As a results, a huge number of studies (and among those the present one) have been performed on flat-surface cooling.

2.2. Experimental Work on Cylindrical and Shaped Holes

In [12] flow-field measurements for film cooling holes with expanded outlets were performed and compared with respective ones for cylindrical holes. One laterally and one both forwardly and laterally expanded hole were tested.The coolant in each case was supplied by a cross-flow channel and the blowing ration was constant ($M = 1$). The use of expanded holes led to a reduce in jet penetration (evident through velocity profiles), velocity gradients and consequently turbulence production. Better adiabatic efficiency was reported for the expanded hole with the laid-back one however presenting some mainstream ingestion as the M was not high enough. Low turbulence level was attributed to the feeding of the coolant through a cross-flow channel (large turning of the fluid associated with the use of a plenum was averted).

In [9] the free-stream turbulence effects on the film cooling were evaluated. Once again the three aforementioned designs were tested for various values of free-stream turbulence intensity. The coolant was supplied with a cross-flow channel for three free-stream turbulence intensities T_u = 3.5, 7.5 and 11%). The M was ranging from 0.5 to 1.5 for the cylindrical holes and up to 2.5 for the shaped holes. The discharge coefficient for the cylindrical holes was significantly lower compared to the ones measured for the shaped holes. No dependency of the coefficient on the intensity or the turbulent length scale was identified. For the cylindrical holes, the increase of the turbulence intensity resulted in losses in terms of effectiveness in low to moderate values of M but brought an increase for higher blowing ratios (by improving lateral spreading and diminishing the tendency to detach). For the shaped holes the effects of increased intensity were always detrimental, especially for smaller M, as the already well-expanded jet just got diluted. Additionally, the impact of the change in M on the heat transfer becomes more pronounced for higher levels of turbulence.

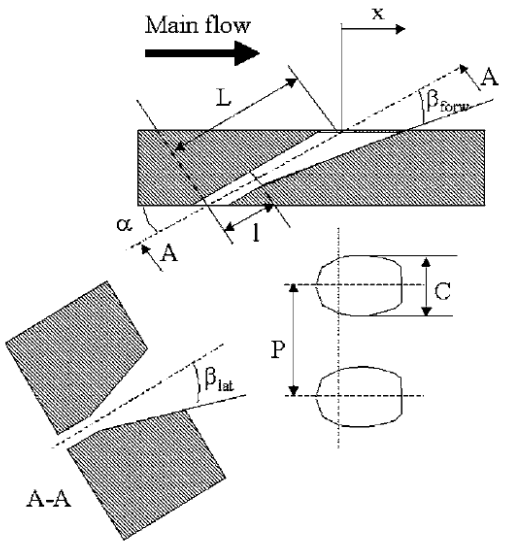

Figure 2.4: *Geometric parameters [13].*

In [13] the effects of the hole geometry on the cooling performance of shaped holes was studied. The length ration (L/D), the aspect ratio (AR), the hole pitch (P/D), the hole coverage (C/P) and the compound angle of the hole (γ) had be chosen as the configuration parameters. The definitions can be seen schematically in figure 2.4. Totally 16 different hole geometries had been created for a systematic study of the singled out effect of each parameter. The discharge coefficient seemed unaffected by the changes in the geometry. In the range of M investigated the changes in the geometry also had a weak effect on the adiabatic effectiveness.

In the same context, in [7] the effect of the inclination angle of the hole, the expansion angle of the diffuser and the length of laterally expanded holes were examined. The M was varied from 0.5 to 2.5 and in each case the effect of the cross-flow Mach (Ma) number in the feeding channel was also studied. For the range of M tested, the increase in the expansion angle led to improved laterally averaged adiabatic efficiency, especially in higher M, providing better coverage and reduced penetration of the jet. The effect of the inclination angle was only pronounced in higher M. As the angle increases the intensively cooled area gets shortened and evident widening of the jet is not sufficient to compensate for the loss in adiabatic effectiveness. The increase in the inclination angle also resulted in greater c_D values. The hole length also had a detrimental effect only in high M were the suppressed separation bubble and the disappearance of the bimodal effect at the footprint resulted in decreased adiabatic effectiveness. In the cases where there was a cross-flow instead of a plenum at the hole's inlet, the results would differ considerably. The fluid went under a swirling motion inside the hole. The hole length would define the number of revolutions the fluid could perform inside the hole and in that way the resulted adiabatic effectiveness outside the hole as the velocity profiles at the exit would differ considerably and were mainly driven by the cross-flow itself.

In [8] the effects of the free-stream conditions were once again addressed. Cylindrical and fan-shaped holes had been investigated in variations of the Ma number of the mainstream, the turbulence intensity, turbulent length scale and the Strouhal (St) number of periodic unsteady wakes designed to simulate the unsteady effects inside an engine's turbine. They observed that the increase in free-stream Ma leads to a thinner boundary layer which in turn results to greater bending of the jet towards the wall and thus improved adiabatic effectiveness. However there was also a correlation between the Ma of the free-stream and the M, which in many case led to increased pressure losses and a dramatic drop in effectiveness due to separation phenomena inside the hole. The results in the effect of turbulence intensity validated the ones from [9]. Finally, it was exhibited that the shaped holes were far more sensitive to periodic unsteady wakes (compared to cylindrical ones) as they presented considerable reduction in effectiveness and discharge coefficients.

2.3. Numerical Study of Film Cooling

One of the first systematic CFD investigations of film-cooling holes has been performed in [14]. Following the computational work of Laylek and Zerkle, Garg and Gauler, Berhe and Patankar as well as experimental work described in the previous section, they studied the effect that the way the feeding of the hole with coolant is done has on the cooling performance. One cylindrical and one shaped hole were tested for plenum and (three) cross-flow conditions at the hole's inlet. In each cross-flow simulation the direction of the flow was modified. A 3D Navier-Stokes solver was used with a $k-epsilon$ model for turbulence. Their study was focused on the flow field inside the hole which affects the velocity profiles at the hole exit which in turn have a huge effect on the adiabatic effectiveness. For the cylindrical holes, due to the large turning of the coolant, a separation zone after the holes' inlet (separation bubble on leeward side of the hole) was identified leading to the concentration of the fluid at the windward side of the hole (jetting effect). For the plenum case, this led to the generation of a counter rotating vortex pair inside the hole, with its axis of rotation normal to the hole's cross section. For the cross-flow case a swirling motion inside the hole was documented instead. In each case, a longitudinal counter rotating vortex pair in the mainstream direction was observed outside the hole meaning that this was a result of the interaction of the jet with the mainstream flow and not due to the CRVP generated inside the hole. The resulted footprint of adiabatic effectiveness in the cross-flow case was skewed compared to the plenum one while the laterally averaged adiabatic effectiveness remained somehow unchanged. For the shaped hole case the flow-field inside the hole was quite complex. Along with the separation due to the turning of the coolant at the inlet, a second region was identified in the expanded portion of the hole where a big separation bubble was observed. No counter rotating vortices due to jet-mainstream interaction was noted. Turbulence intensity contours were also provided attesting to the hypothesis that intense turbulence generation is mainly due to the flow conditions inside the hole and high turbulence levels are less associated with the jet-mainstream interaction. The mainstream ingestion was also examined for the different feeding conditions. When the shaped holes are fed by a perpendicular cross-flow the ingestion is important leading to lower adiabatic effectiveness.

In [15] LES of a film cooling flow from an inclined cylindrical hole was performed. The main focus was a systematic study of the resulting flow-field in this type of configuration and the

typical vortical structures due to the jet-mainstream interaction. Their simulation showed good agreement with experimental data available. They identified many structures that had been previously reported in literature and were associated with the vorticity production inside the cooling holes. Specifically, the CRVP effects were described with the utilization of previously documented hairpin vortices, known to result from wall-bounded jet flows. The dynamics of this type of structures were examined along with their influence on the cooling performance and in the passive scalar (temperature) mixing.

Leedom's MSc thesis [16] was also focused on the numerical investigation of film cooling using LES. In his work, he tested cylindrical and shaped hole (laterally diffused and console) designs for the same coolant mass flow rate per unit width. The performance of the shaped holes was found to be superior, with the console holes performing slightly better than the rest while the fan-shaped one was associated with the highest aerodynamic losses. He identified many typical vortical structures, also documented in [15] mentioned previously, which had a great effect on the adiabatic effectiveness. In figure 2.5 iso-surfaces of Laplacian pressure are used to represent these coherent structures.

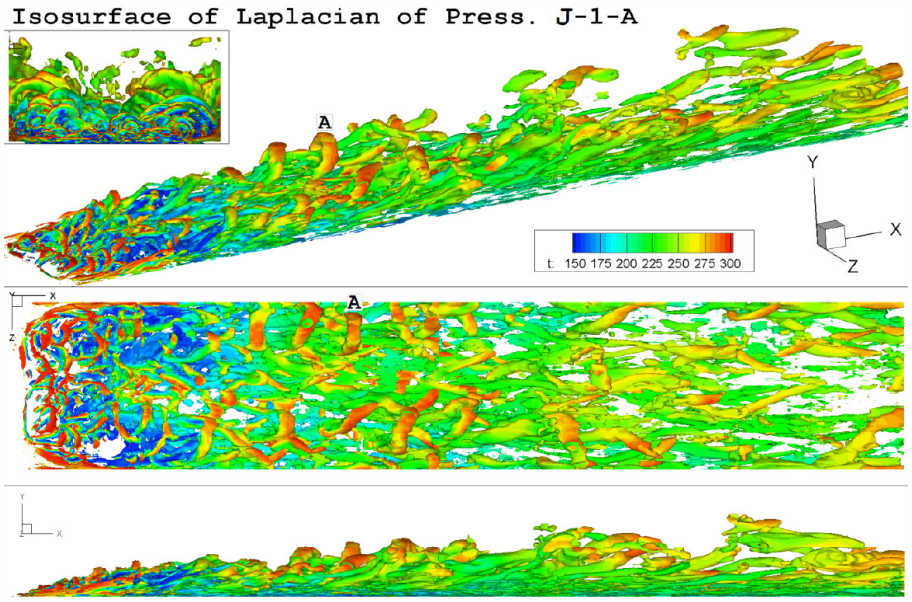

Figure 2.5: *Identification of coherent structures in shaped (laterally expanded) holes,* $L/D = 3.5$, $M = 1$ *[16].*

Cylindrical and Fan-shaped holes where tested in the context of LES in [17] as well. A validated LES method was used to investigate the flow physics and temperature mixing for these two geometries for the same M. The CRVP were well separated in the shaped hole case providing better coverage and lower induced velocity (that generally results in the jet lift-off). Once again, hairpin-like vortical structures seemed to drive the mixing processes in the flow. Higher temperature variance close to the shaped hole was observed due to the large number of smaller coherent structures which result in small scale temperature intermittency. For the cylindrical case, a steady core with low temperature variance resulting from steady exiting hanging vortices was documented instead.

2.4. MOTIVATION

In this project Large Eddy Simulation of film cooling is performed on a flat surface. The hole that provided the coolant had a specific shaping described below. The main motivation behind this study was to perform a systematic LES that will result in a validated tool which can provide a great description over the flow in this type of configuration. The LES approach is justified as it is revealed in literature that the RANS procedure usually underestimates the lateral shear stresses and hence the lateral expansion and mixing [15]. While the experimental work on this subject is wide in terms of publications, the numerical studies have been significantly less. In this project the results from a specific experimental case will be tried to be reproduced.

Since there are still many open questions, many different hypotheses and generally a lack of consensus regarding the nature of the phenomena encountered, this study can only add up to the existing knowledge. That is why, aside from the simulations performed, a wide literature review was carried out so that the reader can have a complete view over the state of the art and the typical directions taken when this type of flows is examined.

2.5. PUBLIC SHAPED HOLES

At this point, it is obvious from what is described in the previous sections, that the application of specific shaping is of great interest as it significantly adds on the cooling performance of the film cooling systems. For that reason, it has become a major field of study for the *Turbine Heat Transfer and Aerodynamics Group* (along with plenty other research teams) of the Department of Mechanical and Nuclear Engineering in the Pennsylvania State University. Within the department, the work of Robert P. Schroeder led to a series of papers ([18], [19], [20], [21], [22]) examining the performance of a proposed hole design.

A big part of Schroeder's work was focused on an extent literature review regarding film cooling applications and designs. He created a database in which he identified more than one hundred and twenty (120) different (in most cases) holes designs studied. Most of the published work he reviewed compared the novel shaped designs with results from cylindrical holes [18]. As discussed in previous sections, this has not much to offer as the cylindrical holes are generally inferior to the shaped ones.

Schroeder proposed a new *"baseline shaped hole geometry"* to be used as a reference for future research. He performed various experiments in order to provide a complete documentation over the performance of his proposed design. The baseline design, the literature review database, the corresponding published work and measurements taken are placed on a public website [2] to be shared with the scientific community. Schroeder chose a laid-back fan shaped design. Each expansion angle in the diffuser (in the forward direction and respectively the half angle in the lateral directions) was 7^o. He named the design "7-7-7 shaped hole". A schematic of the baseline hole design (also named Public Shaped Hole - PSH) can be seen in figure 2.6 along with the values of the geometric parameters found in table 2.1.

[2] https://www.mne.psu.edu/psuturbine/ShapedHole

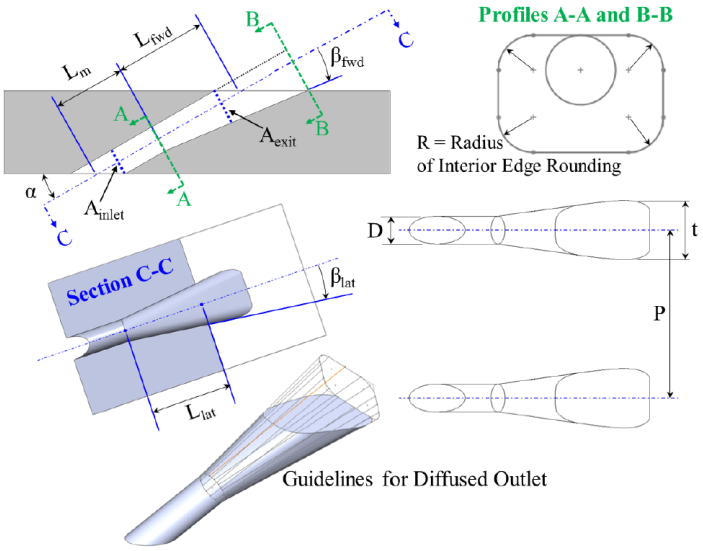

Figure 2.6: *Baseline Shaped Hole Design [18].*

	The 7-7-7 Shaped Hole Design
Metering Section Diameter, D	7.75 (mm)
Injection Angle, α	30^o
Hole Length Ration, L/D	6
L_m/D	2.5
L_{lat}/D, L_{fwd}/D	3.5
Laidback Angle, β_{fwd}	7^o
Lateral Angle, β_{lat}	7^o
Coverage Ration, t/P	6
Aspect Ration, AR	0.35
Rounding of the Diffuser's Edges, R/D	0.5

Table 2.1: *Geometric parameters of the Public Shaped hole [18].*

2.5.1. Studying the "7-7-7" Holes

As has been already mentioned, the work of Schroeder resulted in a series of articles that provide a complete analysis over the performance and the flow/thermal field characteristics of the configuration he designed and tested. Multiple experiments were performed for a row of (5) baseline holes on a flat plate. The holes were fed with coolant through a plenum ejecting it into the mainstream flow realized in a wind tunnel. The shaped holes were machined in Dow Styrofoam brand residential sheathing [18] in order for the flat plate to effectively work as an adiabatic wall for the measurement of effectiveness.

In [18] the holes were tested in low and moderate free-stream turbulence for different values of blowing ratio ($M = 0.5, 1, 1.5, 2, 2.5, 3$). The low turbulence case ($T_u = 0.5\%$) tested two

density ratios (DR = 1.2 and DR = 1.5) while in the moderate turbulence case (T_u = 5.4%) only one density ratio was tested (DR = 1.5). The approaching boundary layer in every case was tripped. Contours of adiabatic effectiveness were provided for each realization along with graphs of the centerline, the laterally-averaged and area-averaged adiabatic effectiveness. It was exhibited that the laterally averaged adiabatic effectiveness increased with the blowing ratio until plateauing for one value (M = 1.5) and then started decreasing again. The difference between the two density ratios was marginal with the greater one giving slightly higher values in terms of effectiveness associated with an (exhibited) better lateral expansion of the jet. The low values of effectiveness in low M were attributed to the ingestion of the cross-flow inside the hole due to the low momentum of the coolant. Increased turbulence level led to a widening of the coolant footprint on the plate and a slight decrease in the area-averaged effectiveness, with a less pronounced effect in higher M. Comparison with other shaped hole designs were also performed.

In [19], the effect that elevated turbulence has on the adiabatic effectiveness and the flow fields was addressed. Indeed, as free-stream turbulence in the flow around real turbine blades can reach up to 15%, a study like this is of great essence. For the same configuration as the one described in [18], additional experiments were performed for T_u = 13.2% and flow field PIV measurements were realized for each turbulence level for two blowing ratios (M = 1.5 and M = 3). Contours and profiles of the time-mean stream-wise averaged velocity, turbulence intensity and turbulent normal and shear stresses were plotted and compared. From the contours the existence of the counter-rotating vortex pair became evident. Supplementary shear stress developed due to the interaction of the main flow with the coolant jet leading to the generation of additional turbulence. The mean velocity field showed almost no change with the elevation of the turbulence intensity but the velocity fluctuations increased in the region around the coolant resulting in complementary lateral spreading. This had a detrimental effect for lower values of M as the laterally averaged adiabatic effectiveness reduced. The detrimental effects of turbulence seemed to recede in high blowing ratios.

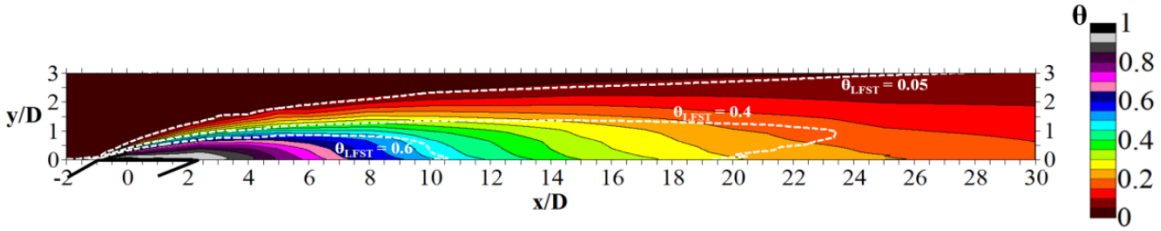

Figure 2.7: *Thermal field contour, z/D = 0, M = 3, T_u = 13.2%, with the white dashed lines the low free-stream turbulence case is denoted [21].*

In [21] thermal field measurements were performed in low and high free-stream turbulence intensity values (T_u = 0.5% and T_u = 13.2%). Thermal field contour were presented for two values of blowing ratio (M = 1.5% and M = 3%) and additional thermal, velocity and turbulent stress profiles. One of the main observations was the increased dilution and dispersion of the coolant jet in elevated turbulence, mainly in the lateral direction and especially further downstream of the hole's exit. The effect in the vertical (defined by the normal to the flat plate) direction was less pronounced. This preferential lateral dispersion was attributed

to the turbulent shear stresses. While elevated free-stream turbulence imposed fluctuations of the same order in every direction, turbulent eddies in the region where the coolant was mainly concentrated were directed laterally to the wall. Finally, it was exhibited that in the high free-stream turbulence case there was an absence of the jet's delayed lift-off which was correlated with the strong dilution of the coolant.

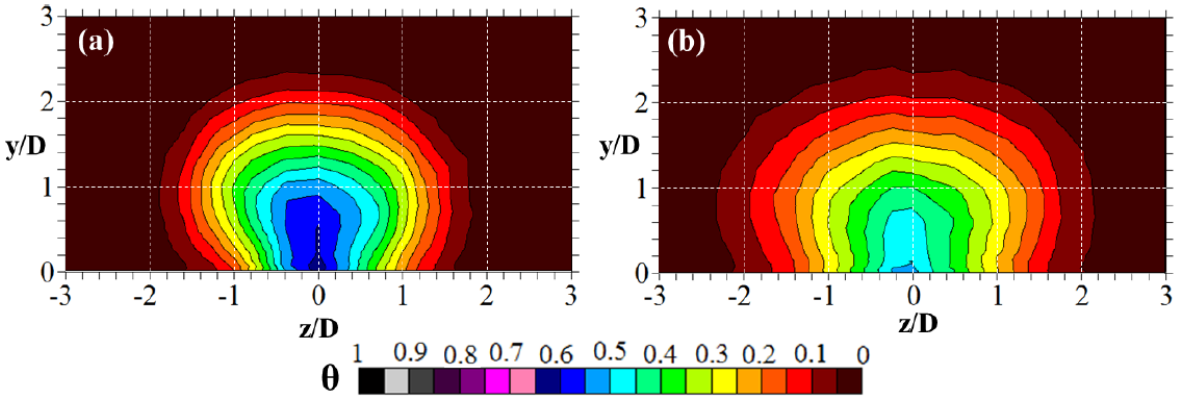

Figure 2.8: *Thermal field contours in the crossplane $x/D = 10$, $M = 3$ for (a) $T_u = 0.5\%$ and (b) $T_u = 13.2\%$ [21].*

Finally, with [20] and [22], additional studies were carried out in order for the community to have a complete view over the PSH's performance. In [20] the effect of blockage on the adiabatic effectiveness of shaped and cylindrical holes was examined through a study that exhibited the superiority of the shaping in terms of cooling performance. In [22] different levels of roughness inside the shaped hole were tested for the cooling performance to be characterized under more realistic (engine-like) conditions, as the effect of roughness can be rather pronounced.

The above reviewed literature was followed by the work of the *Department of Mechanical Engineering* at the *University of Texas at Austin*. In [23] and [24] "7-7-7 shaped holes" configurations were studied for different metering sections. The effect of the free-stream conditions and the substitution of the plenum with a cross-flow channel were thoroughly studied. Additional papers ([25] and [26]) studying this specific design also evince the need for the existence of one baseline shaped hole for the scientific community to share.

2.6. Summing Up

The literature reviewed in this chapter was carefully chosen to be presented here as it gives the reader a quite dense (even if not exhaustive) overview over the technical studies on the film cooling over many years. In the following table (2.2) the papers included in this section are presented.

Ref.	Title	Type of Study	Year
[6]	*"Effects of Hole Geometry and Density on Three-Dimensional Film Cooling"*	Experimental	1974
[10]	*"Hydrodynamic Measurements of Jets in Crossflow for Gas Turbine Film Cooling Applications"*	Experimental	1989
[12]	*"Effects of a Crossflow at the Entrance of a Film Cooling Hole"*	Experimental	1997
[14]	*"A CFD Investigation on the Effect of Entrance Crossflow Directions to Film-Cooling Holes"*	Numerical	1997
[12]	*"Flowfield Measurements for Film-Sooling Holes with Expanded Exits"*	Experimental	1998
[9]	*"Free-stream Turbulence Effects on Film Cooling with Shaped Holes"*	Experimental	2003
[15]	*"Large Eddy Simulation of Film Cooling Flow From an Inclined Cylindrical Jet"*	Numerical	2003
[13]	*"Effect of Hole Geometry on the Thermal Performance of Fan-Shaped Film Cooling Holes"*	Experimental	2005
[16]	*"Numerical Investigation of Film Cooling Fluid Flow and Heat Transfer Using Large Eddy Simulations"*	Numerical May	2009
[7]	*"Effect of Geometry Variations on the Cooling Performance of Fan-Shaped Cooling Holes"*	Experimental	2012
[8]	*"Free-Stream Effects on the Cooling Performance of Cylindrical and Fan-Shaped Cooling Holes"*	Experimental	2012
[17]	*"Large Eddy Simulation of Inclined Jet in Cross Flow with Cylindrical and Fan-Shaped Holes"*	Numerical	2016
[18]	*"Adiabatic Effectiveness Measurements for a Baseline Shaped Film Cooling Hole"*	Experimental (PSH)	2014
[19]	*"Effect of High Freestream Turbulence on Flowfields of Shaped film Cooling Holes"*	Experimental (PSH)	2015
[20]	*"Blockage Effects from Simulated Thermal Barrier Coatings for Cylindrical and Shaped Cooling Holes"*	Experimental (PSH)	2015
[21]	*"Thermal Field Measurements for a Shaped Hole at Low and High Turbulence Intensity"*	Experimental (PSH)	2016
[22]	*"Effect of In-Hole Roughness on Film Cooling from a Shaped Hole"*	Experimental (PSH)	2016
[25]	*"The Effect of a meter-Diffuser Offset on Shaped Film Cooling Hole adiabatic Effectiveness"*	Experimental ("7-7-7")	2016
[26]	*"Dependence of Film Cooling Effectiveness on 3D printed Holes"*	Experimental ("7-7-7")	2016

Table 2.2: *Summary of the literature review.*

3. Flow Field Characteristics

As noted in the previous chapter, there are various flow field structures governing the film-cooling flow. These features have a great impact on the cooling performance as they are directly associated with the behavior of the flow and the thermal field. The basic configuration consists of a jet ejected in a cross-flow under one angle. Under another scope, two flows with different momentum and each with its own boundary layer interact with each other leading to a complicated resulting flow-field. As a matter of fact, in the film-cooling flows finds application the year-long research on the "jet in a cross-flow" subject which counts numerous publications.

3.1. Jet in a Cross flow

It was Fric and Roshko [28] one of the first to identify and categorize the various features present when a transverse jet exits in a cross-flow (their depiction was presented in a previous chapter in figure 2.3). They experimentally studied the different flow structures for various values of the blowing ratio and the Reynolds number which appeared to play a significant role in the resulting flow-field. Their work mainly involved the study of the wake vortices which were proven to be generated due to the realignment of the vorticity in the boundary layer of the mainstream, consisting this type of flow fundamentally different from the flow around a cylinder clamped on a flat plate. In the film cooling applications with shaped holes those wake vortices are not however of great interest as the coolant jet is not supposed to lift-off the surface that much. The main structure of interest is the *Counter Rotating Vortex pair* (CRVP) the generation of which, up to now is not fully understood.

In the work of Andreopoulos and Rodi [27] one can find a description on the generation of the CRVP, the main feature of interest that effectively drives the film cooling flows. To their understanding, based on the work of *Moussa et al.*[3] and *Foss*[4], the stream-wise vorticity associated with the CRVP is the product of two mechanisms in the flow. The first one has to do with the reorientation of the existing vorticity in the boundary layer of the pipe flow resulting in longitudinal vortices. The second one is associated with the generation of vorticity at the interface of the jet with the cross-flow. This "new" vorticity results from the velocity gradient at the interface and forms a vortex sheet around the jet which can be thought to roll up and bent over into the longitudinal direction.

In the same context, *Kelso et al.* [29] performed various wind tunnel and water channel experiments for varying Reynolds and velocity ratios, utilizing flow visualization techniques that aimed to assist in the description of the flow field resulting from a round jet/cross-flow interaction. Their interpretation of the CRVP formation process was quite similar to the one proposed by Andreopoulos and Rodi. They suggested that the vorticity in the shear layer of the interface (quite like the one of a free jet) gets reoriented in a way that *"leads to (or contributes to) the formation of the CVP"* [29]. They associated the initiation of the CRVP with the roll up of the shear layer just above the hole (namely the hovering vortex, visualized as a

[3] *"The near field in the mixing of a round jet with a cross stream"*, Rep. SFB 80/E/161, Univ. Karlsruhe, 1977.
[4] *"Interaction region phenomena for the jet in a cross-flow problem"*, J. of Fluid Mech., Vol. 80, pp. 49-80, 1980.

Kelvin-Helmholtz like instability) and the separation inside the pipe. The main mechanism and their interpretation of the vorticity realignment can be seen in figure 3.1.

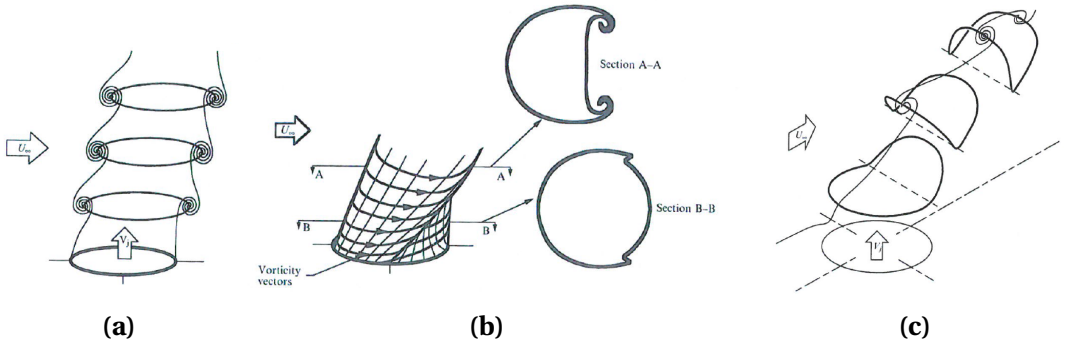

Figure 3.1: *Interpretation of CRVP formation by Kelso et al.. The main mechanism (c) is a combination of the ones shown in (a) and (b) [29].*

3.1.1. Flow Field Structures

Ajersch et al. [30] performed experimental and numerical studies on a row of multiple square jets in a cross-flow. They mainly focused on characterizing the turbulence and on the prediction of the "wake" region of the jet. It was the work of Haven and Kurosaka [31] however that drew a connecting line between the shape of the jet's outlet and the vortical structures observed downstream of the ejection and relatively close to the exit of the jet (near field). According to their interpretation, vorticity generated inside the hole and due to the side walls undergoes twisting and turning while interacting with the mainstream resulting in vorticity realigned with the cross-flow (i.e. CRVP). Having tested various exit hole geometries, they observed multi-decked structures at the curved jet. The way these structures rotated and induced force on the jet seemed to depend on the shape and more importantly on the aspect ratio of the hole's exit (in regards to what the cross-flow was facing).

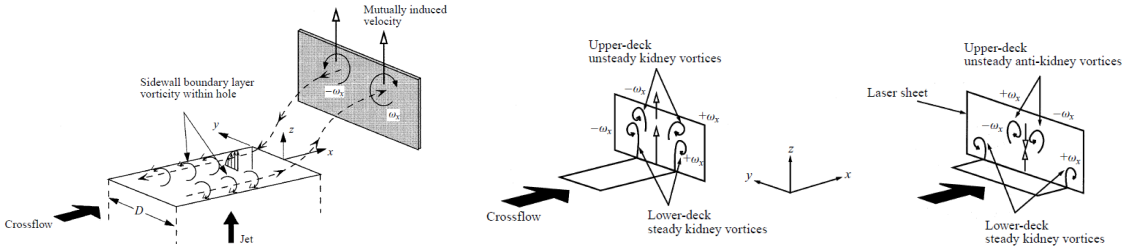

Figure 3.2: *(a) CRVP due to side wall vorticity and (b) double-decked structures [31].*

According to Haven and Kurosaka, the additional vorticity generated in the windward and leeward walls of the jet's tube gets warped as well creating an upper deck structure. This can have the same sense of rotation as the lower one (namely the kidney vortices - a name really common in literature for the CRVP due to the shape of the flow field under their influence) or opposite to that. They visualized the vorticity generated inside the hole as a vortex sheet emanating from the hole and proposed that the rotation of the upper deck structure

depended on the aspect ratio of the hole's exit as it defined the type of warping this sheet would go through (concave or convex).

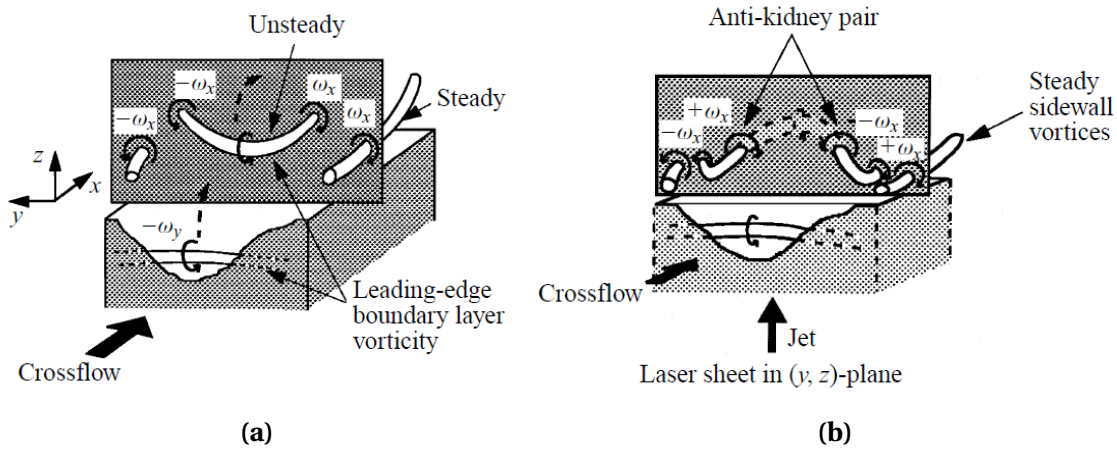

Figure 3.3: *Interpretation of (a) convex and (b) concave warping of the vorticity emanating in the cross-flow resulting in the respective unsteady pair of vortices [31].*

When the upper deck vortices were rotating opposite to the ones of the lower deck they produced an effect opposing to that of the CRVP. Due to that, they named the structures *anti-kidney vortex pair* and they observed that contrary to the steady kidney vortices, these ones were unsteady in nature. Their interpretation was consistent with the experimental visualizations they gathered. They concluded that as the shape of the exit defines the structures of the flow field, the proper shaping can aid in the control of the jet ejected as the detrimental effects of the CRVP on the film-cooling could be contained when anti-kidney vortices were present. Indeed, in their study [32] they exhibited how anti-kidney vortices generated in shaped holes can retain the jet lift of and aid in better lateral spreading of the jet (aside from the mechanisms already discussed), two effects that are significant in the context of film cooling.

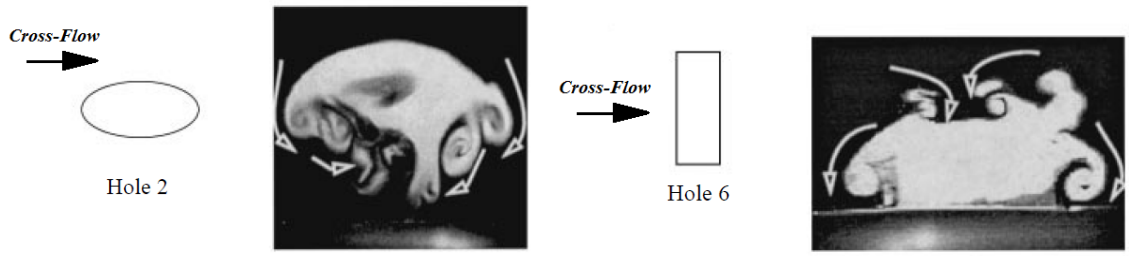

Figure 3.4: *Laser induced fluorescence (LIF) images on the downstream edge of (a) an elliptical (b) a rectangular hole [31].*

The work of Haven and Kurosaka was followed by [34] were the same idea around the warping of vorticity was supported. Elliptic jets with high and low aspect ratio were studied and

multi-decked structures were experimentally observed. They proposed a more complex model according to which the unsteady kidney and/or anti-kidney structures were formed. The common ground in all of those interpretations however, is that the vortices observed in the flow field result from the vorticity generated on the solid walls. However, in studies conducted in [33] it was shown that in fact there is no need for a boundary layer inside the hole to exist in order for the CRVP to develop. Performing CFD simulations of an inclined hole they isolated the jet-mainstream interaction by using slip walls. Indeed, the CVRP did not cease to exist and the vorticity in the hole region was shown to correlate with the velocity gradients in the jet-mainstream interface.

These observations were validated by complimentary studies performed during this project were transverse jet emanating from slip wall tubes were simulated and shown to present a CRVP as well. According to the author, this could also be a result of the strong curvature that the jet undergoes. A similar type of secondary flow has been shown to exist in curved pipes as well [35]. In that study, the secondary flow was a result of the vorticity generated only due to curvature, having singled-out completely the viscous effects of the walls. It could be possible that the jet undergoing strong turning and bounded as it is by the mainstream, could also present a similar secondary flow (i.e. the CRVP) due to the same reason. This mechanism could also contribute to the generation of the CRVP.

3.2. Wall Bounded Jet

In the case of the shaped holes however, and generally in film cooling flows regardless the type of the hole, the coolant is ejected at an angle. As a result, the path that the jet follows is close to the wall (quite less curved) and gets strongly effected by its existence. The descriptions/models of the mechanisms governing the coherent structures of jets discharging over a solid wall could be more relevant to the film-cooling application compared to the ones proposed in studies of the unbounded jet flows.

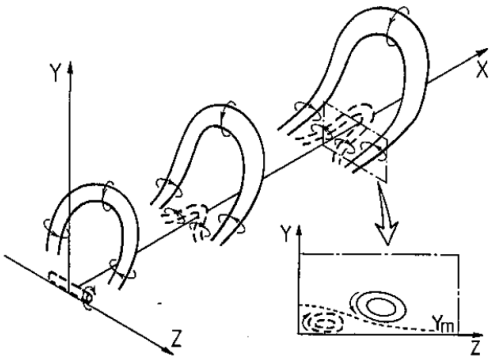

Figure 3.5: *Conceptual model of coherent structures [36].*

In [36] the 3D jet ejected over a solid wall was studied. They were focused in collecting data regarding the velocity variations in the mixing layer in order to define the formation mechanism of the longitudinal (in the direction of the jet) pair of vortices that had been observed in previous studies. They conceptualized a model based on a horseshoe-like structure quasi-periodically shed in the domain from the jet/mainstream interaction. They visualized the longitudinal vortices as a manifestation of this structure whose "legs" bend in a way that promotes lateral spreading and mixing of the jet with the mainstream (quite like the CRVP).

3.3. LES on Inclined Holes

Finally, *Sakai et al.* performed an LES simulation of an inclined round jet issuing into a cross-flow [37]. In their study the performed a systematic investigation to identify the ori-

gins of the CRVP. They observed that even though the averaged vortical structures seemed to be quite similar in all the blowing ratios tested (identified by stream-wise vorticity), the instantaneous vortical structures differed. In low blowing ratio, the CRVP was observed to originate from the hairpin vortices, the same coherent structure that was also identified in [15] and was associated with the CRVP. In higher values of M however, hanging and rear vortices contributed in the formation of the pair and more importantly seemed to improve the adiabatic effectiveness of the jet as (in the case of the cylindrical jet) it helped the coolant reattach to the surface. It is worth noting here that this relation between the blowing ratio values and the nature of the vortical structures had also been made many years earlier by Andreopoulos and Rodi [27] for the case of the transverse cylindrical jet in a cross-flow.

As it has already been noted, in the case of shaped holes there are way more, smaller scale intermittent vortices [17] that in the same way can contribute in the formation of the CRVP or even counter it as Haven and Kurosaka have already established. Finally, it is the impact of the instantaneous field on the film-cooling flows one of the main points that justify once again the use of the LES approach to simulate this type of flow.

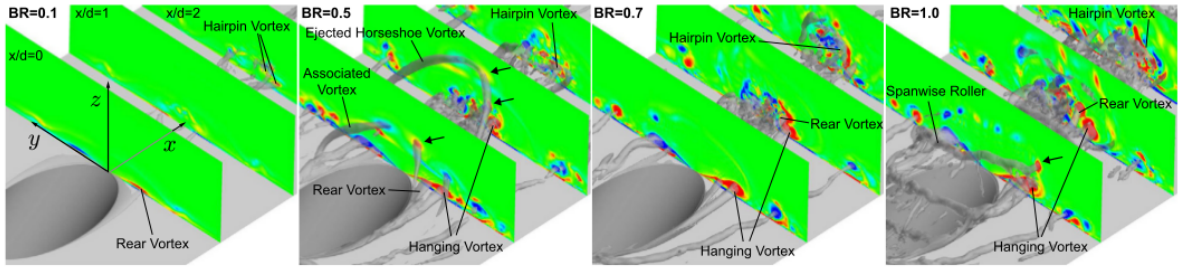

(a) Instantaneous view

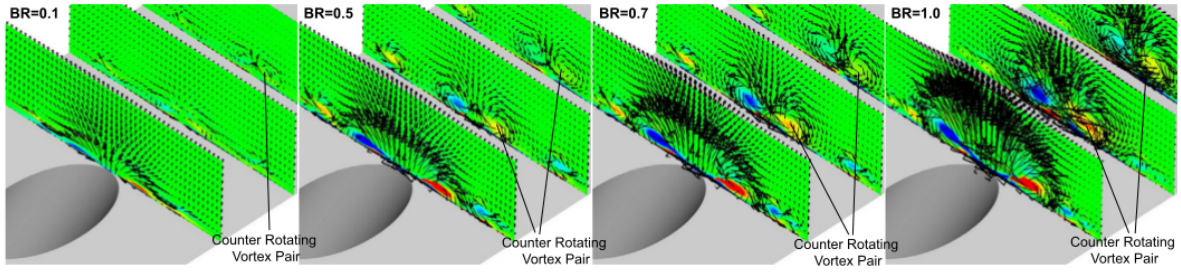

(b) Time averaged view

Figure 3.6: *Origins of CRVP studied by [37]. Positive ω_x vorticity in red/light color.*

This chapter went through many studies dealing with the origins and the description of the flow field structures developed when a jet get ejected in a cross-flow. Over the years, this domain has been the focus of much research. Everything cited up to now will aid in the understanding and analysis of the results obtained from the simulations.

4. Large Eddy Simulation

Large Eddy Simulation (LES) is a higher fidelity approach compared to the Reynolds Averaged Navier-Stokes (RANS) methodology, dedicated to the solution of the Navier-Stokes (NS) equations. In terms of computational expenses, LES lies between the RANS modeling and the Direct Numerical Simulation (DNS) approach, emerging explicitly by the limitations that these approaches come across [38]. Not unlike RANS modeling, the LES approach aims to provide a new set of equations that try to mimic the turbulent characteristics of the flow [39]. However, the two approaches are conceptually very different.

As the DNS deals with the solution of the turbulent spectrum on its whole with a complete lack of modeling for the turbulent scales, the computational cost increases significantly (as the cube of the Reynolds number [38]) making this approach inapplicable to most industrial applications at this point. In RANS, a new set of equations is derived from the Navier-Stokes equation by averaging temporally over a set of realizations [38]. The unclosed terms are representative of the physics governing the flow and covering the whole spectrum of frequencies present in this ensemble of realizations. With proper modeling, the closed set of derived equations can be solved and provide statistical information on turbulence.

However, in LES, the large-scale dynamics of the flow are explicitly solved whilst only the influence of the smaller-scale dynamics remain to be modeled. Thus, the computational cost is significantly reduced compared to the DNS and at the same time the approach remains more universal when compared to the RANS one, by maintaining the transient nature of the phenomena through the contribution of the large scale dynamics. The new set of equations is derived by applying a time independent spatially localized filter of a given size [39] and the unclosed terms resulting from this operation are only associated with the smaller scales (high frequencies in the spectrum) of the flow. With proper modeling of those terms (subgrid-scale or SGS models) the solution of the closed set of derived equation provides an estimation of one realization of the (turbulent) flow.

4.1. About AVBP

AVBP is a modern software tool for Computational Fluid Dynamics (CFD) based on the LES approach. It is a massively parallel code that solves the compressible Navier-Stokes equations for both laminar and turbulent problems. Developed for both two and three dimensional problems aims to provide an accurate flow prediction on unstructured and hybrid meshes, for highly complex geometries, utilizing high order schemes. Its development started in 1993 upon an initiative of Michael Rudgyard and Thilo Schönfeld[5]. Although originally designed for non-reactive, steady state flows for external aerodynamics, its main application nowadays is the modeling of reactive flows for internal configurations (e.g. combustion). AVBP represents one of the most advanced CFD tools worldwide used by multiple laboratories and companies for basic and applied research of industrial interest.

AVBP was originally written in standard FORTRAN 77 and later on gradually upgraded with FORTRAN 90 compilers being available [39]. The key feature of AVBP is the flexibility it pro-

[5] http://www.cerfacs.fr/avbp7x/ (restricted access)

vides in the handling of unstructured and hybrid grids with different cell types. This was motivated by the efficiency regarding the grid generation, mesh adaptation as well as the increased accuracy of the computational results (compared to codes that are not build to explicitly handle hybrid grids). For the handling of such grids specific numerical methods and discretization schemes are implemented in combination with appropriate artificial viscosity models. It was used for this project and what follows is a brief reference on the equation, models and schemes solved and implemented in AVBP.

4.2. Basic Notion on Filters

Let us define a low pass filter (which will be associated to a cut-off length for the separation of the scales) applied to a spatial and temporal field $\phi(\mathbf{x}, t)$. The filtered field can be defined as:

$$\bar{\phi}(\mathbf{x}, t) = \int\int_{-\infty}^{+\infty} \phi(\mathbf{x}', t')\mathbf{G}(\mathbf{x}-\mathbf{x}', t-t')d^3\mathbf{x}'dt' \tag{4.1}$$

where $\mathbf{G}$ is a kernel. The convolution with a kernel in a physical space $\mathbf{G}$ also writes:

$$\bar{\phi} = \mathbf{G} \star \phi \tag{4.2}$$

As a result of the filtering, the field ϕ is split up into two portions as:

$$\phi = \bar{\phi} + \phi' \tag{4.3}$$

where ϕ' represents the unresolved (rejected) part of the field corresponding to the higher (sub-filtered) frequencies and also writes:

$$\phi' = (1-\mathbf{G}) \star \phi \tag{4.4}$$

And in the Fourier space $\hat{\mathbf{G}}$:

$$\hat{\phi}' = (1-\hat{\mathbf{G}})\hat{\phi} \tag{4.5}$$

For variable density problems (i.e. the compressible NS) a density-weighted Favre filtering can be introduced [39] to avoid modeling additional sub-filtered scales, defined for an arbitrary quantity ϕ as:

$$\bar{\rho}\tilde{\phi} = \overline{\rho\phi} \tag{4.6}$$

where the quantity ϕ is decomposed into a low ($\tilde{\phi}$) and a high (ϕ'') frequency part as follows:

$$\phi = \tilde{\phi} + \phi'' \tag{4.7}$$

The following relations can be established [40]:

$$\overline{\rho\phi''} = 0 \tag{4.8}$$

$$\bar{\phi} - \tilde{\phi} = -\frac{\overline{\rho'\phi'}}{\bar{\rho}} = -\frac{\overline{\rho'\phi''}}{\bar{\rho}} \tag{4.9}$$

4.3. Governing Equations for LES

By filtering the instantaneous governing equations for the compressible, non reactive flow [39], the conservation of mass (here for multiple species for completeness) writes:

$$\frac{\partial \bar{\rho}\tilde{Y}_k}{\partial t} + \frac{\partial \bar{\rho}\tilde{Y}_k \tilde{u}_j}{\partial x_j} = -\frac{\partial}{\partial x_j}[\bar{J}_{j,k} + \bar{J}^t_{j,k}] + \bar{\dot{\omega}}_k \tag{4.10}$$

keeping the Einstein notation (the repeated index implies summation over this index). The k index refers to the number of species and does not follow the summation rule. The $\bar{\dot{\omega}}_k$ term corresponds to the filtered source terms. In the same manner, applying the Favre filtering in the momentum equation gives [39] [40]:

$$\frac{\partial \bar{\rho}\tilde{u}_i}{\partial t} + \frac{\partial \bar{\rho}\tilde{u}_i \tilde{u}_j}{\partial x_j} = -\frac{\partial}{\partial x_j}[\bar{P}\delta_{ij} - \bar{\tau}_{ij} - \bar{\tau}^t_{ij}] \tag{4.11}$$

While the total energy equation writes:

$$\frac{\partial \bar{\rho}\tilde{E}}{\partial t} + \frac{\partial (\bar{\rho}\tilde{E}\tilde{u}_j)}{\partial x_j} = -\frac{\partial}{\partial x_j}[\overline{u_i(P\delta_{ij} - \tau_{ij})} + \bar{q}_j + \bar{q}^t_j] + \bar{S} \tag{4.12}$$

where $\bar{S}$ represents the filtered source terms. In the above written equations it is convenient to separate the flux tensor into three components [39]:

Inviscid terms

$$\begin{pmatrix} \bar{\rho}_k \tilde{u}_j \\ \bar{\rho}_k \tilde{u}_i \tilde{u}_j + \bar{P}\delta_{ij} \\ \bar{\rho}_k \tilde{E}\tilde{u}_j + \overline{Pu_j}\delta_{ij} \end{pmatrix}$$

Viscous terms

$$\begin{pmatrix} \bar{J}_{j,k} \\ -\overline{\tau}_{ij} \\ -\overline{(u_i \tau_{ij})} + \bar{q}_j \end{pmatrix}$$

Subgrid scale turbulent terms

$$\begin{pmatrix} \bar{J}^t_{j,k} \\ -\overline{\tau}^t_{ij} \\ \bar{q}^t_j \end{pmatrix}$$

which are the unclosed quantities (the product of filtering) that need to be modeled. In non reactive flows (as the one in subject in this thesis) the laminar filtered stress tensor is given [41]:

$$\bar{\tau}_{ij} = \overline{2\mu(S_{ij} - \frac{1}{3}\delta_{ij}S_{ll})} \approx 2\bar{\mu}(\tilde{S}_{ij} - \frac{1}{3}\delta_{ij}\tilde{S}_{ll}) \tag{4.13}$$

where:

$$\tilde{S}_{ij} = \frac{1}{2}\left(\frac{\partial \tilde{u}_j}{\partial x_i} + \frac{\partial \tilde{u}_i}{\partial x_j}\right)$$

The diffusive species flux writes:

$$\bar{J}_{i,k} = -\overline{\rho\left(D_k \frac{W_k}{W}\frac{\partial X_k}{\partial x_i} - Y_k V_i^c\right)} \approx -\bar{\rho}\left(\tilde{D}_k \frac{W_k}{W}\frac{\partial \tilde{X}_k}{\partial x_i} - \tilde{Y}_k \tilde{V}_i^c\right) \tag{4.14}$$

assuming negligible the effect of higher order correlations [39]. The variable W represents the mean molecular weight of the mixture, D_k is the diffusion coefficients matrix for each species and V_i^c the corrected diffusion velocity [41]. The filtered heat flux [41]:

$$\bar{q}_i = -\overline{\lambda \frac{\partial T}{\partial x_i}} + \sum_{k=1}^{N} \overline{J_{i,k} h_{s,k}} \approx -\bar{\lambda}\frac{\partial \tilde{T}}{\partial x_i} + \sum_{k=1}^{N} \bar{J}_{i,k}\tilde{h}_{s,k} \tag{4.15}$$

for N number of species and assuming that the spatial variations of molecular diffusion fluxes are negligible [39].

4.3.1. Sub-Grid Scale Model [39]

The basic hypothesis explicitly written in [40] goes: *"If subgrid scales exist, then the flow is locally (in space and time) turbulent"*. As a result, the subgrid scale (SGS from now on) models should be built based on the understanding of the turbulent properties in a consistent way, in order to provide a closure to the problem. Indeed, as it will be exhibited later on, the way to proceed in modeling the influence of the SGS on the resolved motion is to assume that its effect is purely dissipative, something that derives from the cascade theory of turbulence.

Let us start by expanding the SGS turbulent flux terms. The Reynolds tensor writes:

$$\bar{\tau}_{ij}^t = -\bar{\rho}(\widetilde{u_i u_j} - \tilde{u}_i \tilde{u}_j) \approx 2\bar{\rho}\nu_t(\tilde{S}_{ij} - \frac{1}{3}\delta_{ij}\tilde{S}_{ll}) \tag{4.16}$$

The SGS diffusive species flux vector:

$$\bar{J}_{i,k}^t = \bar{\rho}(\widetilde{u_i Y_k} - \tilde{u}_i \tilde{Y}_k) \approx -\bar{\rho}\left(D_k^t \frac{W_k}{W}\frac{\partial \tilde{X}_k}{\partial x_i} - \tilde{Y}_k \tilde{V}_i^{c,t}\right)) \tag{4.17}$$

where:

$$D_k^t = \frac{\nu_t}{S_{c,k}^t}, \quad S_{c,k}^t = 0.6 \text{ the turbulent Schmidt number, fixed in AVBP.}$$

Finally, the SGS heat flux writes:

$$\bar{q}_i^t = -\bar{\rho}(\widetilde{u_i E} - \tilde{u}_i \tilde{E}) \approx -\lambda_t \frac{\partial \tilde{T}}{\partial x_i} + \sum_{k=1}^{N} \bar{J}_{i,k}^t \tilde{h}_{s,k} \tag{4.18}$$

where:

$$\lambda_t = \frac{\mu_t \overline{C_p}}{P_r^t}, \quad P_r^t \text{ the turbulent Prandtl number, fixed in AVBP usually at 0.6.}$$

It is evident at this point that a closure of the problem could be given with the modeling of the ν_t, a term that corresponds directly to the turbulent viscosity defined in the RANS approach as well. By introducing the turbulent viscosity, the influence of the SGS on the filtered motion is taken into account.

In AVBP various models for this terms are implemented (some of them recursive), however only the Wall Adapting Linear Eddy (WALE) model is going to be presented here. The WALE model was developed for wall bounded flows (justifying its usage in the present project) in an attempt to recover the scaling laws of the wall [39]. Additionally, this model avoids adding any turbulent viscosity where just a pure shear layer exists. With WALE, the effect of the turbulent viscosity tends to diminish close to the walls mimicking correctly the physics of the turbulent flow. The expression for ν_t is given:

$$\nu_t = (C_w \Delta)^2 \frac{(s^d_{ij} s^d_{ij})^{3/2}}{(\tilde{S}_{ij}\tilde{S}_{ij})^{5/2} + (s^d_{ij} s^d_{ij})^{5/4}} \tag{4.19}$$

with:

$$s^d_{ij} = \frac{1}{2}(\tilde{g}^2_{ij} + \tilde{g}^2_{ji}) - \frac{1}{3}\tilde{g}^2_{kk}\delta_{ij}$$

where $\Delta = V^{1/3}_{node}$ denotes the characteristic filter length with V_{node} being the local node volume, C_w is the model constant set equal to 0.5 and $\tilde{g}_{ij}$ is the resolved velocity gradient. In this type of LES model, variation of the filter size (non uniform mesh) is only accounted for through the change of the local cell volume. Locality is lost and only global quantities are maintained [39].

4.4. Boundary Conditions

The boundary conditions (BC from now on) are of critical essence in every CFD application. In AVBP, like in most CFD codes, a special notice has been taken in the correct implementation and treatment of the BC.This necessity comes mainly from the fact that the high order-low dissipation schemes used, mandatory for an accurate LES, are not able to efficiently/effectively dissipate the (sometimes) excessive production of acoustic waves (inherently present in the governing equations) that can lead to the divergence of a simulation. Additionally, numerical perturbations in the form of wiggled waves are always present in computations and the lack of sufficient artificial viscosity (typical for LES) creates a critical issue in the accuracy of the code.

The BC work in theory impose the desired values in the cells close to the border ($\partial\Omega$) of the computational domain (Ω). If no BC were present, the computed solution would only be driven by the initial solution imposed at the domain and the numerical schemes. One key feature of AVBP is the usage of the so called *characteristic BC* [44], a treatment that decomposes the imposed information in waves in order to enable the handling of the undesired waves (in the sense of permitting them to leave the computational domain with a control on their reflection on the boundaries). It is based on the theory of characteristics for the Navier-Stokes equations (NSCBC) and even though non-characteristic BC are also imple-

mented in AVBP, in this project only the former were used.

This type of BC allows the code to inject and eject turbulence, undesired wiggled waves, manipulate acoustic waves and conserve some mean values around a target value. A specific reference on the turbulence injection technique implemented in AVBP is made in the appendices A.1. A description of the theoretical approach and the principal of the NSCBC method as well as the implementation in the code is far outside the scope of this thesis. The reader is welcome to find more information on this in the corresponding literature ([42], [43], [44], [41], [45], [46]).

4.5. NUMERICS FOR LES

Since in this chapter much reference on AVBP have been made, a discussion about numerics is not out of context. On the contrary, as AVBP handles hybrid (multi-element) grids and complex geometries and as LES is a high fidelity method, a brief overview of the discretization schemes used was required [6].

The LES codes in general handle various physical phenomena, having different time and space scales. Besides the computational intensity of the method for realistic geometries (that require robustness, efficiency in terms of algorithm and parallelization techniques) it is of essence for the code to be able to accurately predict (within reasonable computational cost) the unsteady evolution of these phenomena, which in the context of LES can be elaborate. High order, low dissipation schemes are used, with the proper handling so that the inherent numerical issues (typically of dispersive and dissipative nature) are also treated.

The governing sets of (NS) equations without source terms can be written:

$$\frac{\partial \mathbf{u}}{\partial t} + \nabla \cdot \mathbf{F} = 0 \tag{4.20}$$

where $\mathbf{u} \in R^m$ is the vector of conserved variables and $\mathbf{F}$ the corresponding flux tensor. The fluxes can then be split into two parts, one inviscid convective (indicated by i) and one viscous part (indicated by v):

$$\mathbf{F} = \mathbf{F}_i(\mathbf{u}) + \mathbf{F}_v(\mathbf{u}, \nabla \mathbf{u})$$

AVBP's formulation is based on a *Cell-Vertex (CV) Finite Volume (FV)* method [50]. This formulation belongs in a greater class of schemes know as *Residual Distribution (RD) schemes* [39] and conceptually they could be roughly placed in between the finite volume and the finite element approaches. In principle, with the CV method the conservation laws are applied in the cells of the mesh while the variables are stored at the nodes of each cell.

[6] Parts of what follows is taken from a collection of notes gathered during training sessions on LES at CERFACS

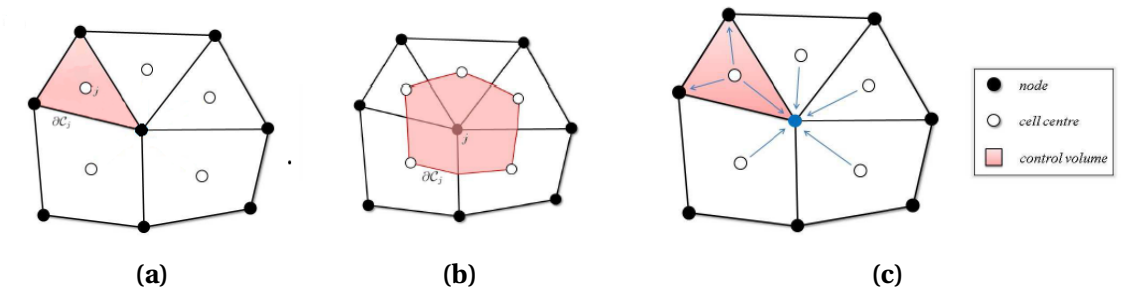

Figure 4.1: *The classic (a) cell-centered FV approach and (b) vertex-centered FV approach compared to the (c) cell-vertex approach [39].*

The idea of the method is described in what follows [39]. The cell residuals (fluctuations) are calculated for each control volume:

$$r_e := \frac{1}{V_C}\int_C \nabla \cdot \mathbf{F}_h dV = \frac{1}{V_C}\oint_{\partial C} \mathbf{F}_h \cdot \mathbf{n} ds = 0 \tag{4.21}$$

where $\mathbf{F}_h$ is a numerical approximation of the fluxes and V_c the control volume. Fractions of the cell residual are then distributed to the respective nodes. The solution must advance in time and the time derivative (equation 4.20) is integrated over the control volume:

$$\int_{C_j} \frac{d\mathbf{u}}{dt} dV \approx \frac{d\mathbf{u}_j}{dt} V_{C_j} \tag{4.22}$$

and the semi-discrete approximation of 4.20 is:

$$\frac{d\mathbf{u}_j}{dt} = -\mathbf{r}_j \tag{4.23}$$

The *Lax-Wendroff* (LW) scheme is implemented in AVBP for the discretization of the convective fluxes. This method is based on adding a second (diffusive) derivative as a streamwise stabilization term. It involves a on-step time marching method [39]. This method is efficient and is not associated with great computational cost. However, the resulting dispersion error is generally increased leading to loss in accuracy. For this, the *Taylor-Galerkin* (TG) convection schemes are also implemented in AVBP. The TG schemes are the generalization of the LW schemes in the frame of the Galerkin finite element method [39]. Many TG schemes have been added in a continuous try to reduce numerical dissipation and dispersion, increase accuracy and correctly preserve the physical properties of the flow in the context of LES. For this thesis, the *Two-Step Taylor-Galerkin 4A* (TTG4A) and the *Two-Step Taylor-Galerkin* (TTGC) schemes were used. The reader is welcome to find more on these in [51].

In AVBP, the solution advances in time explicitly, either with a single or a multi-step sequence. The time advance is incorporated in the schemes of the convective fluxes, in the case of the LW and the TG schemes. The discretized equations used are conditionally stable. As a result, the appropriate time step should be chosen at each numerical iteration for the instabilities to be avoided. In order for the stability to be ensured, the time step is chosen as the minimum between the one derived from the desired CFL (for the convection schemes)

and Fourier (for the diffusion schemes) numbers [39]. If sources are also involved, their respective limitations imposed on the time step should also be taken into account.

Two different schemes for the discretization of the diffusive fluxes are implemented in AVBP. The first one used a 4Δ operator (stencil) which is a typical CV scheme that equally distributes the residuals from the calculated viscous fluxes to the cell nodes [39]. This scheme uses a large stencil that involves a lot of nodes. The second one is a 2Δ operator, a vertex-centered scheme that involves a smaller amount of nodes and also has the ability to dissipate 2Δ wiggles that appear and are often responsible for non-linear instabilities [39]. From those two operators only the latter is used (i.e. the 2Δ operator) due to its improved numerical behavior compared to the former, as described above. The reader is welcome to find more on these in [52].

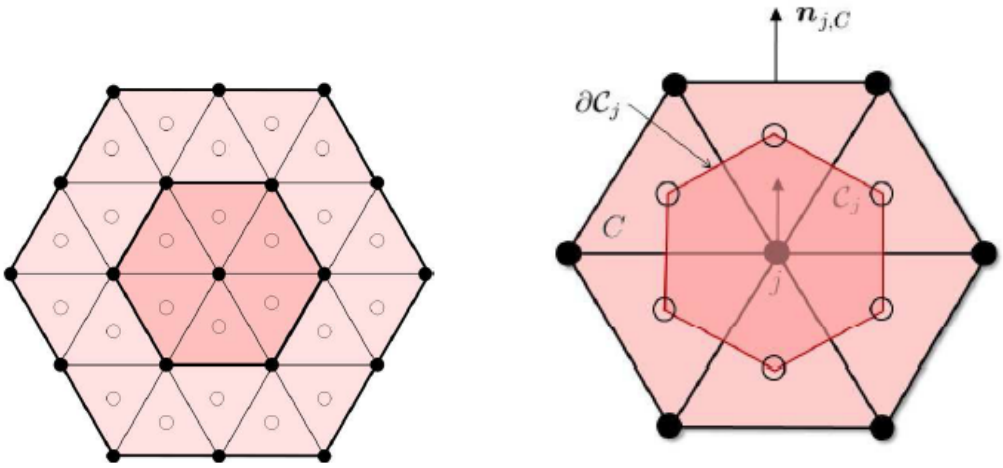

(a) **(b)**

Figure 4.2: *The operators implemented in AVBP for the viscous fluxes discretization, the (a)* 4Δ *and the (b)* 2Δ *stencil [39].*

5. Results & Discussion

In this chapter the validation of AVBP in the film cooling flow with the "7-7-7" laid-back fan shaped hole is carried out. A few cases were tested and the results are presented in the following sections along with the respective experimental ones. For this, a specific geometry and a mesh were developed to represent as faithfully as possible the configuration tested by [2]. The test bench included five holes bringing cold fluid in the mainstream generated by a wind tunnel. The coolant film was formed above a flat surface of a low conductivity material, suitable for adiabatic effectiveness measurements. The coolant flow was supplied by a plenum. A schematic of the test configuration can be seen in figure 5.1.

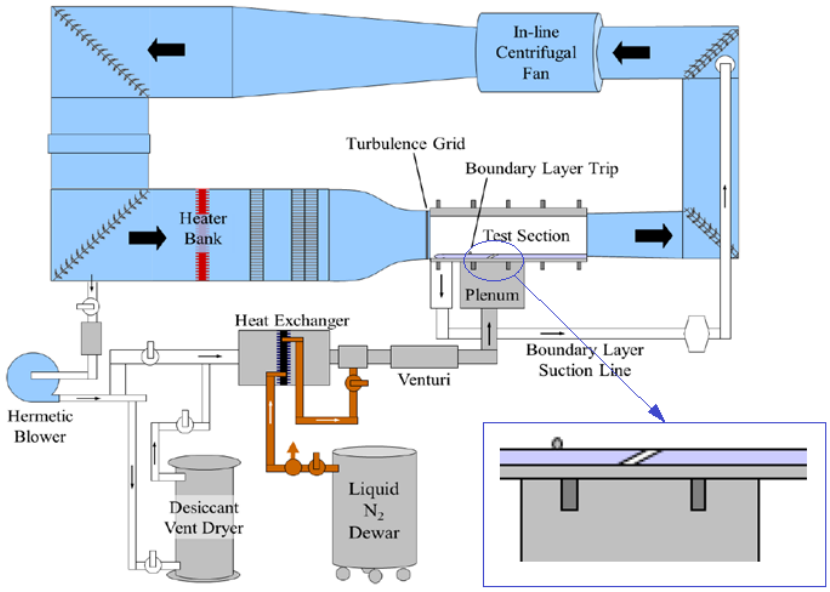

Figure 5.1: *Schematic of the wind tunnel used for film cooling measurements by Schroeder [2].*

5.1. Description of the Problem

As in every CFD problem, a computational domain had to be created. The geometry constructed for this purpose can be seen in figure 5.2. It comprises of only one hole bringing the cold flow into a small part of the wind tunnel. The height of the wind tunnel part was set to be more than three times the height of the incoming boundary layer and was assessed (through tests) to be enough not to have any significant effect on the computed flow. A part of the plenum that supplies the hole with the coolant was also included in the design. The hole geometry was provided by the *Turbine Heat Transfer and Aerodynamics Group* of the Pennsylvania State University as it can be found in the group's website[7] in $.igs$ format. It was scaled up ($D = 7.75\ mm$ for the circular cross-section) and the domain around was designed so as to represent the experimental configuration. In the same context, the proper boundary conditions had to be chosen in accordance.

[7] https://www.mne.psu.edu/psuturbine/ShapedHole

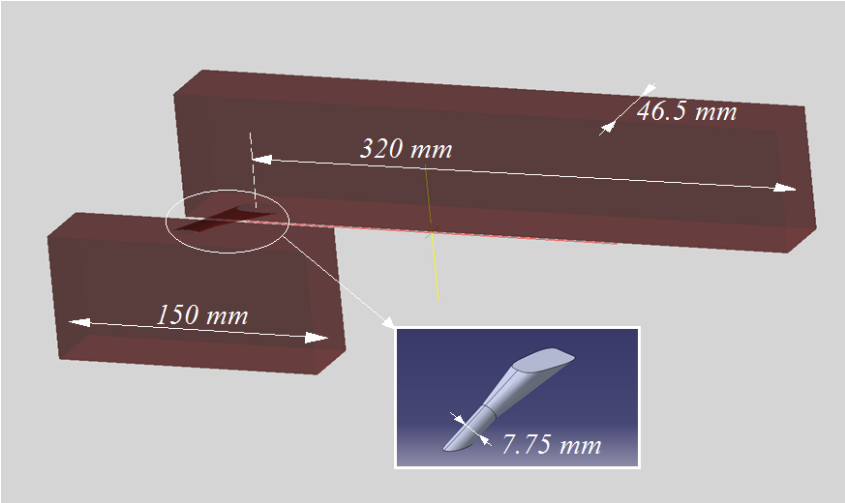

Figure 5.2: *Geometry of the problem's domain.*

The domain was meshed with CENTAUR, a grid generator software developed for the fast generation of hybrid meshes. The generated mesh can be seen in figure 5.4 along with the chosen boundary conditions. A *velocity inlet*, with a specific profile and a constant value for the temperature ($T_{atm} = 295K$) was set at the domain's left boundary. This profile was chosen according to experimental data providing information on the turbulent boundary layer at a position right before the hole exit. A *total pressure inlet* was chosen for the plenum's inlet. The correct value for the total pressure was established after various tests trying to accomplish a target mass flow through the hole and a specific density ratio between the coolant and the mainstream. The pressure at the outlet of the domain was $P_{atm} \approx 14\ psia$ in order to match the experimental conditions. All the boundary patches at the third dimension (the one normal to the figure's plane) were given a *symmetry* boundary condition as the *periodic* boundary conditions in the cases tested were found to lead to divergence of the jet towards the sides. Finally, the walls were given an adiabatic no-slip condition.

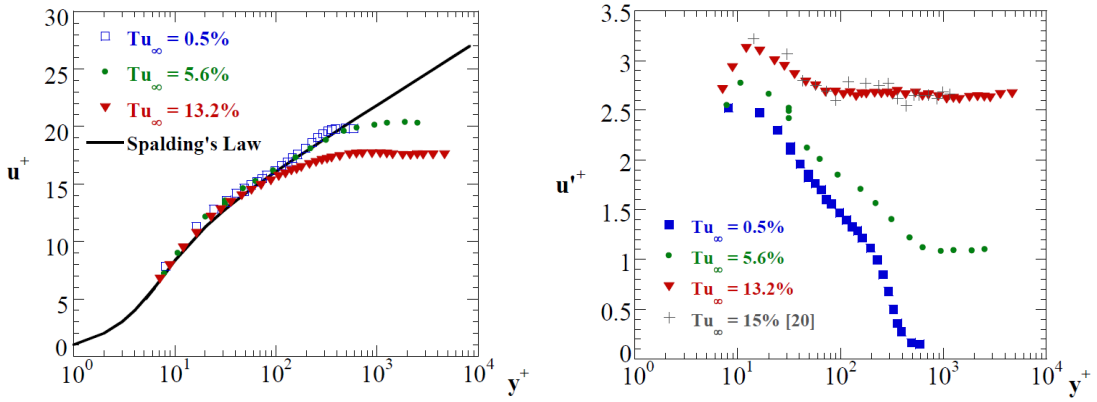

(a) **(b)**

Figure 5.3: *Turbulent boundary layer (a) velocity and (b) stream-wise velocity fluctuation profiles, measured before the hole's exit, $u_\tau = 0.5\ m/s$, $U_\infty = 10\ m/s$.*

The low free-stream turbulence ($T_u = 0.5\%$) case was chosen to be simulated, for $M = 1.5$

and $DR = 1.5$. No turbulence grid was used in the experiments, the bulk velocity was $U_\infty = 10\ m/s$ and the tripped boundary layer had the characteristics shown in figure 5.3.

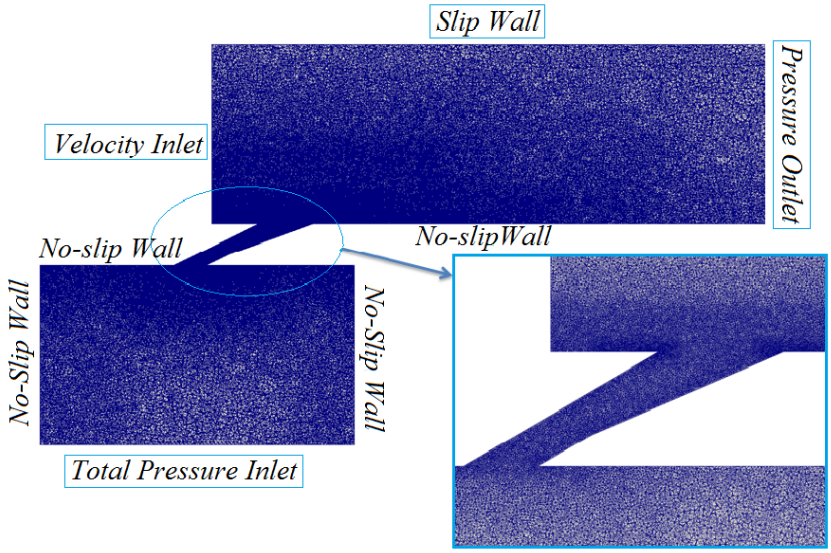

Figure 5.4: *A 2D slice on the plane of symmetry of the computational domain meshed with* 19 *mil. cells, along with the boundary conditions.*

The original mesh presented in figure 5.4 had a little less than 19 million cells. In an effort to reduce the computational cost but also keeping the good grid characteristics in the regions of interest (i.e. close to the walls and the mixing region), a mesh adaptation was performed. The aim was to coarsen the mesh in the region away from the walls and the mixing zone of the two flows.

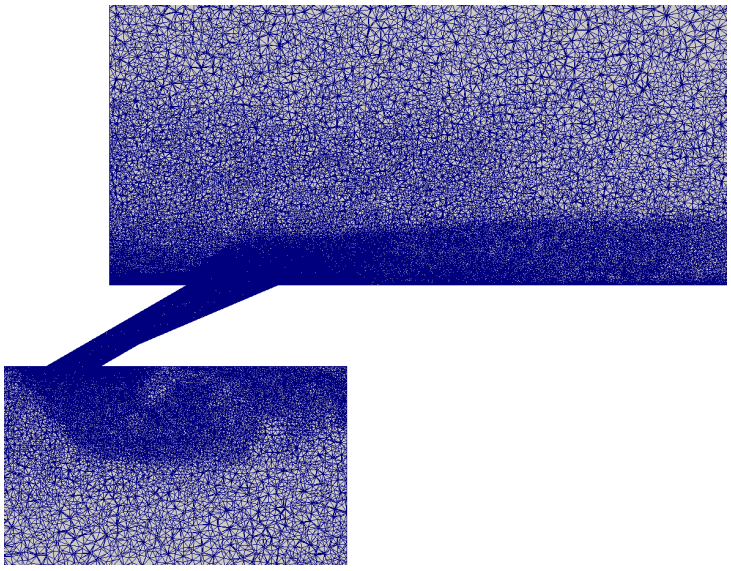

Figure 5.5: *A 2D slice on the plane of symmetry of the coarsened mesh, adapted according to the losses in kinetic energy.*

An adaptation technique based on the computed losses in kinetic energy had been devel-

oped in [53] and has been put into practice in this case as well. The resulted adapted mesh, with a little bit over 13 million cells can be seen in figure 5.5. The mesh is significantly coarsened in the far field while keeping the same cell size in the region of interest. No mesh convergence study was carried out as it could not be accomplished within the duration of this thesis.

In the following sections the validation of the code in this test case is carried out. Various simulations were launched and a few of them are presented in order to provide the reader with an evaluation of the code's sensitivity. The flow field is included as estimated by AVBP along with some results plotted versus experimental ones.

5.2. VALIDATION

The first simulation to be carried out aimed to the estimation of a converged solution of the problem. A LW convective scheme was used to avoid the excessive computational cost. A converged solution in terms of mean kinetic energy was established after $\Delta T = 0.1\ sec$, which corresponds to almost three times the "flow-through time". By this term we define the time that the mainstream flow needs in order to reach the pressure outlet starting from the inlet of the tunnel. The CFL number for the computation was set to 0.7 and the resulting time step (deduced from the CFL for the smallest cell of the grid) was $\Delta t \approx 0.6 \cdot 10^{-7} sec$.

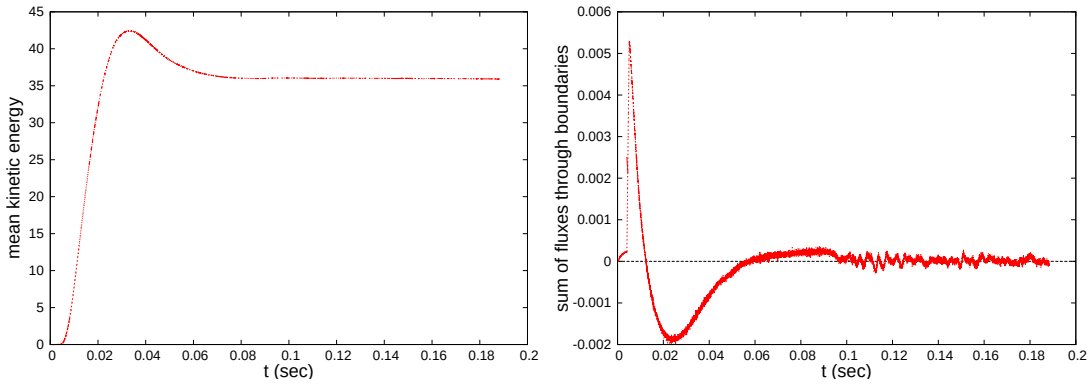

(a) **(b)**

Figure 5.6: *Convergence of (a) the mean kinetic energy and (b) the sum of the fluxes through the boundaries, Lax-Wendroff convective scheme.*

For this specific time step value 700000 iterations need to be completed for the flow to sweep the computational domain from the inlet to the outlet plane. For the same grid size and CFL number, the computational time of the calculation varies according to the architecture of the machine used for the computations, the number of nodes and of course the convective scheme. Just for the reader to have an idea on the computational cost of this simulation, the CPU time would exceed the forty (40) hours when the TTGC scheme was used and the simulation was launched in NEMO (one of the internal calculators of CERFACS[8]) using 15 nodes of 24 processors each.

[8]The reader can find information regarding the CERFACS' internal resources at: https://cerfacs.fr/

Starting from the converged estimation provided by the code with the LW convection scheme, different cases were tested in search for an accurate solution and in order for the sensitivity of the acquired estimation to be assessed. The cases tested in this project are presented in the table 5.1. In all of them the $WALE$ sub-grid scale model implemented in AVBP was used and the FE_2delta scheme (the 2Δ operator in accordance to what it was described in the previous chapter) for the discretization of the diffusive fluxes. The same artificial viscosity model was also utilized and the CFL was identical (0.7).

They y^+ values on the flat plate and on the walls of the hole can be seen in figure 5.7 computed with the TTGC convective scheme with a wall-resolved LES approach. With the grid used, the y^+ values on the largest part of the plate would range around $8-13$ which was assessed as acceptable (even if high for the wall-resolved LES cases) considering the limitations imposed in terms of computational cost. Some regions with greater values (close to 20) can also be identified. The y^+ values on the walls of the tube are considerably higher.

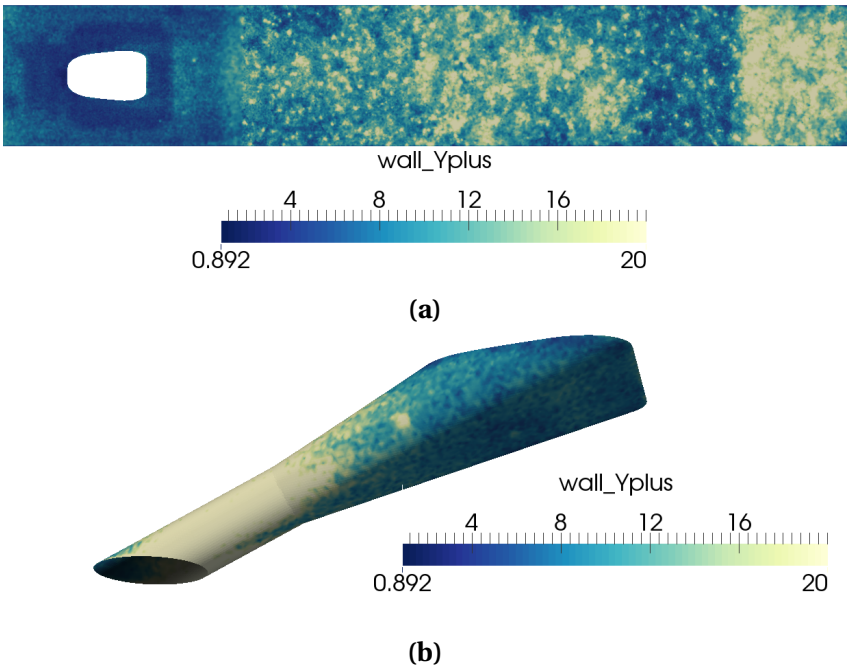

Figure 5.7: *Values of wall y^+ on the (a) flat plate and (b) on the walls of the hole, computed with the TTGC convective scheme, targeting $M = 1.5$, $DR = 1.5$, isotropic turbulence injected, wall resolved LES approach.*

In the following sections, the results obtained from the numerical simulations are presented. First, the flow field feature are included providing a description of the flow both inside and outside the hole. They are followed by plots of averaged thermal and velocity profiles versus the experimental ones that can be found in [2]. Plots of adiabatic effectiveness, velocity and velocity fluctuations profiles are included. Finally, plots of laterally averaged (over the flat surface area) adiabatic effectiveness are also provided. From hereon, the x axis refers to the stream-wise direction (defined by the mainstream flow) the xz plane is the parallel

`les-calculateurs-du-cerfacs`

to the flat surface and consequently y axis is normal to that plane. Even if redundant, it is explicitly noted that the lateral direction will be the one defined by the z axis. The results presented in the following sections derive from temporally averaging the solution over three flow-through times (except if it is explicitly mentioned otherwise).

Case Number	Convective Scheme	Wall Modeling	Turbulence Injection	Blowing Ratio	Density Ratio	Discharge Coefficient[9]
1	LW	No	Isotropic	1.51	1.47	0.74
2	TTGC	No	Isotropic	1.55	1.48	0.76
3	TTG4A	No	Isotropic	1.45	1.47	0.77
4	TTGC	No	Anisotropic	1.54	1.48	0.76
5	TTGC	Yes	Isotropic	1.54	1.48	0.75

Table 5.1: *Summary of the validation cases tested.*

5.3. Flow Field

In this section the flow field both inside and outside the hole is going to be examined. Starting with figure 5.8 the instantaneous temperature field is presented. Large scale unsteady vortical patterns can be observed in the mixing zone of the jet with the cross-flow. The jet gets entrained and moves further downstream providing a film coverage of the flat surface (the footprint of the jet onto the adiabatic wall can also be observed). The time evolution of the thermal field is presented in a collection of figures available at the appendix B.1.

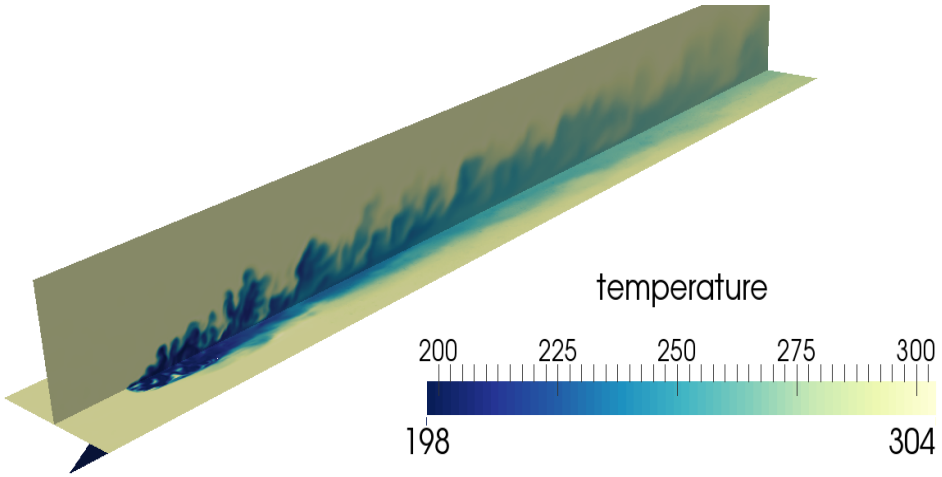

Figure 5.8: *Contour plot of the instantaneous temperature field on the flat plate (xz plane) and on the xy symmetry plane, results from Case 2.*

In figures 5.9b and 5.9d the planar averaged velocity field on the symmetry plane is depicted. The large turning of the coolant supplied by the plenum leads to the known jetting

[9] The discharge coefficient is estimated with equation 1.4 given in a previous chapter. It is compared to the value of 0.75 estimated experimentally in [20].

effect. The fluid tends to concentrate close to the windward wall of the hole forming a high velocity jet. Below that, a low momentum recirculation region is developed. A separation bubble inside the diffuser part of the hole can be identified as well. Both of these observations are well described in literature and were expected. The incoming boundary layer seems to smoothly pass over the jet and no detached flow is present before the hole exit. The effect on the jet's momentum reduction is due to the geometric jet outlet expansion and is obvious.

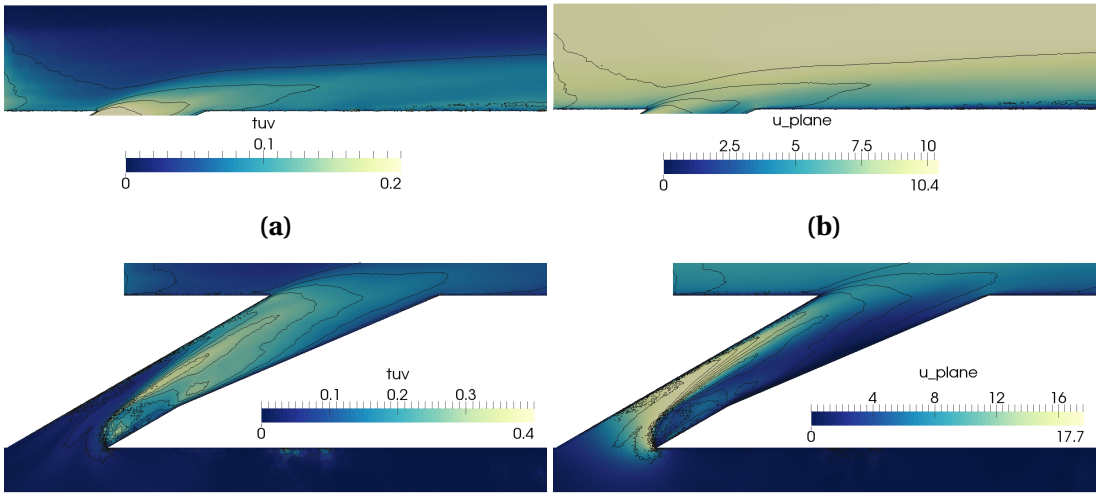

Figure 5.9: *Slices of the xy symmetry plane, solution from Case 2, (a) and (c) present the $T_{uv} = \sqrt{(u\prime^2 + v\prime^2)/2}/U_\infty$ field while (b) and (d) the magnitude of the (temporally) averaged velocity on that plane. Iso-contour lines of T_{uv} values are plotted in all the figures.*

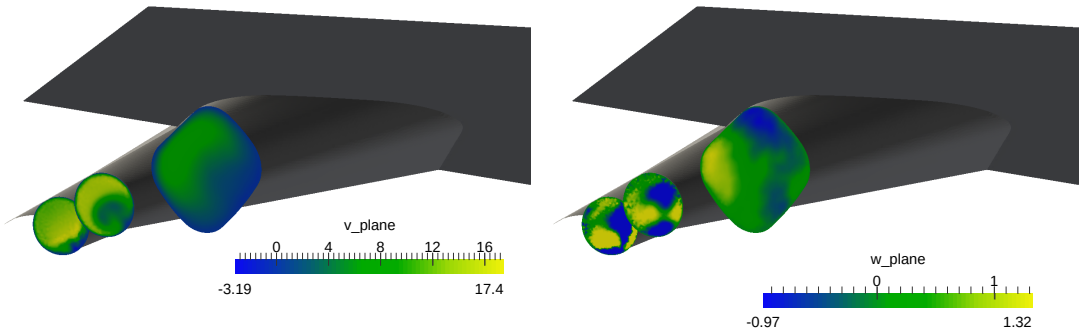

Figure 5.10: *Averaged velocity fields inside the hole for Case 2, the two components of the planar velocity are depicted where (b) presents the tangential velocity (has the direction of the z axis) and (a) the second planar component normal to w.*

In figure 5.9a and 5.9c the turbulence intensity ($T_{uv} = \sqrt{(u\prime^2 + v\prime^2)/2}/U_\infty$) on the same ($xy$ symmetry) plane is pictured. It is evident that the higher values of turbulence come from within the hole. Iso-contour lines of the intensity are also plotted in all the figures. The shear layer created by the jetting effect and the recirculation leads to turbulence levels that exceed those brought by the incoming turbulent boundary layer (from the inlet) or the ones resulting from the jet/cross-flow interaction. This is also consistent to what has been reported in the literature [14].

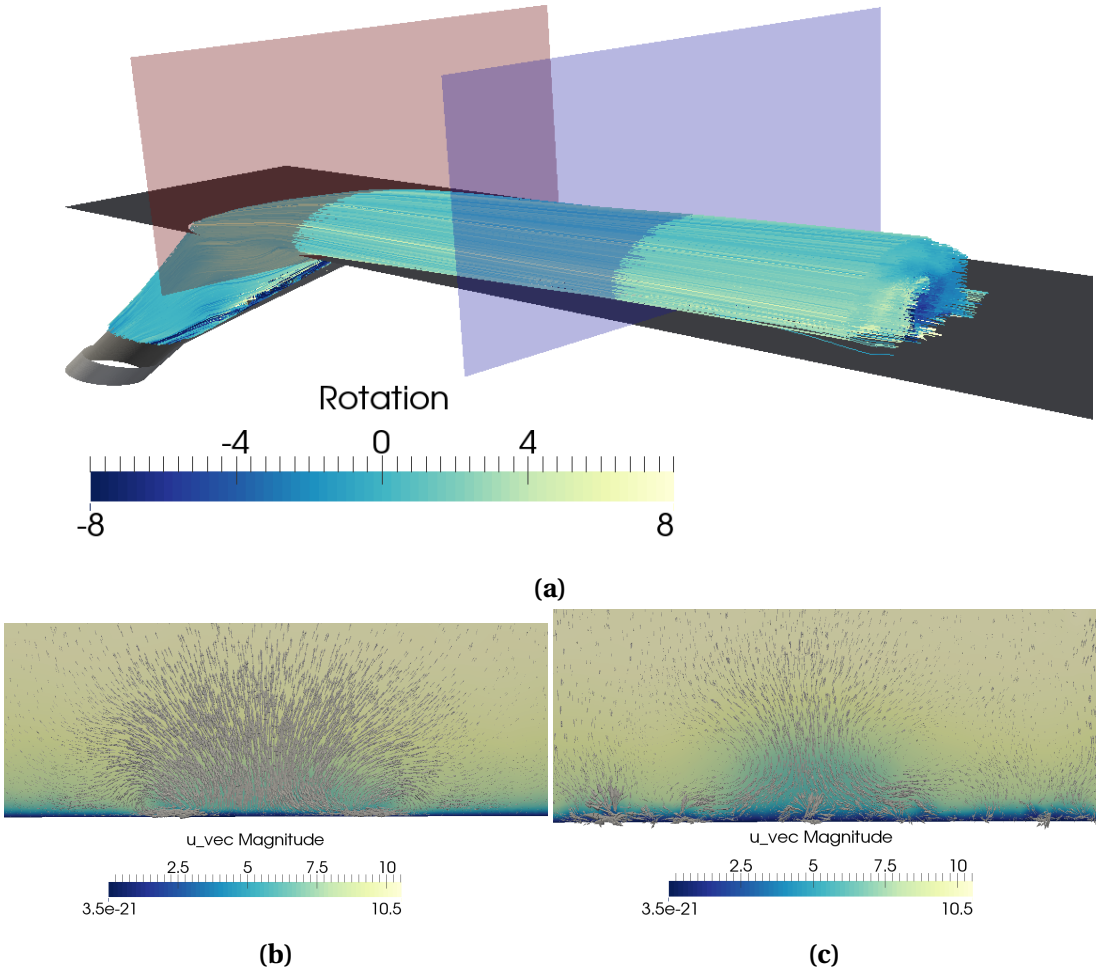

Figure 5.11: *(a) Streamlines of the jet's path and (b), (c) glyphs of the vectorial components of the (temporally) averaged planar velocity of the Plane A and Plane B respectively along with the magnitude of the averaged velocity field. The existence of the CRVP is evident both by the rotation of the streamlines (positive values signify rotation in the direction of the cross-flow) and by the direction of the vectors on the planes. The CRVP's centers C1 and C2 are also noted on the figures.*

The two remaining (temporally) averaged planar velocity components are plotted in the figures 5.10a and 5.10b. The generation of a CRVP inside the hole due to the large turning of the coolant is evident. This pair however seems to get dissipated inside the diffuser support-

ing the view that these vortices are not the ones responsible for the CRVP in the mainstream direction and outside the hole.

The existence of the CRVP outside the hole is confirmed by taking a look at the figure 5.11. The streamlines exiting the hole get twisted in with a rotational direction that attests to the effect of the CRVP. This becomes more obvious by examining the figures 5.11b and 5.11c depicting the *planes A* and *B*. Glyphs of the planar components of the averaged velocity evidence a rotating motion alike to the one of the CRVP. The centers of this vortex pair are also identified and noted on the figures. Theses vortices seem to expand as they develop and also lift of the surface as we move downstream, due to the induced lift deriving from the vortex dynamics and has already been addressed. The detrimental effects that these vortices have on the cooling application has also been discussed extensively and figure B.1 in the appendices can attest to that as it presents the entrainment of the (hot) mainstream under the jet and above the surface due to the CRVP.

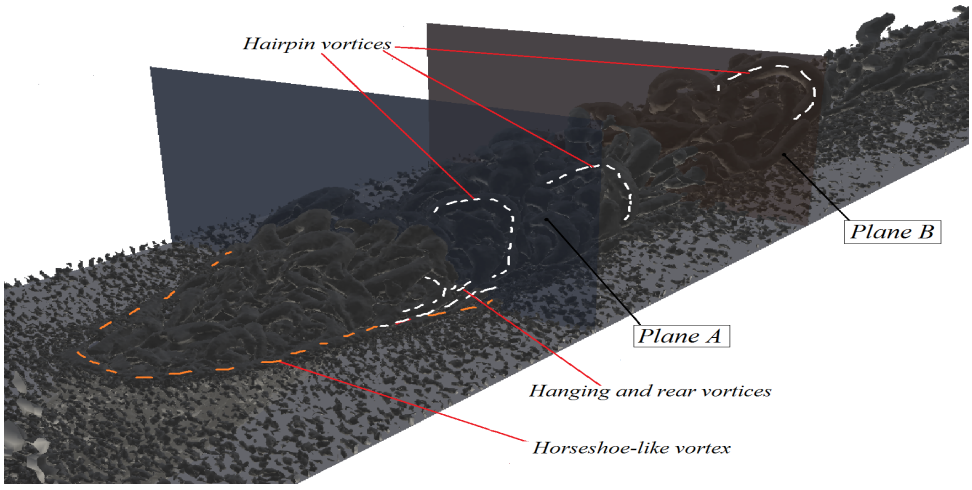

(a)

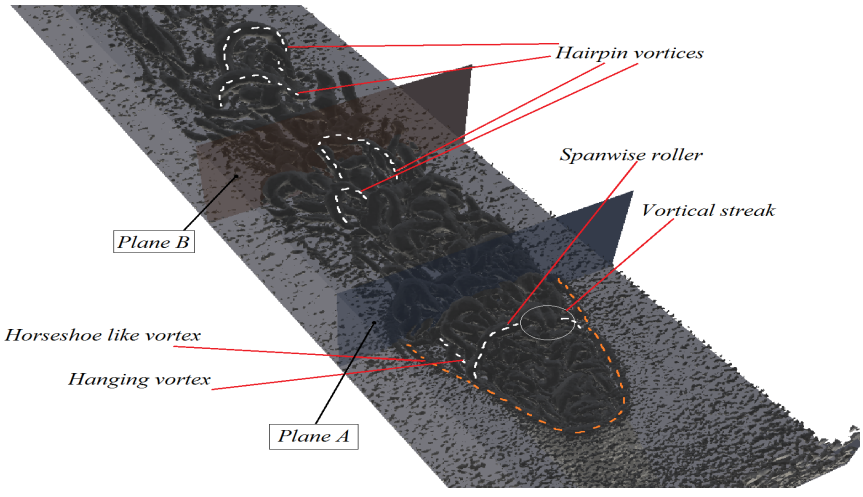

(b)

Figure 5.12: *Q criterion plots: volumes of iso-Q values ($Q = 4 \cdot 10^5$) along with planes A and B defined in a previous figure. No turbulence was injected so that the figure could be clear. With dotted lines, typical coherent structures are marked.*

Finally, it would be interesting to examine the field of the coherent structures. For that reason in figure 5.12 Q criterion plots are presented. In those figures typical coherent structures (already identified by *Sakai et al.* [37] for the cylindrical hole) are marked with dotted lines. With cross-examining figures 5.11 and 5.12 one could hypothesize that close to the hole exit, for this M and this laid-back fan shaped hole design, the initiation of the CRVP comes mainly from the hanging and rear vortices developed from the jet mainstream interaction on the hole sides. They are close to the wall and define the flow field just after the hole exit. This pair seems to evolve and interact with the rest of the small scale structures of the flow. Further downstream, where the CRVP has already been lifted-off the wall, the development of hairpin vortices is also observed. Instead of having one main big centered hairpin vortex though (as observed by *Sakai et al.* for the cylindrical hole), it seems that these structures come in smaller pairs quasi-periodically [36] shed, each with a small translation to the left and to the right of the plane of symmetry. These seem to assist in the formation of the large CRVP downstream (as their "exterior legs" have the same longitudinal orientation) which is a steady structure in a temporally averaged sense. This could bring to someone's mind the warping procedures described by *Haven and Kurosaka* [31]. According to the author's interpretation, the one main hairpin structure that emits us a result of the jet/cross-flow interaction could undergo a process of warping (due to the velocity profiles) leading to the apparent formation of the pair of hairpin vortices that are observed. One could also assume that the region noted as IR in figure 5.11c could result from the passing of the hairpin pair's "interior legs" (which are rotating in an opposite sense). It would be really interesting if this process is to be studied more carefully since the post processing of numerical results can provide a wide dataset of relative information. Finally, the effect that the hairpin "heads" have on the (thermal) flow field can be seen in figure A.1a as they correspond to the large scale vortical structures observed in the mixing zone.

5.3.1. Convective Schemes

The results of *Cases 1-3* are presented in this section. Different convection schemes were used. Additional results can be found in the appendix B.2 for completeness. The (temporally) averaged thermal footprint on the plate (starting right after the hole) can be seen in figure 5.13 where the adiabatic effectiveness computed with three different convective schemes is plotted. The experimental data are also available. It is evident that the main effect that the change in the convective scheme has is on the lateral expansion of the jet (coverage). The TTGC seems to provide an estimation that is closer to the experiments in terms of coverage close to the hole while it gets more expanded further downstream.

In figure 5.14 the characteristics of the averaged thermal field are plotted. The variable θ seen in the following figures is defined in a similar way to the adiabatic effectiveness:

$$\theta = \frac{T - T_{atm}}{T_{atm} - T_c} \tag{5.1}$$

where T the computed local averaged temperature. For the centerline (on the $z = 0$ line) and the laterally averaged adiabatic effectiveness the start ($x = 0$) is on the leeward edge of the hole's exit. For the rest of the profiles, the $x/D = 0$ is inside the hole outlet, on the imaginary axis passing through the center of the circular cross-section and normal to that.

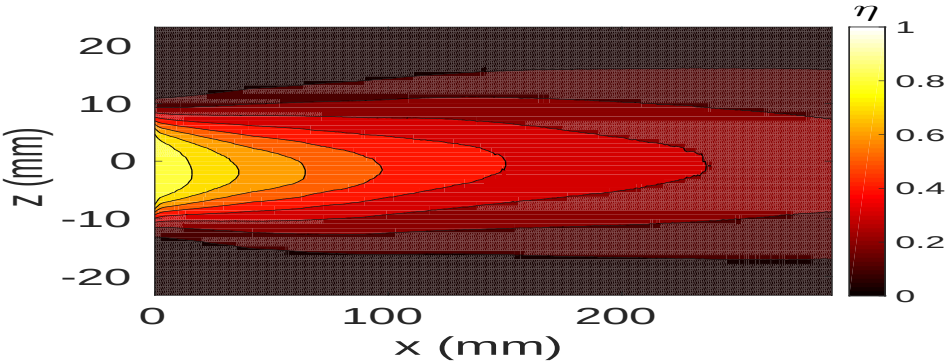

(a) *EXPERIMENTS*

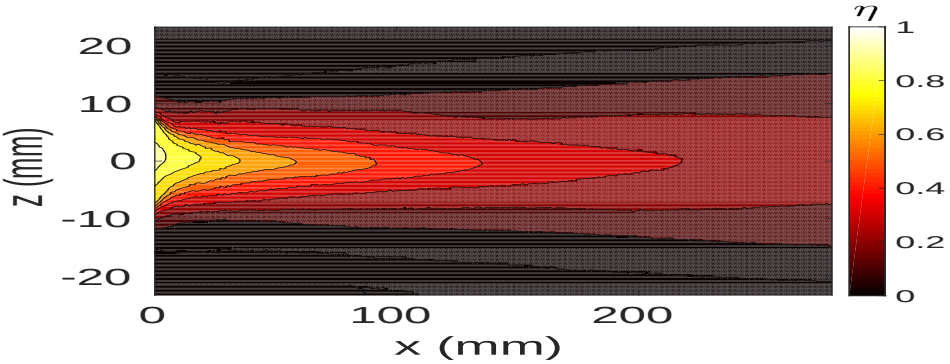

(b) *LW*

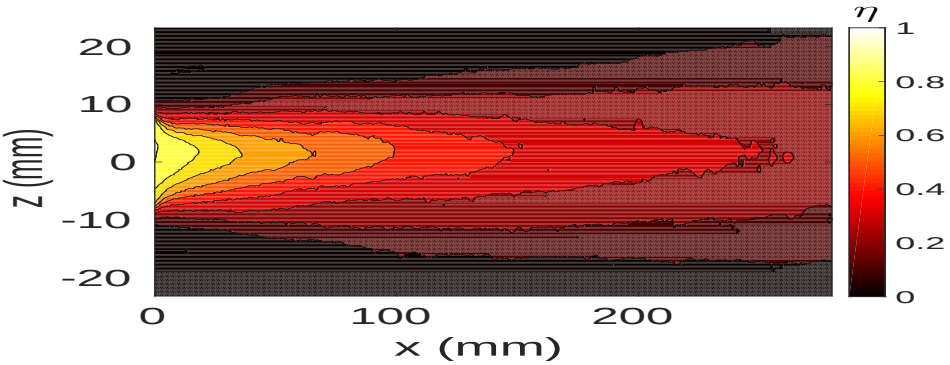

(c) *TTGC*

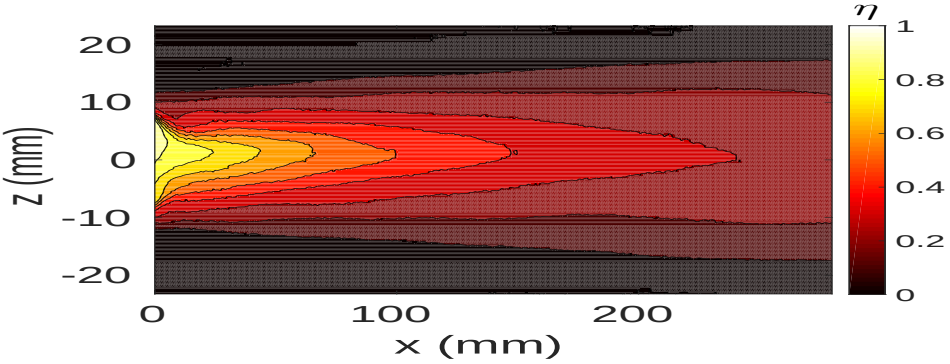

(d) *TTG4A*

Figure 5.13: *Contours (thermal footprint) of adiabatic effectiveness on the flat surface, averaged over time, just after the hole's exit, taken from (a) experiments [19] (spatially) averaged over five holes and (b)-(d) with LES, solution (temporally) averaged over three flow through times, targeting* $M = 1.5$, $DR = 1.5$, *isotropic turbulence injected.*

The agreement with the experimental results in terms of adiabatic effectiveness and θ is quite good for all the schemes used. Only downstream there seems to be a slight deviation as the jet gets more expanded in the normal direction. In terms of averaged adiabatic effectiveness, the TTGC gives the best prediction among the others. This was expected having gone through figures 5.13a-5.13d. Still, the jet does not get expanded enough at the outlet leading to lower values of $\bar{\eta}$ close to the break out point. Any difference in the averaged adiabatic effectiveness could derive from a number of factors, from errors due to numerics (SGS model, numerical schemes) to problems related to the modeling of the problem (grid resolution, boundary conditions, the fact that only one jet is simulated).

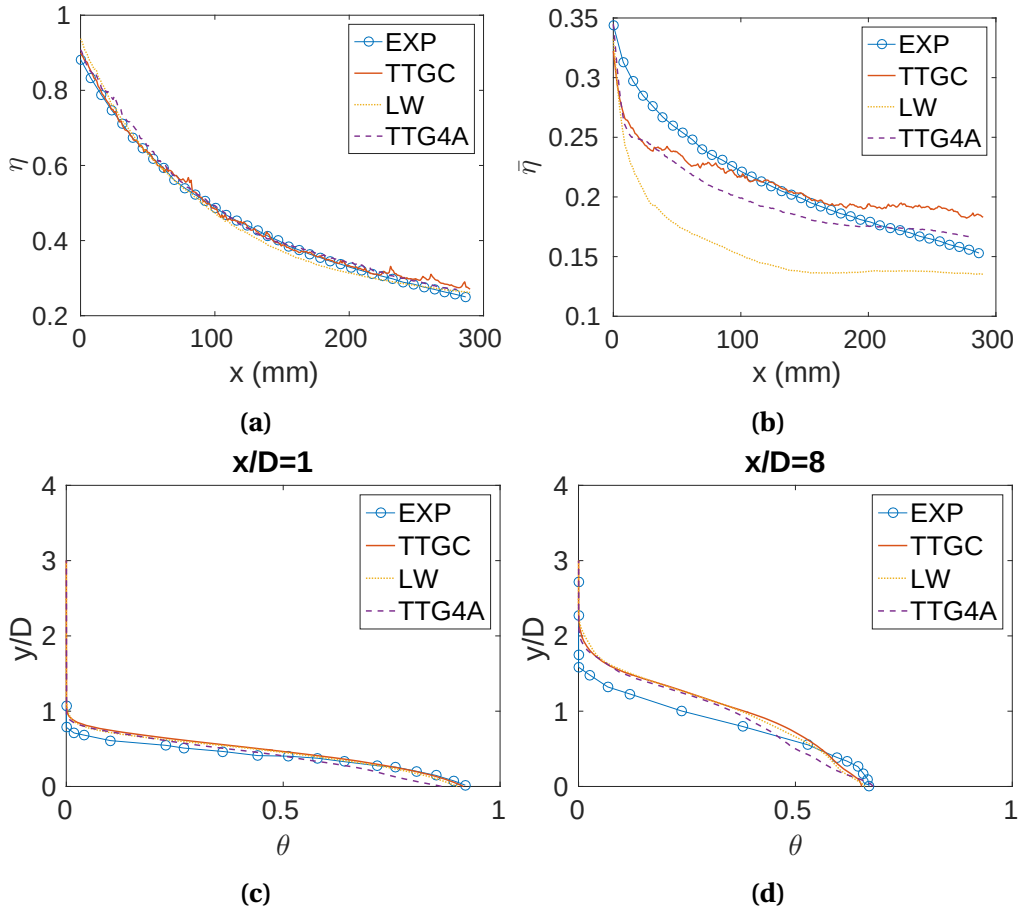

Figure 5.14: *Cases 1 to 3: Three different convective schemes, (a) centerline and (b) laterally averaged adiabatic effectiveness and (c)-(d) (temporally) averaged thermal profiles on the xy symmetry plane, low free-stream turbulence.*

In figure 5.15 the stream-wise (along x axis) velocity and velocity fluctuation profiles are presented. All the schemes give a good estimation of the velocity profile with the TTGC being once again more exact, especially for $x/D = 0$. The agreement in the $u\prime$ values is good, with the TTGC slightly overestimating the maximum value close to the wall. This overestimation was more pronounced in the estimation of the tangential (figure 5.15f) and normal velocity fluctuations components (plots provided in the appendices), even if the physical trends were correctly computed. The turbulent shear stress (figure 5.15e), is correctly estimated as well.

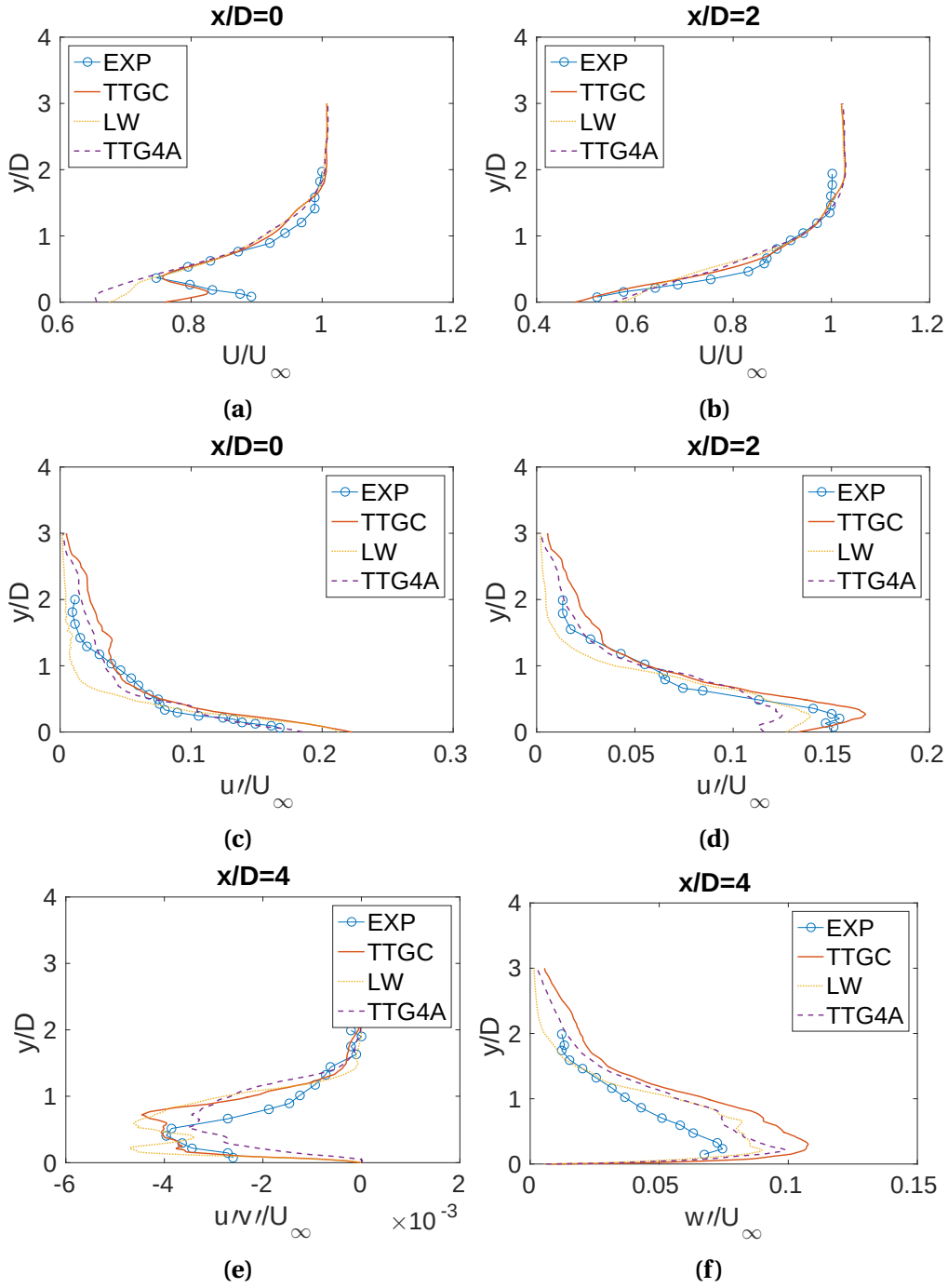

Figure 5.15: *Cases 1 to 3: Three different convective schemes, (a)-(b) stream-wise (temporally) averaged velocity, (c)-(f) profiles of (temporally) averaged turbulent normal and shear stresses on the xy symmetry plane, low free-stream turbulence.*

5.3.2. Turbulence Injection

The results of *Cases 2* and *4* are presented here. The synthetic turbulence injected in the previous simulations was isotropic. However, this specific boundary condition implemented in AVBP gives the user the capability to inject anisotropic turbulence as well. Turbulence in the

boundary layer is in theory highly anisotropic. As for the cases tested turbulence is only injected in the (tripped) boundary layer. The effect that could arise from injecting anisotropic turbulence has been examined. The aim was to inject information closer to a turbulent field inside the boundary layer and this was done in search for a solution were the turbulent stresses are not overestimated. For the same given $\sqrt{u\prime^2}$ profile used up to now, the rest of the components at the inlet had been set in order to mimic more appropriately the turbulence in the boundary layer:

$$\sqrt{v\prime^2} = \lambda\sqrt{u\prime^2}, \quad \sqrt{w\prime^2} = u\prime \cdot w\prime = v\prime \cdot w\prime = 0, \quad u\prime v\prime = C_{uv}\, u\prime \cdot v\prime \tag{5.2}$$

where: $\lambda = 0.8$ given in [21], $C_{uv} = -0.5$ a typical value when the two velocity components are correlated (Prandtl's description of the turbulent boundary layer). Comparing the reduced turbulence level pictured in figures 5.16a and 5.16c with the ones in 5.9c and 5.16b respectively, the difference due to the injection of anisotropic turbulence can be seen.

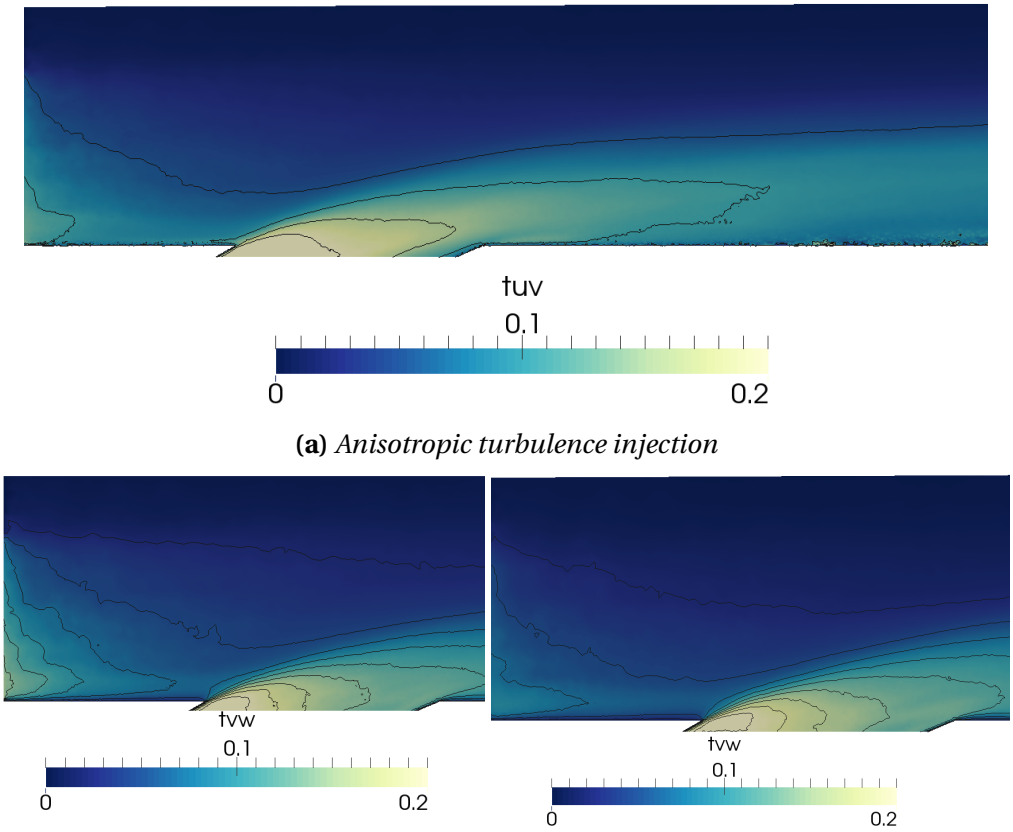

(a) *Anisotropic turbulence injection*

(b) *Isotropic turbulence injection*

(c) *Anisotropic turbulence injection*

Figure 5.16: *Slices of the xy symmetry plane, solution from Cases 1 and 4, (a) presents the $T_{uv} = \sqrt{(u\prime^2 + v\prime^2)/2}/U_\infty$ contours while (b) and (c) the $T_{vw} = \sqrt{(v\prime^2 + w\prime^2)/2}/U_\infty$ ones. Iso-contour lines of T_{uv} and T_{vw} values are plotted respectively.*

In figures 5.17 and 5.18 the respective results are plotted. The reader can find additional data available in appendix B.3. The difference in the two computations are marginal with the anisotropic case giving a slightly worse prediction far downstream. This lack in any remark-

able difference between the two cases comes to complete the experimental studies up to now concluding that the turbulence generated inside the hole is the main factor that drives these flows and dominates the interactions taking place. Indeed, as mentioned previously, the turbulence generated inside the hole exceeds by far the levels of turbulence injected or produced in the mixing of the mainstream with the jet. This can also be supported by the contour of the production of turbulent kinetic energy B.3 included in the appendix.

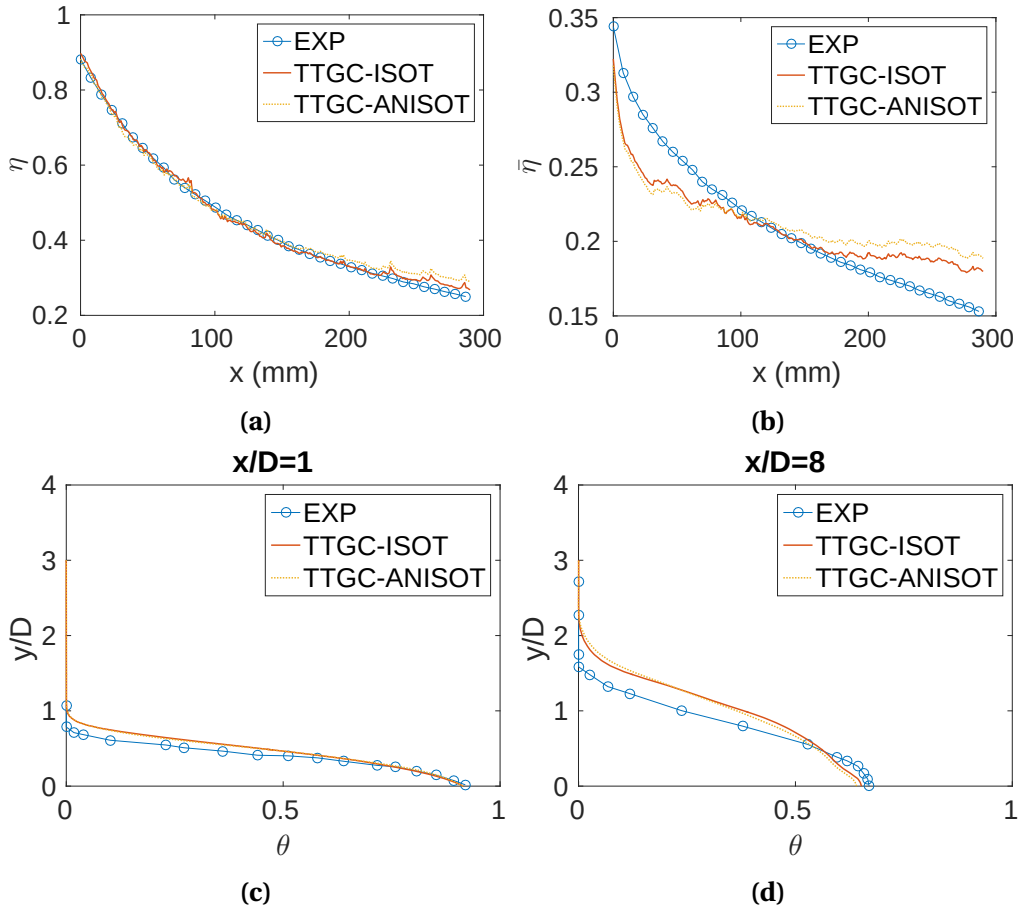

Figure 5.17: *Cases 2 and 4: Injection of isotropic and anisotropic turbulence, (a) center-line and (b) laterally averaged adiabatic effectiveness and (c)-(d) (temporally) averaged thermal profiles on the xy symmetry plane, low free-stream turbulence.*

5.3.3. Wall Modeling

In this section the *Cases 2* and *5* are presented. In the previous simulations a wall resolved LES approach was followed. A simulation were the results of wall modeling are tested was carried out as well. A wall boundary condition equipped with a *wall-law model* was set on the plat plate and on the walls of the tube instead of the *no-slip conditions* used until now. The *wall-law model* derives the velocities in the first cell above the wall according to the empirical law of the wall and the local y^+ value. These models are typically based on the solution for the flat plate fully turbulent boundary layer and in that case are well defined in order to accurately estimate the velocity gradient on the wall when the grid resolution is not

sufficient for a wall resolved LES. With this test case it could be established whether different (more accurate) turbulence levels could be generated inside the hole.

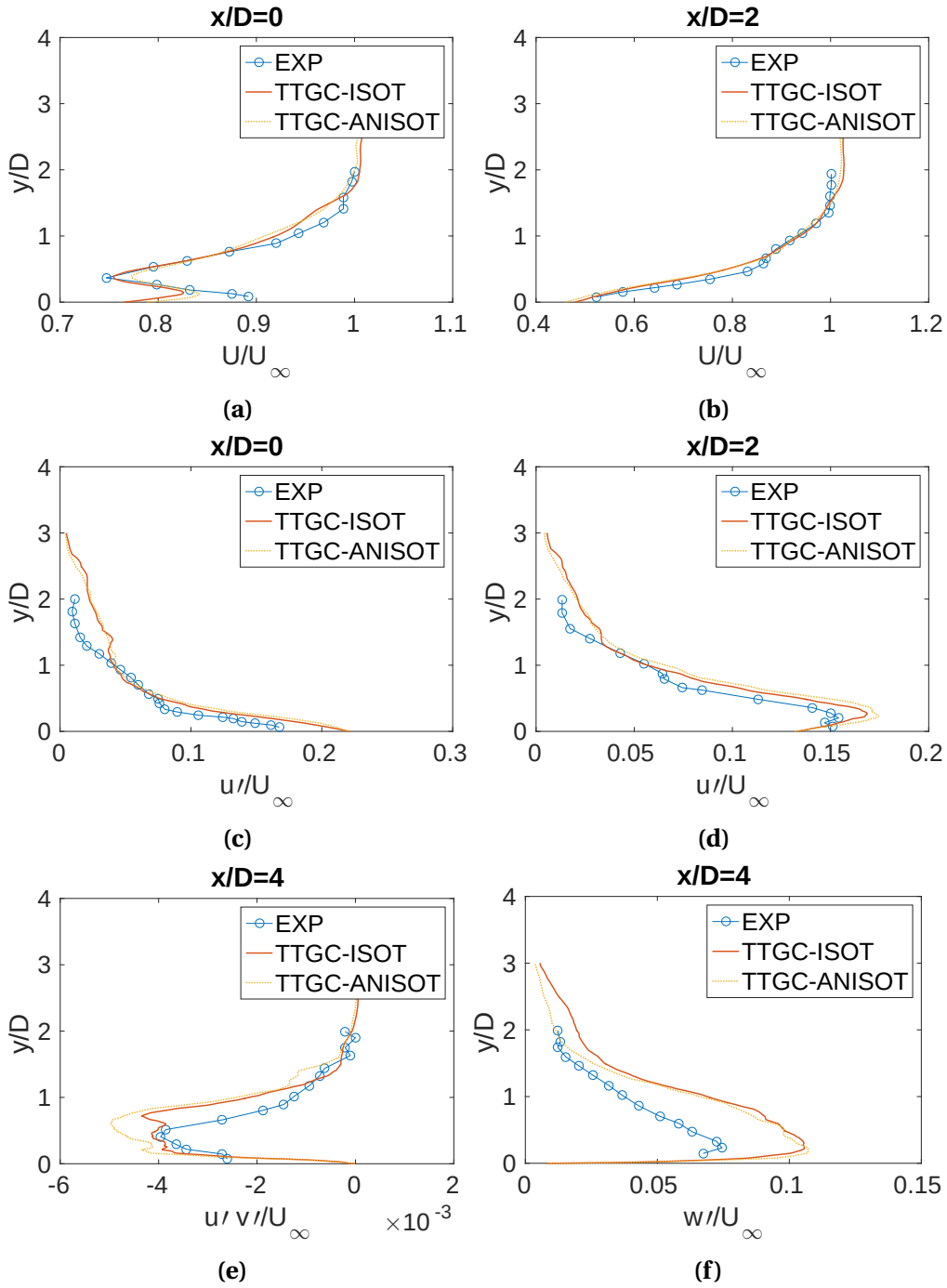

Figure 5.18: *Cases 2 and 4: Injection of isotropic and anisotropic turbulence, (a)-(b) stream-wise (temporally) averaged velocity, (c)-(f) profiles of (temporally) averaged turbulent normal and shear stresses on the x y symmetry plane, low free-stream turbulence.*

In figures 5.19 and 5.20 the respective data are presented. The reader is welcome to find additional plots in appendix B.4. The estimated solution does not present any improve. The

laterally averaged adiabatic effectiveness is well estimated further downstream but the jet seems to get even less expanded at the outlet leading to even lower values of $\bar{\eta}$ close to the hole's outlet. The averaged axial velocity profile is better resolved at the outlet centerline but the peaks of the turbulent stresses are overestimated everywhere else.

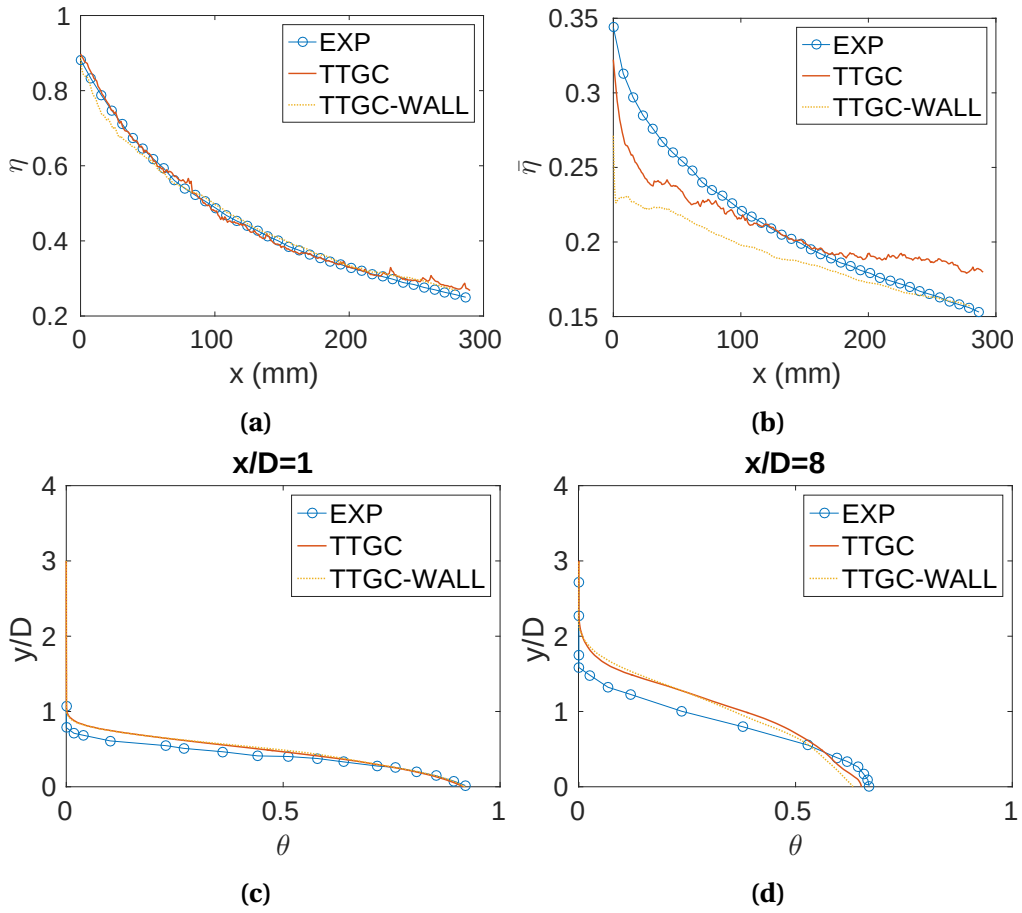

Figure 5.19: *Cases 2 and 5: Testing the wall modeling approach, (a)-(b) effectiveness and (c)-(d) (temporally) averaged thermal profiles on the xy plane (trough the centerline), low free-stream turbulence,* $M = 1.5$, $DR = 1.5$, .

The y^+ values on the plate were around 10 with the wall modeling as it is depicted in figure 5.21. As a matter of fact, this corresponds to a region inside the buffer zone of the turbulent boundary layer. The *law of the wall* models usually use empirical expression describing the boundary layer either in the viscous sub-layer or in the logarithmic zone. This could be a reason due to which a more accurate prediction is not obtained.

More importantly however, the poor prediction of the solution right after the hole's exit may be mainly due to this: the wall modeling is (as is already mentioned) well defined for a fully turbulent boundary layer. Inside the hole, the flow undergoes transition on the walls and due to the jetting effect. It is possible that the wall modeling in this case cannot provide an accurate solution as the turbulence inside the hole is not fully developed. The reader could examine the difference on the turbulence intensity and the (temporally) averaged velocity inside the hole for the wall modeling in figure 5.22. Slightly higher T_{uv} intensities mainly due

to the higher values of the velocity profiles are observed. Same goes for the T_{vw} values even if not presented here. It is possible that the higher levels of turbulence lead to an immediate dilution of the jet right after the exit resulting in the reduce of adiabatic effectiveness right after the hole exit.

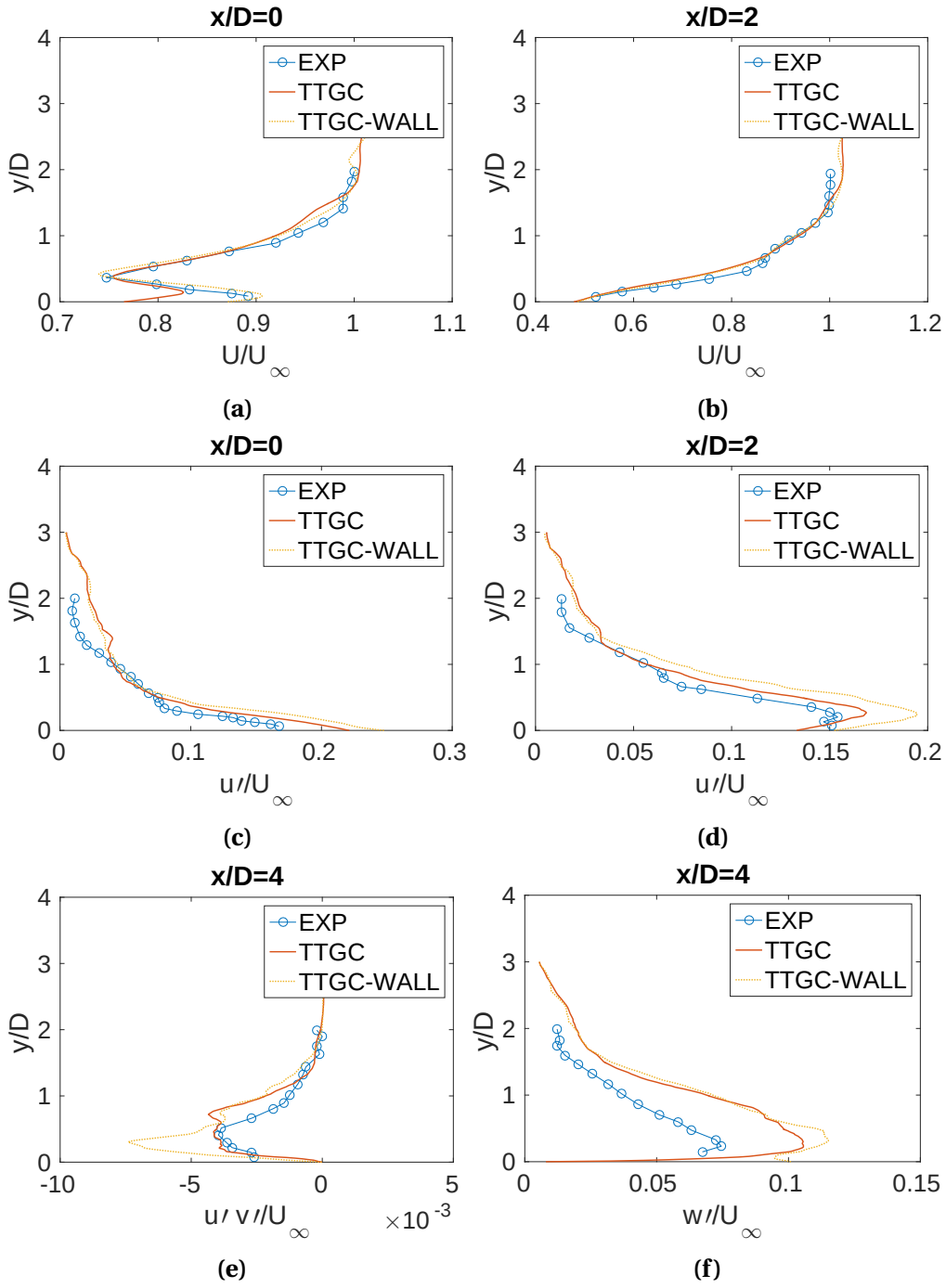

Figure 5.20: *Cases 2 and 5: Testing the wall modeling approach, (a) centerline and (b) laterally averaged adiabatic effectiveness and (c)-(d) (temporally) averaged velocity fluctuations profiles on the xy symmetry plane, low free-stream turbulence.*

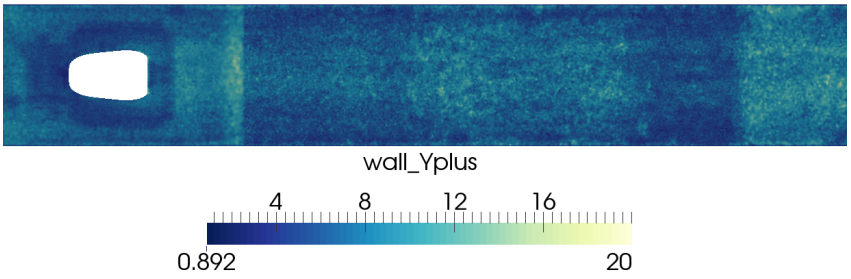

(a)

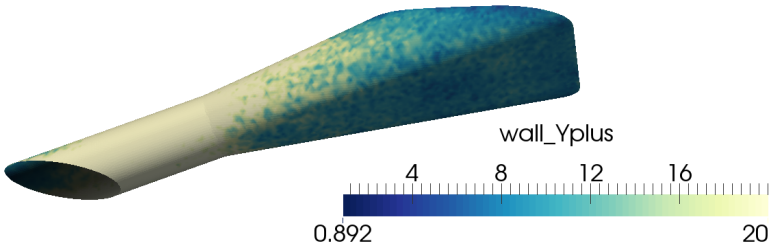

(b)

Figure 5.21: *Values of wall y^+ on the (a) flat plate and (b) on the walls of the hole, computed with the TTGC convective scheme, targeting $M = 1.5$, $DR = 1.5$, isotropic turbulence injected, wall modeling.*

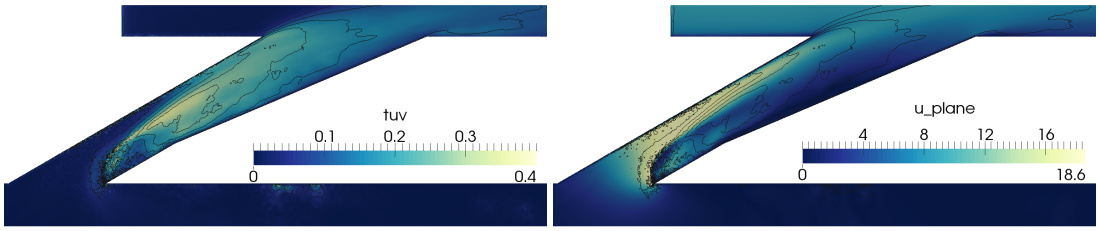

(a) **(b)**

Figure 5.22: *Slices of the xy symmetry plane, solution from Case 5, (a) presents the $T_{uv} = \sqrt{(ur^2 + vr^2)/2}/U_\infty$ field while (b) the magnitude of the (temporally) averaged velocity on that plane. Iso-contour lines of T_{uv} values are plotted in all the figures.*

6. CONCLUSION

Having reached the final chapter of this thesis it is essential to go over what has been examined in oder for some concluding remarks to be drawn. The first part of this thesis was devoted to an extensive (even if not exhaustive) literature review. Film cooling has been utilized over many years as an external cooling technique of the turbine blades in order to aid in the increase of the thermal efficiency of engines. Experimental and numerical studies of film cooling on flat surfaces over many years have been reviewed. In that way the reader could get an idea on the basics of this field of research and on some technicalities typically involved. What is of interest and what could we expect from studying film cooling configurations are some of the questions answered from this survey. It also became obvious that the add of shaping in the holes used for film cooling can lead to a by far improved cooling efficiency (compared to simple cylindrical holes). It is a technique feasible in terms of manufacturing and (as a result) applicable to the industrial needs. Over multiple publications, the shaped holes have been studied up to a point where their behavior is well described, even if it is considered a multi-parametric study case. The geometric parameters and the operating conditions usually have significant effects on film cooling and have been widely surveyed.

However, this domain is not only interesting due to its industrial application. As it turned out studying the film cooling flow can also be conducted following a more "academic" approach. Essentially, this type of flow could be viewed as a jet flow ejected to a cross-flow or even as a wall-bounded jet discharging over a solid boundary. This domain has been researched a lot over the years with many questions still remaining unanswered. Scientists have proposed various interpretations and models to describe the flow field resulting from this type of configurations which typically is rich in coherent vortical structures[10]. Out of all, the Counter Rotating Vortex Pair (CRVP) is the main feature that drives these flows and is essential to the film cooling study as well. This pair has a sense of rotation that brings the hot mainstream flow under the jet just above the surface that is intended to be cooled. That behavior constitutes this pair detrimental for the cooling procedure. More importantly, the generation process of the CRVP is still under debate. An interpretation of this mechanism is attempted in this thesis in order to provide some added value to the LES study, taking into account structures and functions already identified in past literature.

On the second part of this thesis the Large Eddy Simulation approach has been applied to the study of a fan-shaped laidback hole. This specific design named the *"7-7-7"* shaped hole (every expansion angle was 7^o) was proposed by R. P. Schroeder who performed various experimental studies in order to create a wide dataset fully describing its performance. He aimed for a baseline design to be established as a common reference for the scientific community that studies the film cooling application. For this reason the shaped holes design along with results acquired from experiments are available at the site of the laboratory he worked in. Indeed his attempt was deemed successful as various studies were then carried out later on, utilizing his design further expanding the available dataset.

[10] The words "structures" and "vortices" had been equivalently used throughout this thesis. In many occasions the term "vortical structure" has been used as well in the same context even if redundant. It is in the author's best of hopes not to have caused any confusion to the reader.

6.1. Validation Assessment

In the same context, this thesis also deals with a study on the *"7-7-7"* holes. Various simulations were carried out using AVBP, an LES code developed and used in CERFACS, where this thesis was carried out during a six-month internship. It aimed to the validation of the code for this specific complex flow problem and to the assessment of its sensitivity through various test cases. A simplified geometry including one hole was meshed and given appropriate boundary conditions representing as close as possible the experimental configuration. The effect of numerical schemes, wall modeling and turbulent injection were studied. The thermal and flow profiles were compared to the experimental ones.

The code was successfully validated. The TTGC (a Taylor-Galerkin based) convective scheme provided the best results among the others and a quite good prediction in general when compared to the available experimental dataset. The wall modeling approach did not seem to lead to an improvement of the estimation and the turbulence injected at the inlet of the computational domain had no apparent effect on the computed solution. Through flow field plots all the typical feature of the film cooling flow already identified in past literature were observed constituting AVBP a solver capable to predict the phenomena taking place. Any difference observed could be a result of the modeling regarding the mesh resolution and the fact that the flow of only one hole was simulated and then compared to results spatially averaged over five holes.

6.2. The Next Step

Having established that AVBP is capable of providing a quite accurate prediction of the film cooling flow the question would be on how this could be utilized for future work. On one hand, it would be interesting (even if quite elaborate) for the coherence between the various flow structures to be examined. A validated numerical tool like AVBP could provide sufficient information on the secondary flows observed and can add up to the existing knowledge on this type of phenomena. On the other hand, this application is also of great interest to the industrial world. Simulations in engine-like operating conditions could be performed to determine the gain in effectiveness in a more realistic environment were experimental work can be prohibited. Finally, new designs or improvements on the existing one could be tested. In the interest of completeness, some ideas are cited in these following concluding paragraphs.

Typically, the experimental procedures can become quite costly when examining various geometries in order for a wide dataset to be established. Performing numerical simulation with (relatively) lower cost can assist in the industrial search for optimal film cooling designs. One idea that could be tested (in terms of design optimization) would be the adding of a vortex generator inside the hole. As the outflow is mainly driven by structures generated and interacting with each other, their coherence could be broken and potentially lead to improved cooling performance. In fact, the effect of the vortex generator inside a cylindrical hole was examined in [54]. A transverse jet ejected to a cross-flow was experimentally studied. It was found that when the vortex generator was placed in the windward side of the hole, the jet's penetration would reduce and the bound vortex pair would be also weakened. Following, in the experimental study of *Matsuda et al.* [55] a diffusion shaped hole

having a vortex generator was tested among other designs for a low blowing ratio ($M = 0.5$). It provided the best results in terms of film cooling effectiveness. This could be tested by complimentary numerical studies that could provide an idea on the impact that the vortex generator has on the vortical structures of the flow field.

In the same context a numerical study was carried out in [56]. Having established that the CRVP is the main structure governing the cooling flow having detrimental effects on the adiabatic effectiveness, a new design was proposed exploring the "anti-vortex" concept instead of the shaping. They studied two designs. The first one was a cylindrical hole equipped with two additional smaller sized holes on the sides that would be provided with coolant from the same (original) drilled hole as well. The second would have only one additional cylindrical hole that would eject a jet upstream of the (original) inclined hole. The additional holes aimed into creating vortices with a sense of rotation that would negate (reduce) the effects of the CRVP. Improvement in the computed adiabatic effectiveness was observed in both cases with the first one performing even better. More innovative designs in terms of shaping were also tested in following studies. Advanced [57],[58] and slot-based [60] shaping of holes have been studied. The effect of radiusing (rounding the edges of the hole's exit) studied in [59] for cylindrical holes also seemed quite promising and could be easily examined as well for the shaped holes.

REFERENCES

[1] Je-Chin Han, Sandip Dutt, Srunath V. Ekkad, *"Gas Turbine Heat Transfer and Cooling Technology"*, Taylor & Francis, 2000.

[2] Robert P. Schroeder, *"Influence of in-hole Roughness and High Freestream Turbulence on Film Cooling from a Shaped Hole"*, Dissertation in Mechanical Engineering, PhD, 2015.

[3] Jenn-Jiang Hwang, Chau-Shing Lu, *"Lateral-Flow Effect on Endwall Heat Transfer and Pressure Drop in a Pin-Fin Trapezoidal Duct of Various Pin Shapes"*, Journal of Turbomachinery, Copyright by ASME, Vol. 123/133, January 2001.

[4] Ronald S. Bunker, *"A Review of Shaped Hole Turbine Film-Cooling Technology"*, Journal of Heat Transfer, Copyright by ASME, Vol. 127/441, April 2005.

[5] P. M. Kodzwa Jr., J. K. Eaton, *"Measurements of Film Cooling Performance in a Transonic Single Passage Model"*, Report No. TF 93, Standford University, June 2005.

[6] Goldstein R. J., Eckert E. R. G., Burggraf F., *"Effects of Hole Geometry and Density on Three-Dimensional Film Cooling"*, Journal of Heat Mass Transfer, 17 pp. 595-607, 1974.

[7] Saumweber C., Shulz A., *"Effect of Geometry Variations on the Cooling Performance of Fan-Shaped Cooling Holes"*, Journal of Turbomachinery, Vol. 134, Copyright by ASME, November 2012.

[8] Saumweber C., Shulz A., *"Free-Stream Effects on the Cooling Performance of Cylindrical and Fan-Shaped Cooling Holes"*, Journal of Turbomachinery, Vol. 134, Copyright by ASME, November 2012.

[9] Saumweber C., Schulz A., Wittig S., *"Free-stream Turbulence Effects on Film Cooling with Shaped Holes"*„ Journal of Turbomachinery, Vol. 125, Copyright by ASME, January 2003.

[10] Pietrzyk J. R., Bogard D. G., Crawford M. E., *"Hydrodynamic Measurements of Jets in Crossflow for Gas Turbine Film Cooling Applications"*, J. Turbomachinery, Vol. 111, 1989.

[11] Thole K., Gritsch M., Schulz A., Wittig S., *"Effects of a Crossflow at the Entrance of a Film Cooling Hole"*, Journal of Fluids Engineering, Vol. 119, 1997.

[12] Thole K., Gritsch M., Schulz A., Wittig S., *"Flowfield Measurements for Film-Sooling Holes with Expanded Exits"*, Journal of Turbomachinery, Vol. 120, Copyright by ASME, April 1998.

[13] Gritsch M., Colban W., Schär H., Döbbeling K., *"Effect of Hole Geometry on the Thermal Performance of Fan-Shaped Film Cooling Holes"*, Transactions of ASME, Vol. 127, October 2005.

[14] Khli A., Thole K. A., *"A CFD Investigation on the Effect of Entrance Crossflow Directions to Film-Cooling Holes"*, ASME paper, 1997.

[15] Mayank Tyagi, Sumanta Acharya, *"Large Eddy Simulation of Film Cooling Flow From an Inclined Cylindrical Jet"*, Transactions of ASME, Vol. 125, October 2003.

[16] Leedom D. H., *"Numerical Investigation of Film Cooling Fluid Flow and Heat Transfer Using Large Eddy Simulations"*, MSc Thesis in the Department of Mechanical Engineering, Copyright by Leedom D.H., Louisiana State University, May 2009.

[17] Lingxu Zhong, Chao Zhou, Shiyi Chen, *"Large Eddy Simulation of Inclined Jet in Cross Flow with Cylindrical and Fan-Shaped Holes"*, proceedings of ASME Turbo Expo 2016: Turbomachinery Technical Conference and Exposition, GT2016-56840, June 2016.

[18] Schroeder R. P., Thole K. A., *"Adiabatic Effectiveness Measurements for a Baseline Shaped Film Cooling Hole"*, proceedings of ASME Turbo Expo 2014: Turbine Technical Conference and Exposition, GT2014-25993, June 2014.

[19] Schroeder R. P., Thole K. A., *"Effect of High Freestream Turbulence on Flowfields of Shaped film Cooling Holes"*, proceedings of ASME Turbo Expo 2015: Turbine Technical Conference and Exposition, GT2015-43339, June 2015.

[20] Whitfield C. A., Schroeder R. P., Thole K. A., Lewis S. D., *"Blockage Effects from Simulated Thermal Barrier Coatings for Cylindrical and Shaped Cooling Holes"*, Journal of Turbomachinery, Vol. 137, copyright by ASME, September 2015.

[21] Schroeder R. P., Thole K. A., *"Thermal Field Measurements for a Shaped Hole at Low and High Turbulence Intensity"*, proceedings of ASME Turbo Expo 2016: Turbine Technical Conference and Exposition, GT2016-56967, June 2016.

[22] Schroeder R. P., Thole K. A., *"Effect of In-Hole Roughness on Film Cooling from a Shaped Hole"*, proceedings of ASME Turbo Expo 2016: Turbine Technical Conference and Exposition, GT2016-56978, June 2016.

[23] Wilkes E., Anderson J., McClintic J., Bogard D., *"An Investigation of Turbine Film Cooling effectiveness with Shaped Holes and Internal Cross-Flow with Varying Operational Parameters"*, proceedings of ASME Turbo Expo 2016: Turbomachinery Technical Conference and Exposition, GT2016-56162, June 2016.

[24] Wilkes E., Anderson J., McClintic J., Bogard D., *"Effects of Freestream Mach Number, Reynolds Number and Boundary Layer Thickness on Film Cooling Effectiveness of Shaped Holes"*, proceedings of ASME Turbo Expo 2016: Turbomachinery Technical Conference and Exposition, GT2016-56152, June 2016.

[25] Haydt S., Lynch S., Lewis S., *"The Effect of a meter-Diffuser Offset on Shaped Film Cooling Hole adiabatic Effectiveness"*, proceedings of ASME Turbo Expo 2016: Turbomachinery Technical Conference and Exposition, GT2016-56135, June 2016.

[26] Aghasi P., Gutmark E., Munday D., *"Dependence of Film Cooling Effectiveness on 3D printed Holes"*, proceedings of ASME Turbo Expo 2016: Turbomachinery Technical Conference and Exposition, GT2016-56698, June 2016.

[27] Andreopoulos J., Rodi W., *"Experimental Investigation of Jets in a Crossflow"*, J. Fluid Mech., Vol. 138, pp. 33-127, 1984.

[28] Roshko A., Fric T.F., *"Vortical Structure in thw wake of a transverse jet"*, J. Fluid Mech., Vol. 279, pp 1-47, 1994.

[29] Kelso R. M., Lim T. T., Perry A. E., *"An experimental study of round jets in cross-flow"*, J. Fluid Mech., Vol.306, pp. 111-114, 1996.

[30] Peter Ajersch, Jian-Ming Zhou, Steven Ketler, Martha Salcudean, Ian S. Gartshore, *"Multiple Jets in a Crossflow: Detailed Measurements and Numerical Simulations"*, J. of Turbomachinery, Vol. 119, pp. 330-342, 1997.

[31] Haven B. A., Kurosaka M., *"Kidney and anti-kidney vortices in crossflow jets"*, J. Fluid Mech., Vol. 352, pp. 27-64, 1997.

[32] Haven B. A., Yamagata D. K., Kurosaka M., Yamawaki S., Maya T., *"Anti-kidney pair of vortices in Shaped holes and their influence on film cooling effectiveness"*, presented at ASME International Gas Turbine & Aeroengine Congress & Exhibition, Vol. 3: Heat Transfer; Electric Power; Industrial and Cogeneration, 1997.

[33] Lemmon C. A., Kohli A., Thole K. A., *"Formation of Counter-Rotating Vortices in Film-Cooling Flows"*, presented at ASME International Gas Turbine & Aeroengine Congress & Exhibition, 1999.

[34] New T. H., Lim T. T., Luo S. C., *"elliptic Jets in a Cross Flow"*, Journal of Fluid Mechanics, Vol. 494, pp. 119-140, November 2003.

[35] Ralph William Detra, *"The secondary flow in Curved Pipes"*, PhD thesis, ETH Zürich, 1953.

[36] Hisashi Matsuda, Sei-ichi Iida, Michio Hayakawa, *"Coherent Structures in a Three-Dimensional Wall Jet"*, Transactions of ASME, Vol. 112, December 1990.

[37] Sakai E., Takahashi T., Watanabe H., *"Large Eddy Simulation of an Inclined Round Jet Issuing into a Crossflow"*, J. of Heat and Mass Transfer, Vol. 69, pp. 300-311, 2014.

[38] Pope S. B., *"Turbulent Flows"*, Cambridge University Press, 2000.

[39] *"The AVBP HandBook"*, CERFACS, Reviewed Version, December 2011.

[40] Garnier E., Adams N., Sagaut P., *" Large Eddy Simulation for Compressible Flows"* , 2009, IX, 276p.

[41] Poinsot T., Veynante D., *" Theoretical and numerical combustion"*, R.T. Edwards, 2nd edition, 2005.

[42] Nicoud F., *"Defining wave amplitude in characteristic Boundary Conditions"*, Journal of Computational Physics, vol. 149, p. 418-422, 1999.

[43] Nicoud F., Poinsot T., *"Boundary Conditions for compressible unsteady flows"*, Tech. rep., CERFACS, Toulouse/France, 1999.

[44] Poinsot T., Lele S., *Boundary conditions for Direct Numerical Simulations of compressible viscous flows"*, J. Comput. Physics, vol. 101,1 p. 104-129, 1992.

[45] Lodato G., Domingo P., Vernisch L., *"Three Dimensional Boundary Conditions for Direct and Large Eddy Simulation of Compressible Viscous Flows.*, J. of Computational Physics, Vol. 227, No. 10, pp. 5105-5143, 2008.

[46] Granet V., Vermorel O., Poinsot T., *"Comparison of non-reflecting Outlet Boundary Conditions for Compressible Solvers on Unstructured Grids"*, AIAA Journal, Vol. 48, No. 10, October 2010.

[47] Guezénnec N., Morata E. C., *"Injection of vortices and turbulence"*, AVBP Quality Program Form (restricted access), April 2012.

[48] Kraichnan R. H., *"Diffussion by a Random Velocity Field"*, The physics of Fluids, 13:22-31, 1970.

[49] Smirnov A., Shi S., Celik I., *"Random Flow Generation technique for Large Eddy Simulations and Particle-Dynamics modeling"*, Trans. ASME, Journal of Fluids Engineering, 123:359-371, 2001.

[50] Schönfeld T., Rudgyard M, *"Steady and Unsteady Flows Simulations using the hybrid flow solver AVBP"*, AIAA Journal 37, p. 1378-1385, 1999.

[51] Colin O., Rudgyard M., *"Development of high-order taylor-galerkin schemes for unsteady calculations"*, J of Comp. Phys., Vol. 162, 2000.

[52] Colin O., Benkenida A., Angelberger C., *" 2D modeling of mizing, ignition and combustion phenomena in highly stratified gasoline engines"*, Oil & Gas & Science and Texhnology, IFP, Vol. 58 of Rev. IFP, January 2003.

[53] Daviller G., Brebion M., Xavier P., Staffelbach G., Müller J.D., Poinsot T., *"A mesh Adaptation Strategy to predict pressure losses in LES of swirled flows"*, paper under review, submitted for publishing in J. Flow, Turbulence and Combustion.

[54] Zaman K. B. M. Q., Foss . K., *"The effect of Vortex generators on a jet in a Cross-Flow"*, NASA Lewis Research Center, Physics of Fluids, Vol. 9, 1997.

[55] Hisashi Matsuda, Kazutaka Ikeda, Yuji Nakata, Fumio Otomo, Takeo Suga, Yoshitaka Fukuyama, *A new thermochromic liquid crystal temperature identification technique using color space interpolations and its application to film cooling effectiveness measurements"*, J. of Flow Visualization & Image processing, Vol. 7, pp. 103-121, 2000.

[56] James D. Heidmann, *"A Numerical Study of Anti-Vortex Film Cooling Designs at High Blowing Ratio"*, NASA Glenn Research Center, paper prepared for Turbo Expo 2008: Gas Turbine Technical Congress and Exposition, 2008.

[57] Siavash Khajehhasani, *"Numerical Modeling of Innovative Film Cooling Hole Schemes"*, PhD dissertation, 2014.

[58] Kusterer K., Dickhoff J., Campana N. T., Sugimoto T., Tanaka R., Kazari M., Bohn D., *"Automated Design Space Exploration of Advanced-Shaped Gilm Cooling Holes Using the Sherpa Algorithm"*, proceedings of ASME Turbo Expo 2016: Turbomachinery Technical Conference and Exposition, 2016.

[59] Antar M. M. Abdala, Fifi N. M. Elwekeel, Qun Zheng, *"Effects of Film Hole Exit Radiusing on Film Cooling performance"*, proceedings of ASME Turbo Expo 2016: Turbomachinery Technical Conference and Exposition, 2016.

[60] Bai-Tao AN, Jian-Jun LIU, Si-Jing Zhou, Xiao-Dong Zhang, Chao Zhang, *"Film Cooling Investigation of a Slot Based Diffusion Hole"* , proceedings of ASME Turbo Expo 2016: Turbomachinery Technical Conference and Exposition, 2016.

Appendices

A. Turbulence Injection [47]

In this section a narrow reference is made on the technique used to inject synthetic turbulence in the computation. In a computation, turbulence can be developed from the non-linear (chaotic) inherent behavior of the NS equations. With a fine enough mesh and the passage of sufficient computational time, turbulence can be generated even with mean statically stationary boundary conditions. However it is really important to try and surpass the need for additional computation time, especially in the context of three-dimensional LES where the cost is already high enough. One come technique that accomplishes that is the turbulence injection method.

Since most meshes are constructed in a way that the grid regions close to the boundaries are generally coarser (in the context of aerodynamics at least were the target is the estimation of the flow accurately close to a body's surface), it is difficult for a reliable transition to turbulence to be provided. By injecting synthetic turbulence with realistic statistical properties at the inlet, the results and the reduce in computational time can be significantly improved. In AVBP, the turbulent (spatio-temporal) signal is generated with the Kraichnan/Celik method.

This method was originally proposed by Kraichnan [48] and later on extended by Celik et. al [49] for the boundary condition used in LES. The concept of this method is to generate a fluctuating field from a sample of random Fourier harmonics. This field is then added to the statistically mean flow using Taylor's hypothesis [11] (*frozen field hypothesis*).

Let us consider the fluctuating velocity field $\underline{u}' = u - \bar{u}$ of a turbulent flow added at the inlet. Its Fourier transformation at a wave number $\underline{k}$ gives:

$$\underline{u}'(\underline{r},t) = \int_{D(\underline{k})} \underline{\hat{u}}(\underline{k},t) e^{j\underline{k}\cdot\underline{r}} d^3\underline{k} \tag{A.1}$$

where: $j^2 = -1$, $\underline{r}$ the coordinate vector in physical space and $D(\underline{k})$ the spectral domain. With Taylor's assumption:

$$\underline{\hat{u}}(\underline{k},t) = \underline{\hat{u}}(\underline{k}) e^{j\underline{k}\cdot\bar{\underline{u}}t} \tag{A.2}$$

leading to:

$$\underline{u}'(\underline{r},t) = \int_{D(\underline{k})} \underline{\hat{u}}(\underline{k}) e^{j(\underline{k}\cdot\underline{r}+\omega t)} d^3\underline{k} \tag{A.3}$$

where $\omega = \underline{k}\cdot\bar{\underline{u}}$. The discrete equations for N modes $\underline{k}^n$, assuming incompressible flow are:

[11] The hypothesis roughly translates to this: the isotropic harmonic turbulent field, at the scale of observation, can be considered to be simply transfered by the main flow as the spatial decrease of turbulence under diffusion is negligible compared to the temporal decrease due to dissipation. This can be directly used to describe turbulence generated by a grid but does not stand close to the solid wall region.

$$\underline{u}'(\underline{r},t) = \sum_{n=1}^{N} \underline{\hat{u}}^n(\underline{k}^n) e^{j(\underline{k}^n \cdot \underline{r} + \omega^n t)} \quad \text{and} \quad \underline{\hat{u}}^n \cdot \underline{k}^n = 0 \quad \forall n \tag{A.4}$$

and since $\underline{u}'$ is real in the physical space, it is equal to its conjugate:

$$\underline{u}'(\underline{r},t) = \underline{u}'^*(\underline{r},t) = \sum_{n=1}^{N} \underline{\hat{u}^*}^n(\underline{k}^n) e^{j(-\underline{k}^n \cdot \underline{r} + \omega^n t)} \tag{A.5}$$

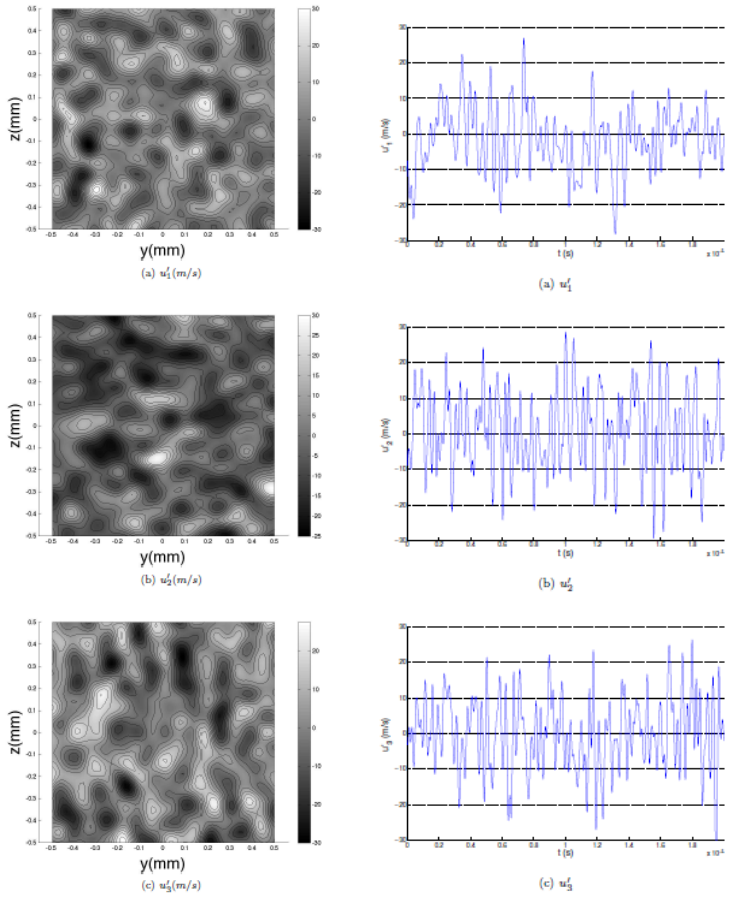

(a) **(b)**

Figure A.1: *Realization of the Kraichnan/Celik method on a plane to generate (a) instantaneous velocity fields and (b) the temporal variation signal, for 5000 Fourier modes and $\lambda_e = 165\mu m$ the wavelength of the most energetic scales of the Passot-Pouquet spectrum [47].*

By summing A.4 and A.5 we get:

$$\underline{u}'(\underline{r},t) = \sum_{n=1}^{N} \left[\underline{\hat{v}}^n(\underline{k}^n) \cos(\underline{k}^n \cdot \underline{r} + \omega^n \cdot t) + \underline{\hat{w}}^n(\underline{k}^n) \sin(\underline{k}^n \cdot \underline{r} + \omega^n \cdot t) \right] \tag{A.6}$$

where $\underline{\hat{v}}^n$ and $\underline{\hat{w}}^n$ the real and the imaginary part respectively of the complex $\underline{\hat{u}}^n$, for which we write:

$$\underline{\hat{v}}^n \cdot \underline{k}^n = 0 \quad \text{and} \quad \underline{\hat{w}}^n \cdot \underline{k}^n = 0 \quad \forall n \tag{A.7}$$

According to the Kraichnan/Celik method, the $\underline{\hat{v}}^n$ and $\underline{\hat{w}}^n$ vectors are such as the incompressibility condition A.7 is satisfied:

$$\underline{\hat{v}}^n = \underline{\zeta}^n \times \underline{k}^n \quad \text{and} \quad \underline{\hat{w}}^n = \underline{\xi}^n \times \underline{k}^n \quad \forall n \tag{A.8}$$

where the vectors $\underline{\zeta}^n$ and $\underline{\xi}^n$ are picked from Gaussian distributions with a standard deviation of $\sigma_N = \sqrt{2/N}$. The wave vectors $\underline{k}^n$ and pulsations ω^n are then chosen from isotropic distribution in the proper way to represent the desired turbulent spectrum. This method has low computational cost (no inverse Fourier transformation needed) and provides a quite simple way to generate a turbulent condition at the inlet. Finally, in terms of memory usage it has a great advantage as it only generates a plane entering the computational domain and not a full three dimensional turbulent field. Realizations of this method on an inlet patch can be seen in figure A.1, generated in the same manner as it is implemented in AVBP.

B. Additional Results

The reader can find here plots of results omitted from the main part of the thesis.

B.1. Flow Structures

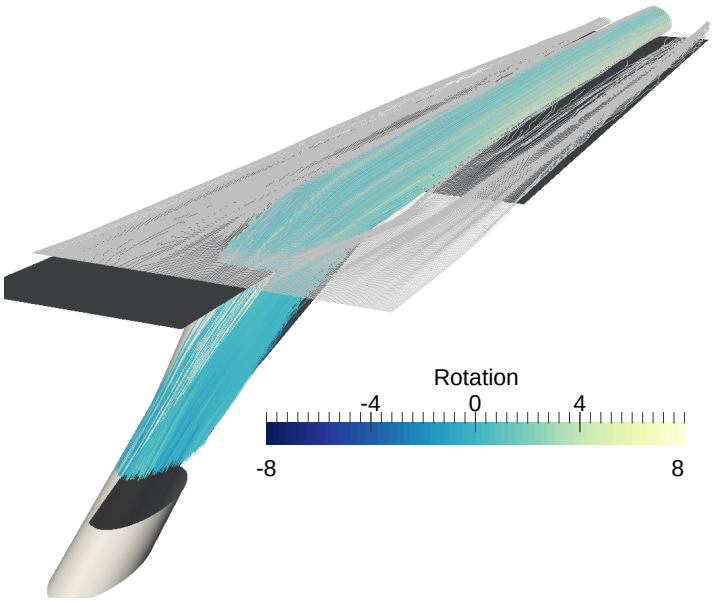

(a)

Figure B.1: *Entrainment of the mainstream streamlines by the CRVP of the jet, simulation Case 2.*

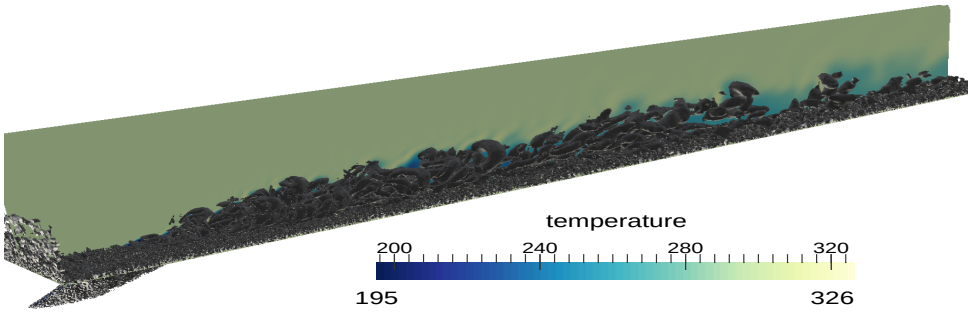

Figure B.2: *Q criterion plots: iso-volumes of* $Q = 4 \cdot 10^5$ *along with the instant thermal field on the x y symmetry plane.*

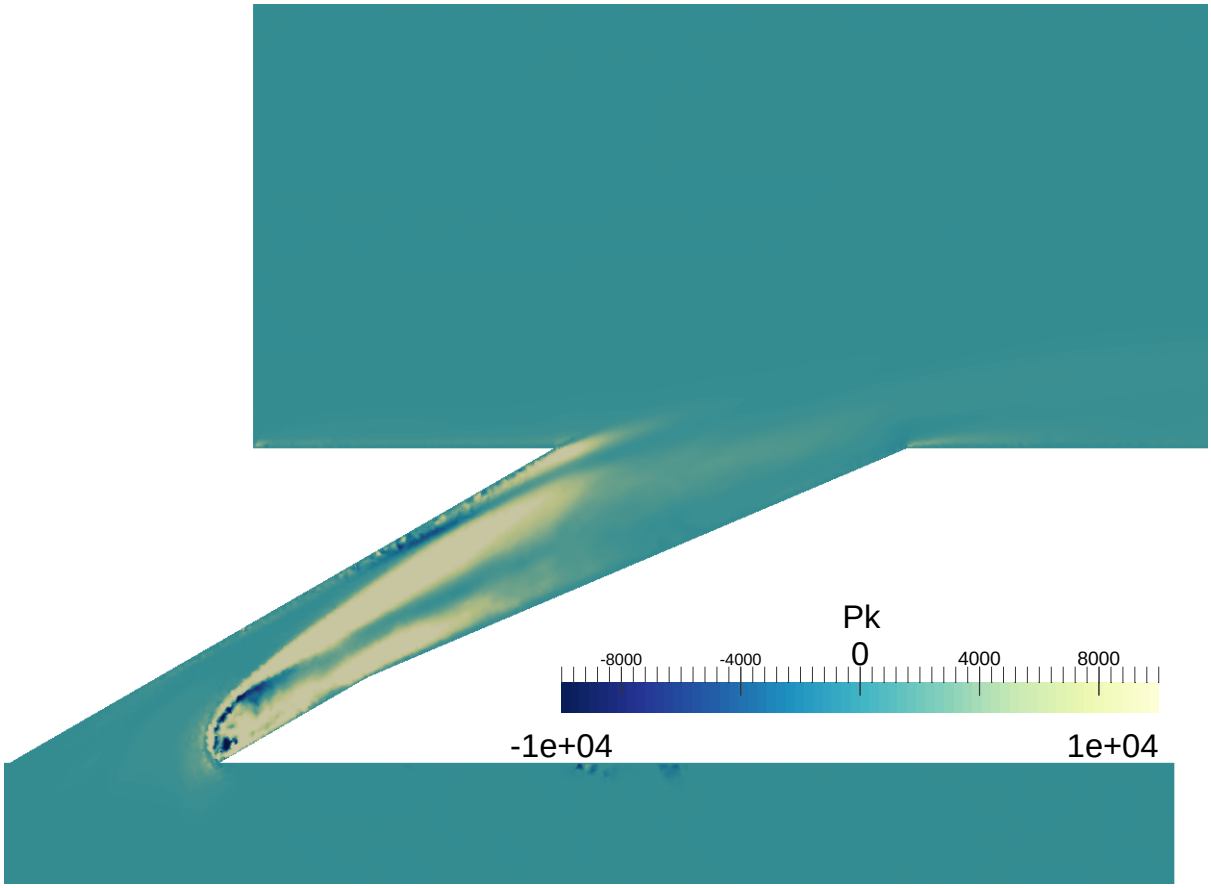

Figure B.3: *Production of turbulent kinetic energy, $P_k = -\overline{u_i' u_j'} \frac{\partial U_i}{\partial x_j}$. Negative values of production could be associated with the transitional detached flow.*

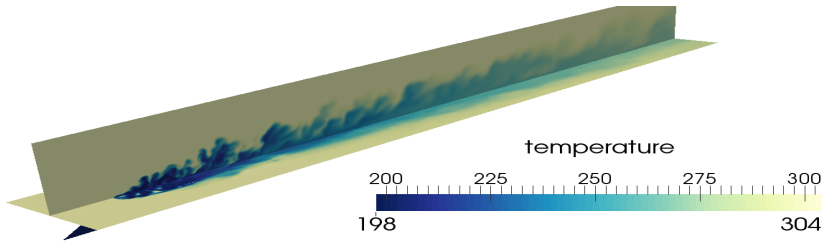

(a) $t = 0$

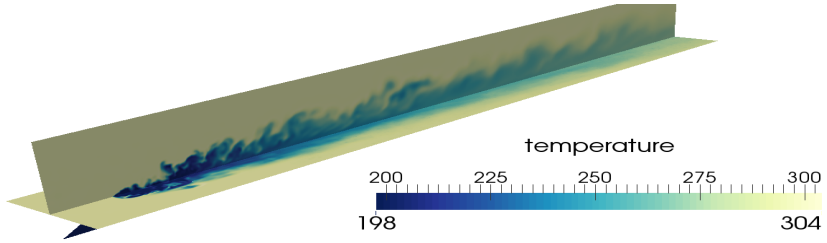

(b) $t = T/5$

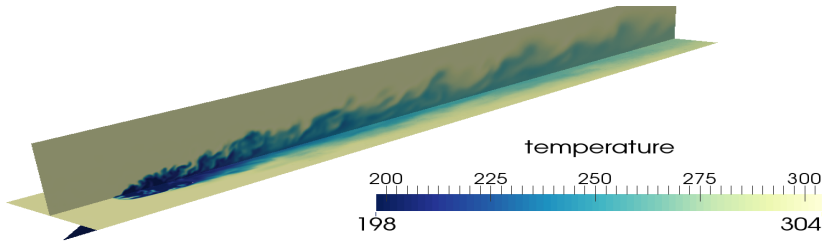

(c) $t = 2T/5$

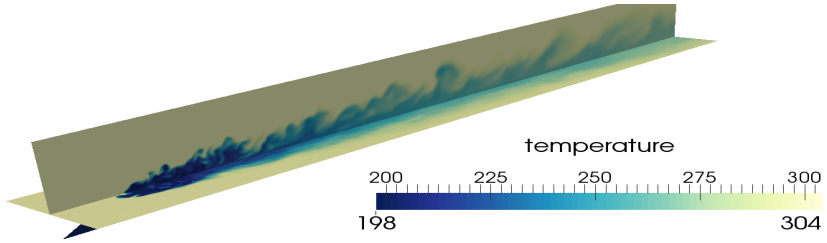

(d) $t = 3T/5$

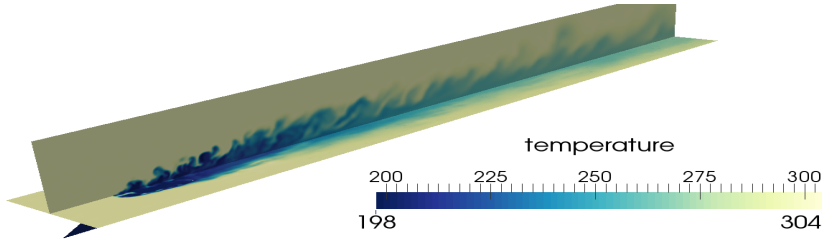

(e) $t = 4T/5$

Figure B.4: *Contour plot of the instant temperature field on the flat plate (xz plane) and on the xy symmetry plane. T is the time the mainstream flow needs to swipe through the computational domain from the velocity inlet to the pressure outlet.*

B.2. Convective Schemes

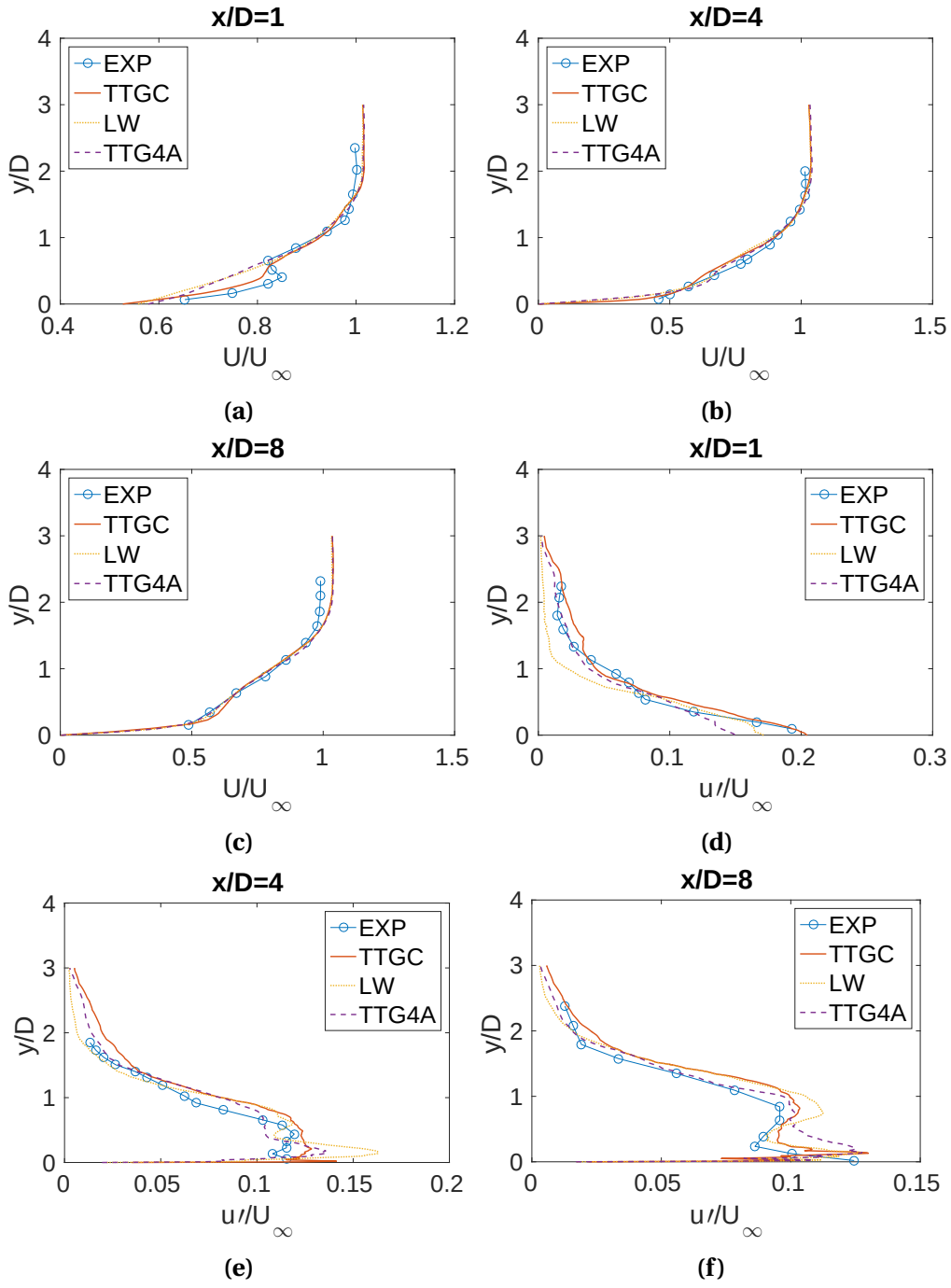

Figure B.5: *Cases 1 to 3: Three different convective schemes, (a)-(c) stream-wise (temporally) averaged velocity and (d)-(f) (temporally) averaged velocity fluctuations profiles on the xy symmetry plane, low free-stream turbulence.*

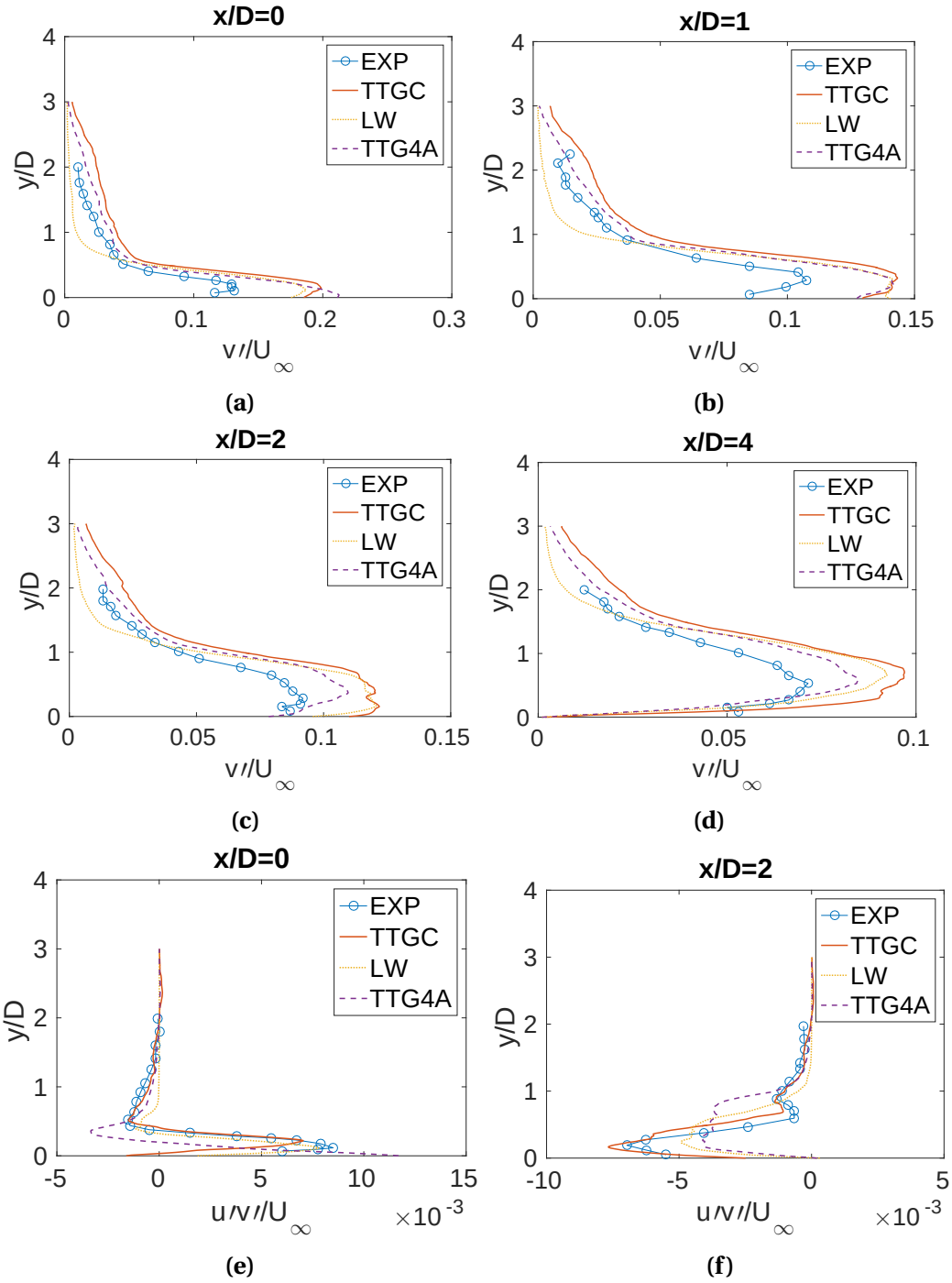

Figure B.6: *Cases 1 to 3: Three different convective schemes, (temporally) averaged normal velocity fluctuations profiles on the xy symmetry plane, low free-stream turbulence.*

B.3. Turbulence Injection

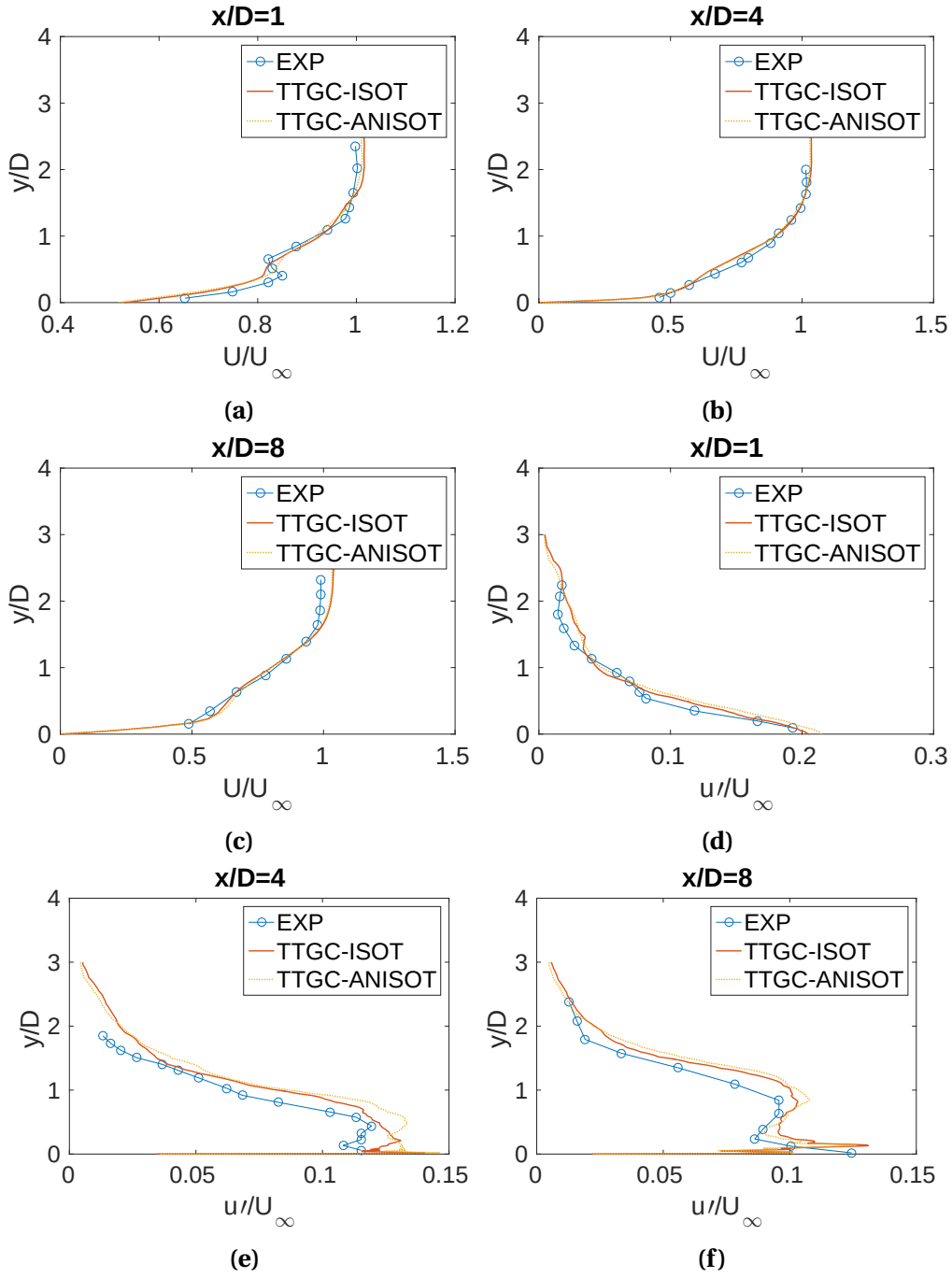

Figure B.7: *Cases 2 and 4: Injection of isotropic and anisotropic turbulence, (a)-(c) stream-wise (temporally) averaged velocity and (d)-(f) (temporally) averaged velocity fluctuations profiles on the xy symmetry plane, low free-stream turbulence.*

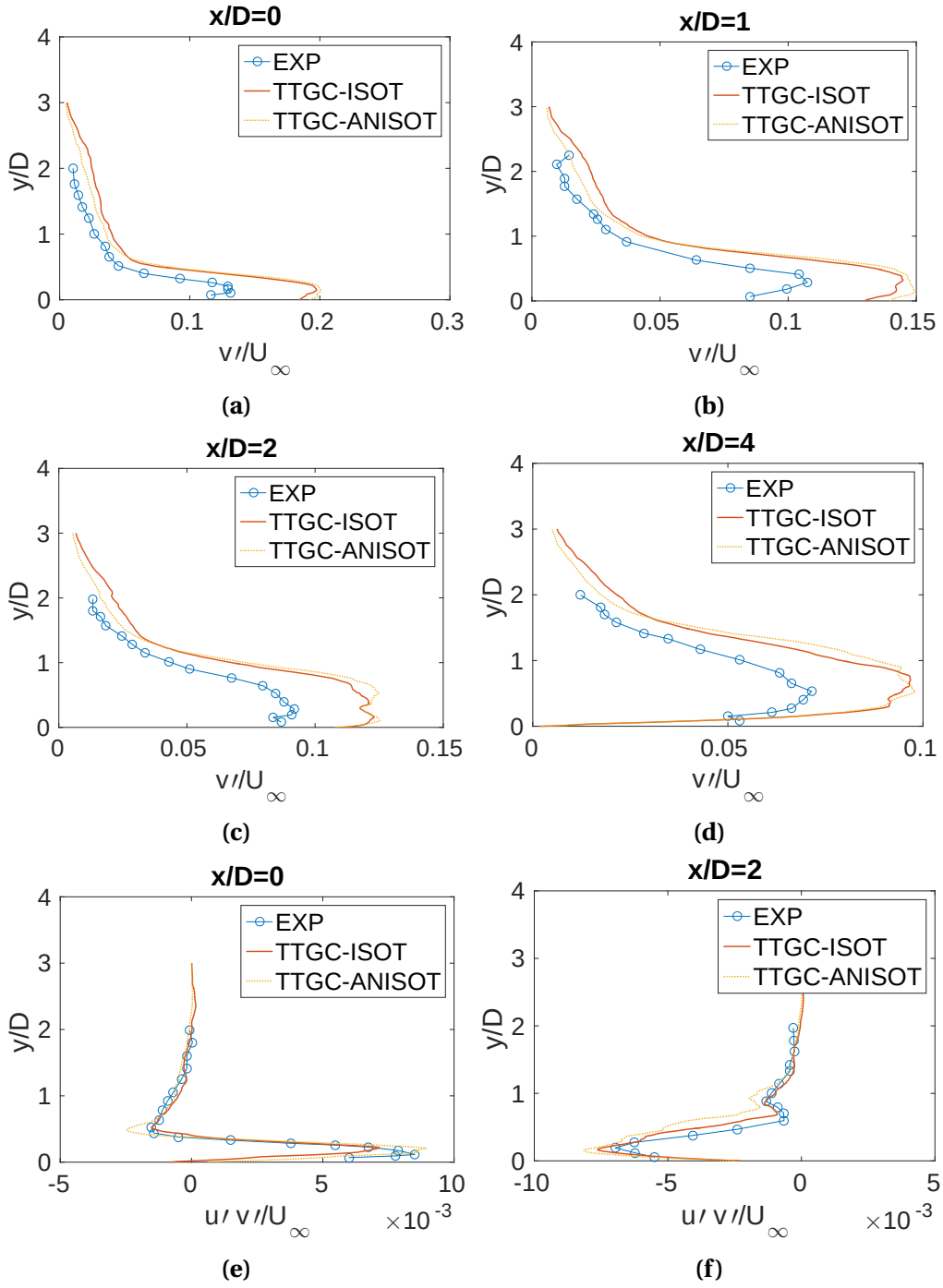

Figure B.8: *Cases 2 and 5: Injection of isotropic and anisotropic turbulence, (temporally) averaged normal velocity fluctuations profiles on the xy symmetry plane, low free-stream turbulence.*

B.4. Wall Modeling

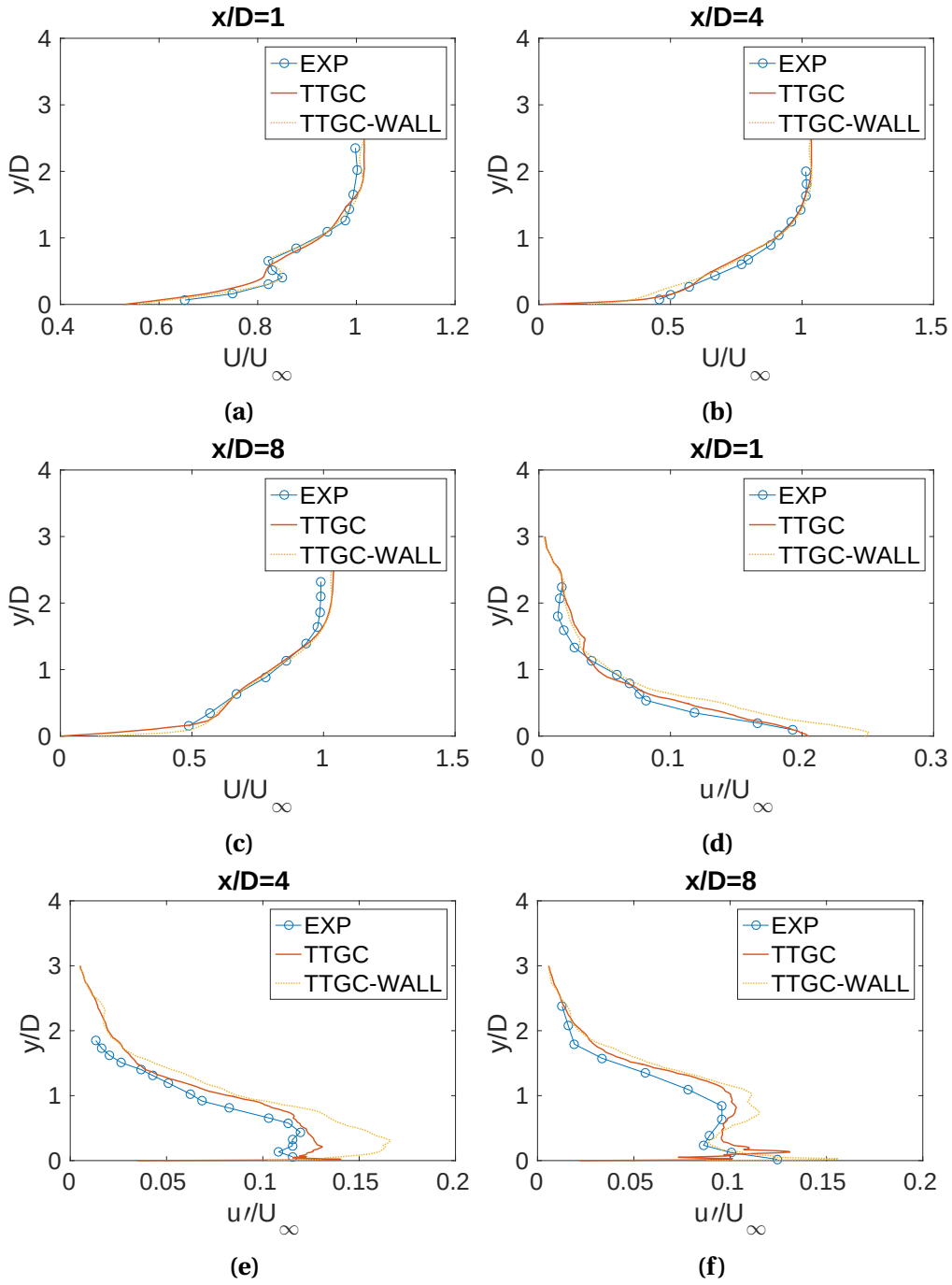

Figure B.9: *Cases 2 and 5: Testing the wall modeling approach, (a)-(c) stream-wise (temporally) averaged velocity and (d)-(f) (temporally) averaged velocity fluctuations profiles on the xy plane, low free-stream turbulence.*

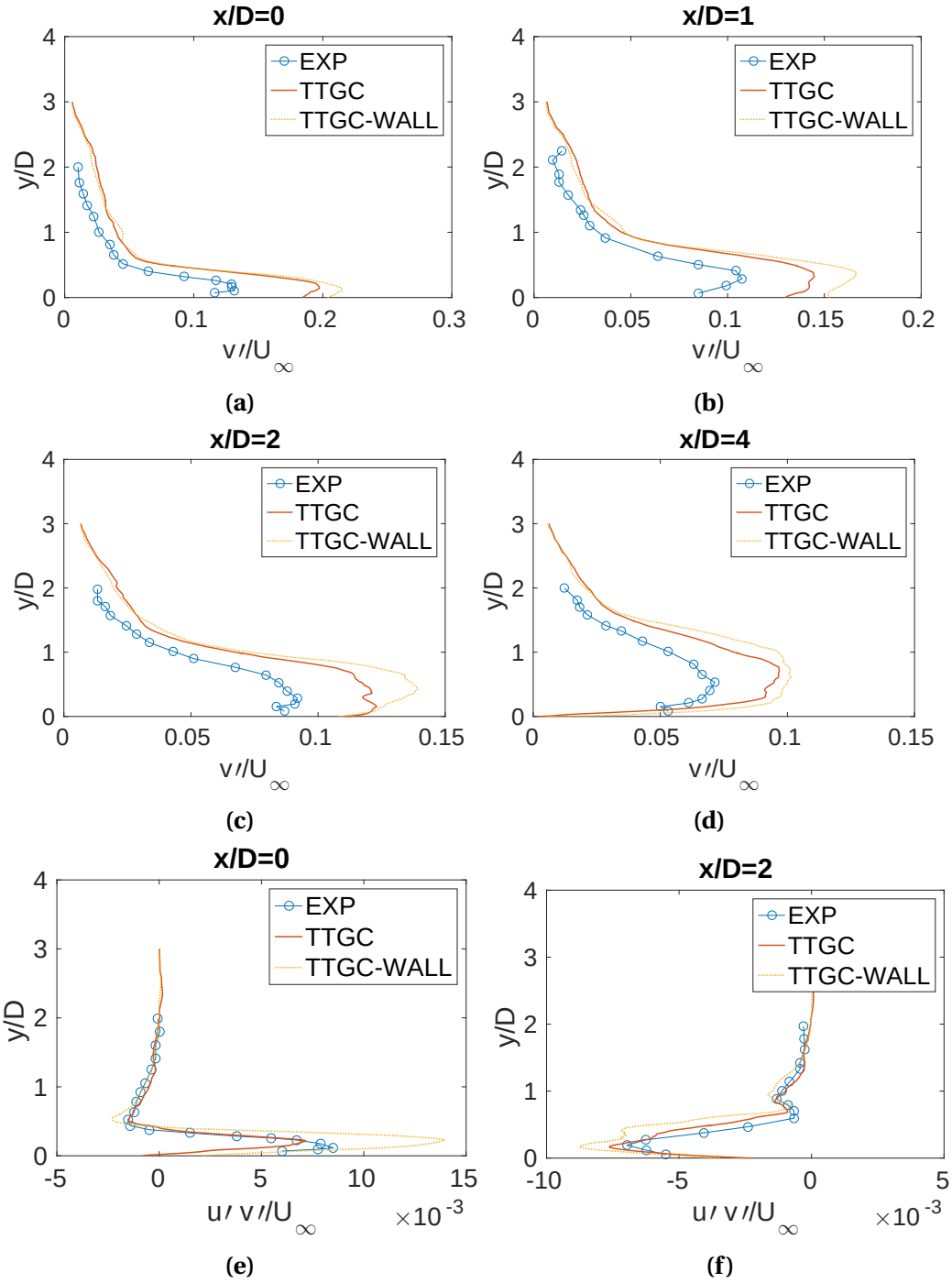

Figure B.10: *Cases 2 and 5: Testing the wall modeling approach, (temporally) averaged normal velocity fluctuations profiles on the xy plane, low free-stream turbulence.*